The first image of a black hole

Luciano Rezzolla

Institute for Theoretical Physics, Frankfurt
Event Horizon Telescope (EHT) Collaboration

Milano
09.10.19

Plan of the talk

- The first image of a black hole: M87*
- How do you take a picture of a BH: **observations?**
- How do you take a picture of a BH: **theory?**
- Alternatives to Einstein and to black holes

M87, center of the Virgo cluster

The first image of a black hole

How was this accomplished?

ESO

VLBI: Very Long Baseline Interferometry

$$\text{resolution} = \frac{\text{wavelength}}{\text{telescope size}}$$

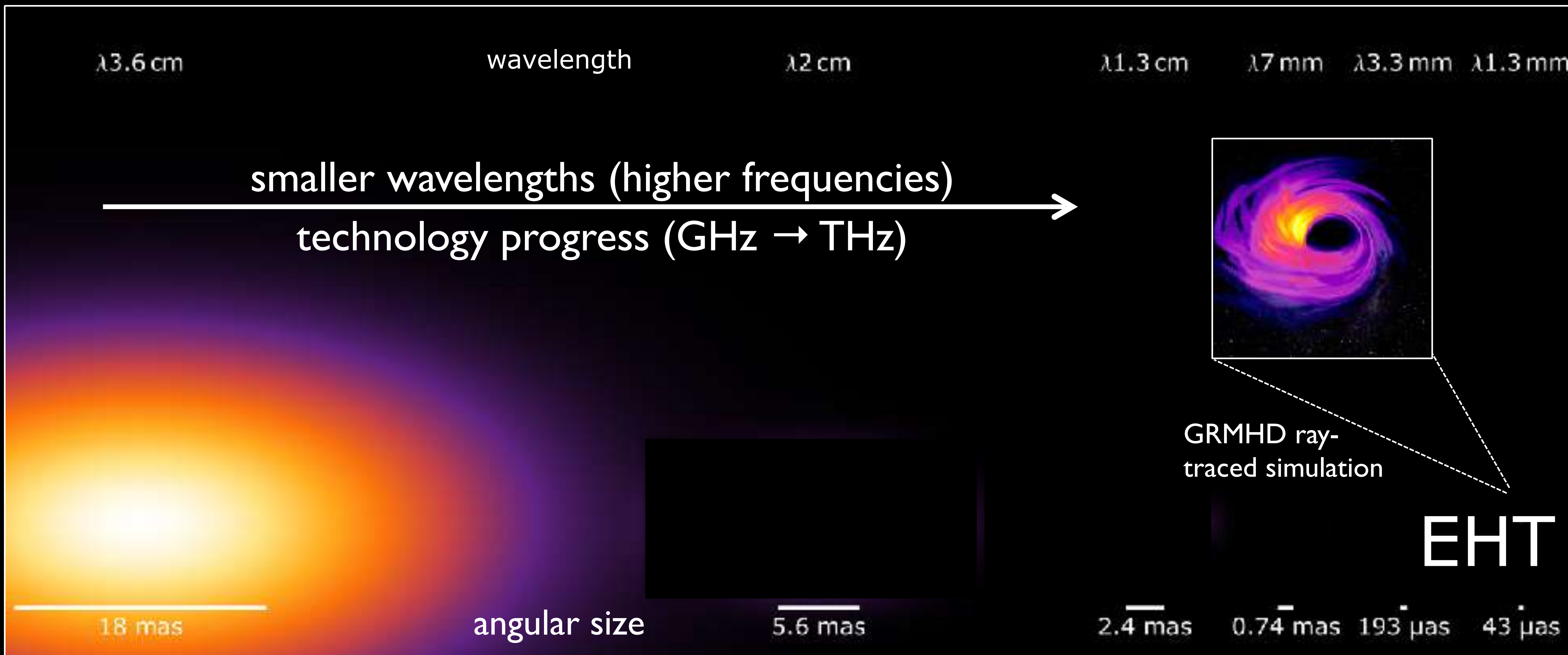

- The shorter the wavelength, the smaller the emitting source
- At 1.3 mm the source becomes of the size of the horizon

mas = milli-arcsecond = 5×10^{-9} rad

μas = micro-arcsecond = 5×10^{-12} rad

VLBI: Very Long Baseline Interferometry

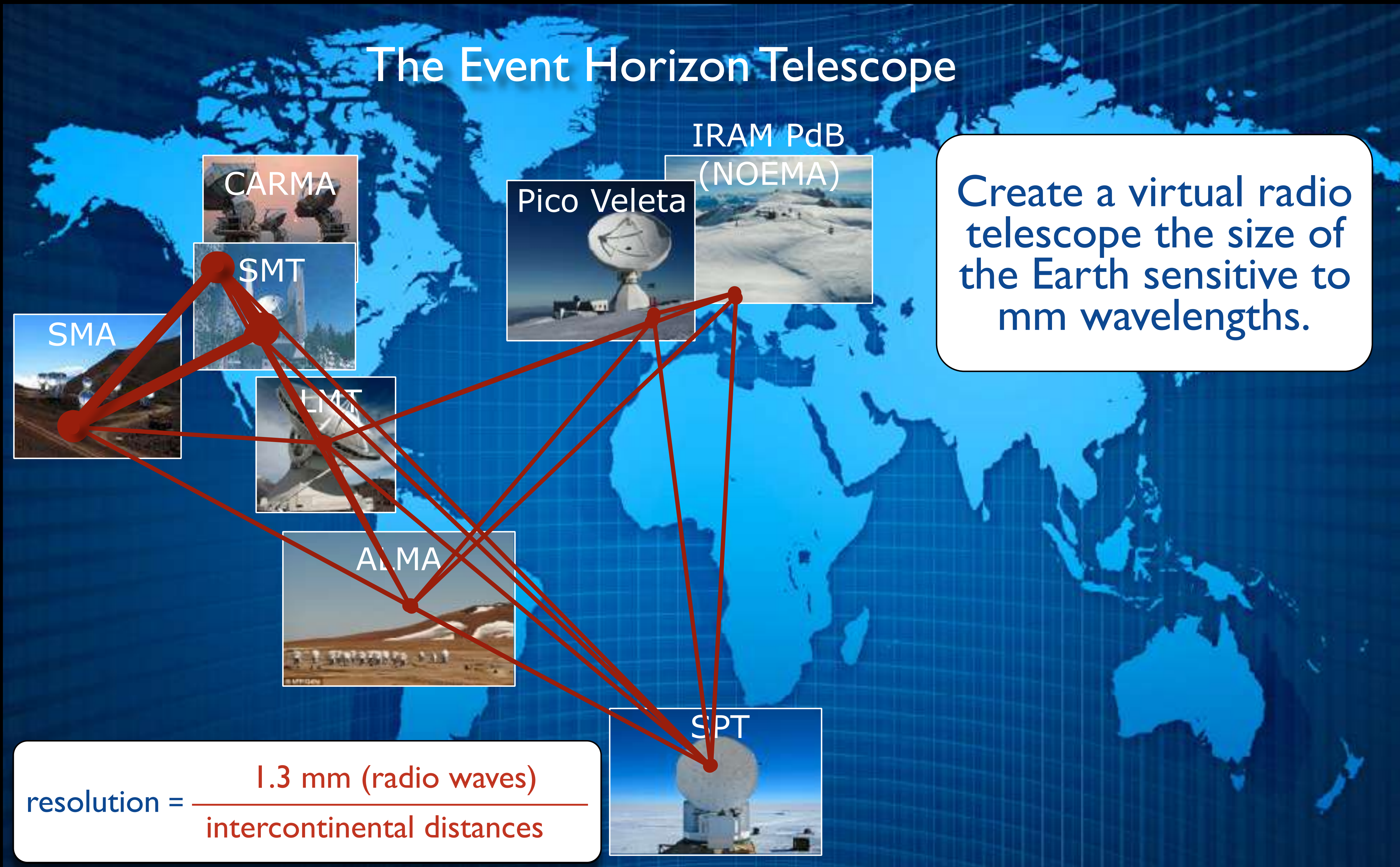

Create a virtual radio telescope the size of the Earth sensitive to mm wavelengths.

$$\text{resolution} = \frac{\text{1.3 mm (radio waves)}}{\text{intercontinental distances}}$$


Mexico
(LMT)
Hawaii
(SMA/JCMT)
Arizona
(SMT)
South Pole
(SPT)
Chile
(ALMA/APEX)
Spain
(IRAM 30m,
Pico Veleta)

The image has soon gone around the world…

becoming a great resource for social media…

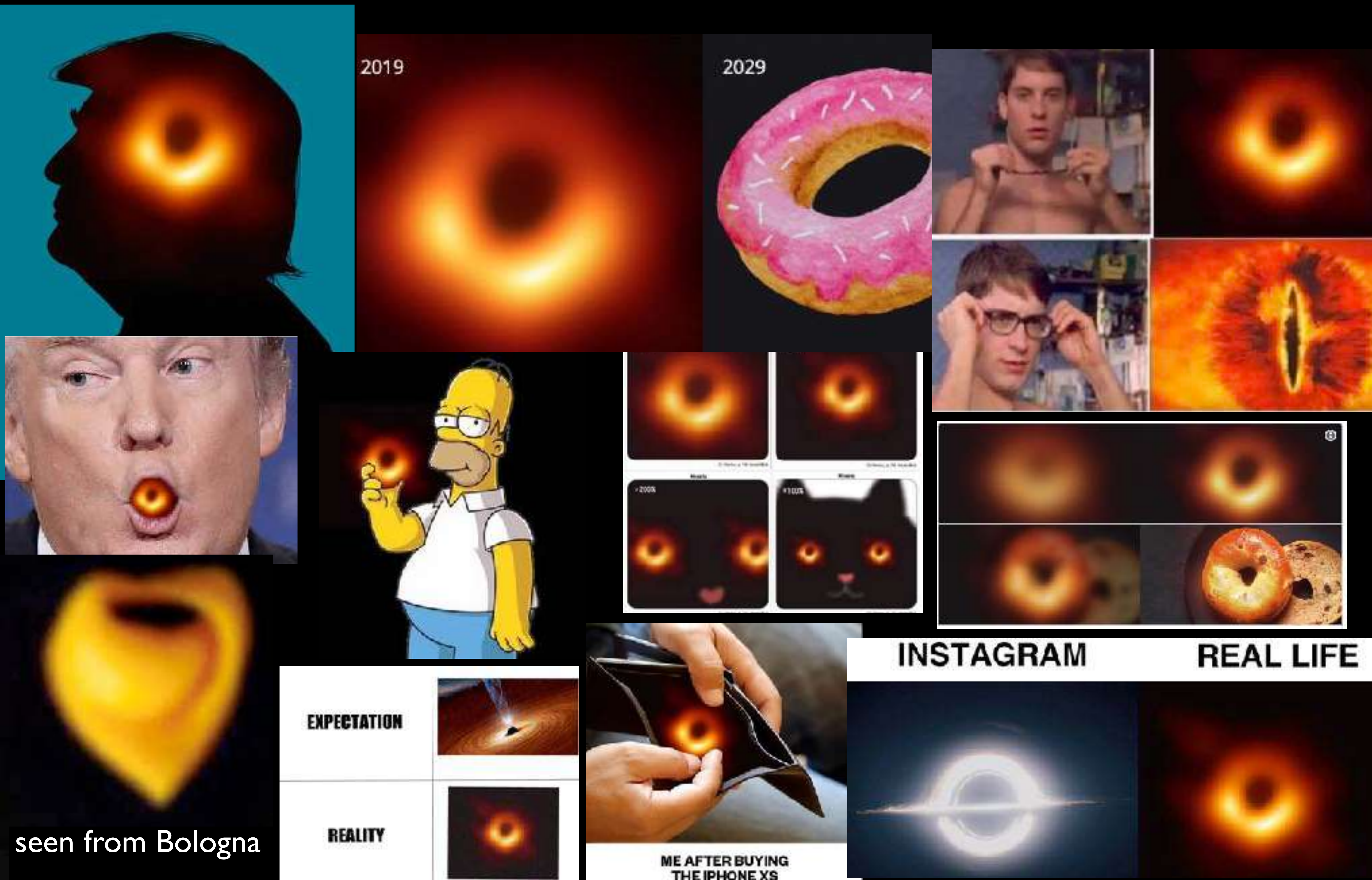

Elliptical galaxy in center of Virgo cluster 55 Million light years away

There is evidence for a central dark mass of $3\text{-}6\times10^{9}\ M_{sun}$

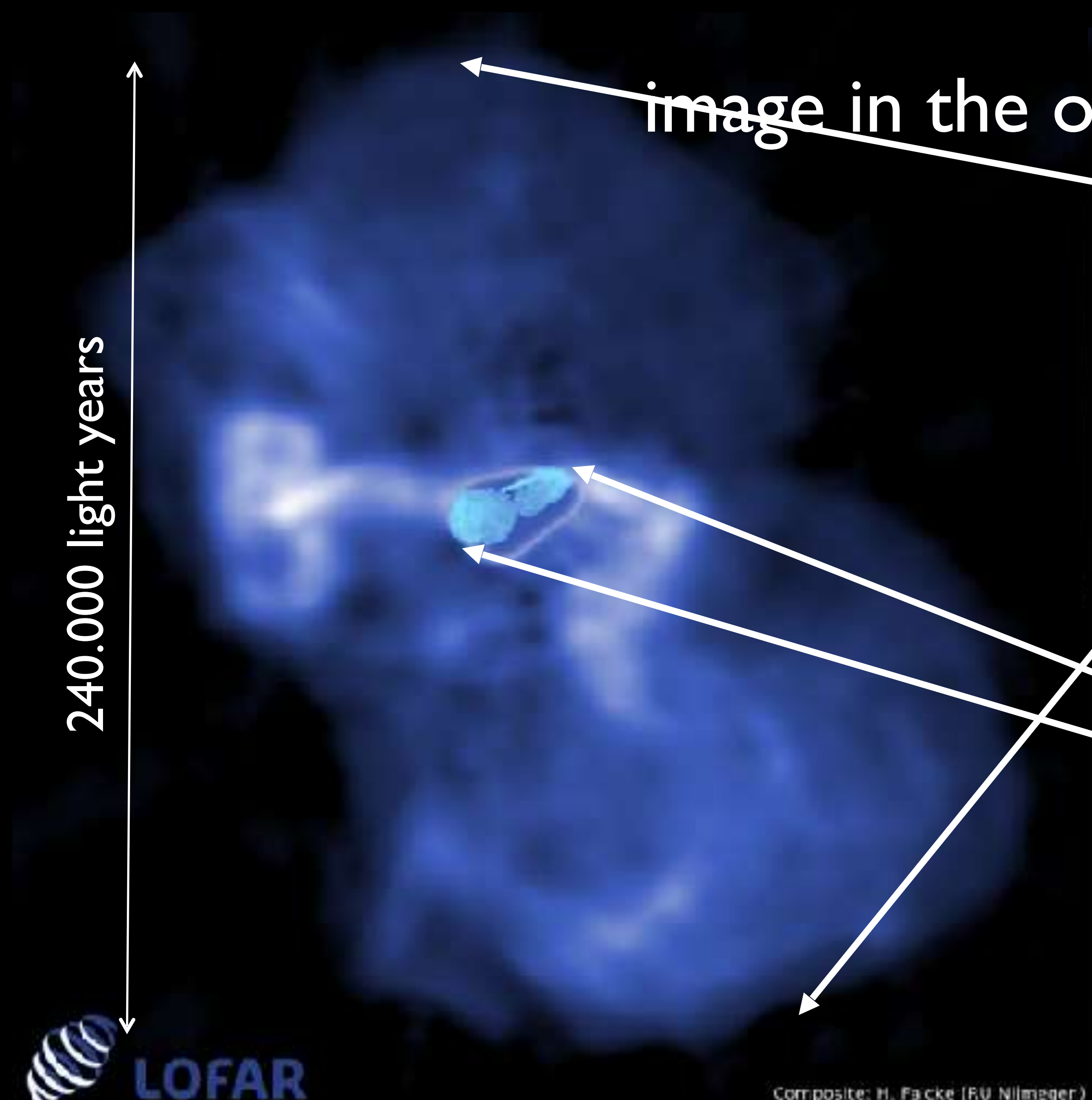

Elliptical galaxy in center of Virgo cluster 55 Million light years away

There is evidence for a central dark mass of $3\text{-}6\times10^{9}\,M_{sun}$

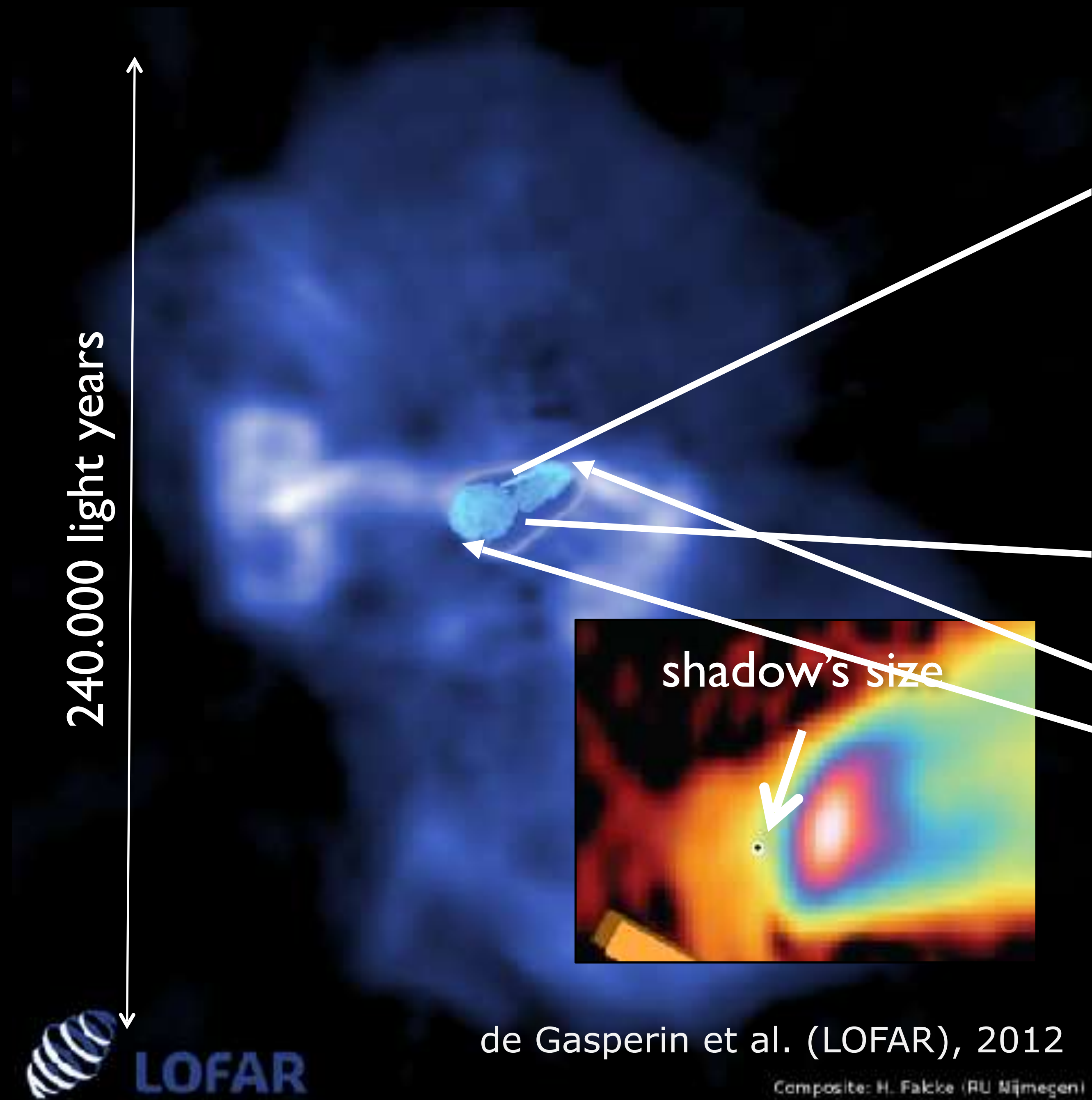

small-scale radio map of the core (cm wavelength)

… to have an idea of the scales…

https://xkcd.com/2135/

How do we do this in practice?
Observations

How do we do this in practice?
Observations

$\mathcal{V}(u,v)$: complex visibilities

$$\mathcal{V}(u,v) = \int\int e^{-2\pi i(ux+vy)} I(x,y)dxdy$$

(x,y) : angular coordinates on the sky

(u,v) : projected baseline coordinates

$I(x,y)$: brigthness distribution

$$\mathcal{V}(f) = \int e^{-2\pi i f t} I(t)dt$$

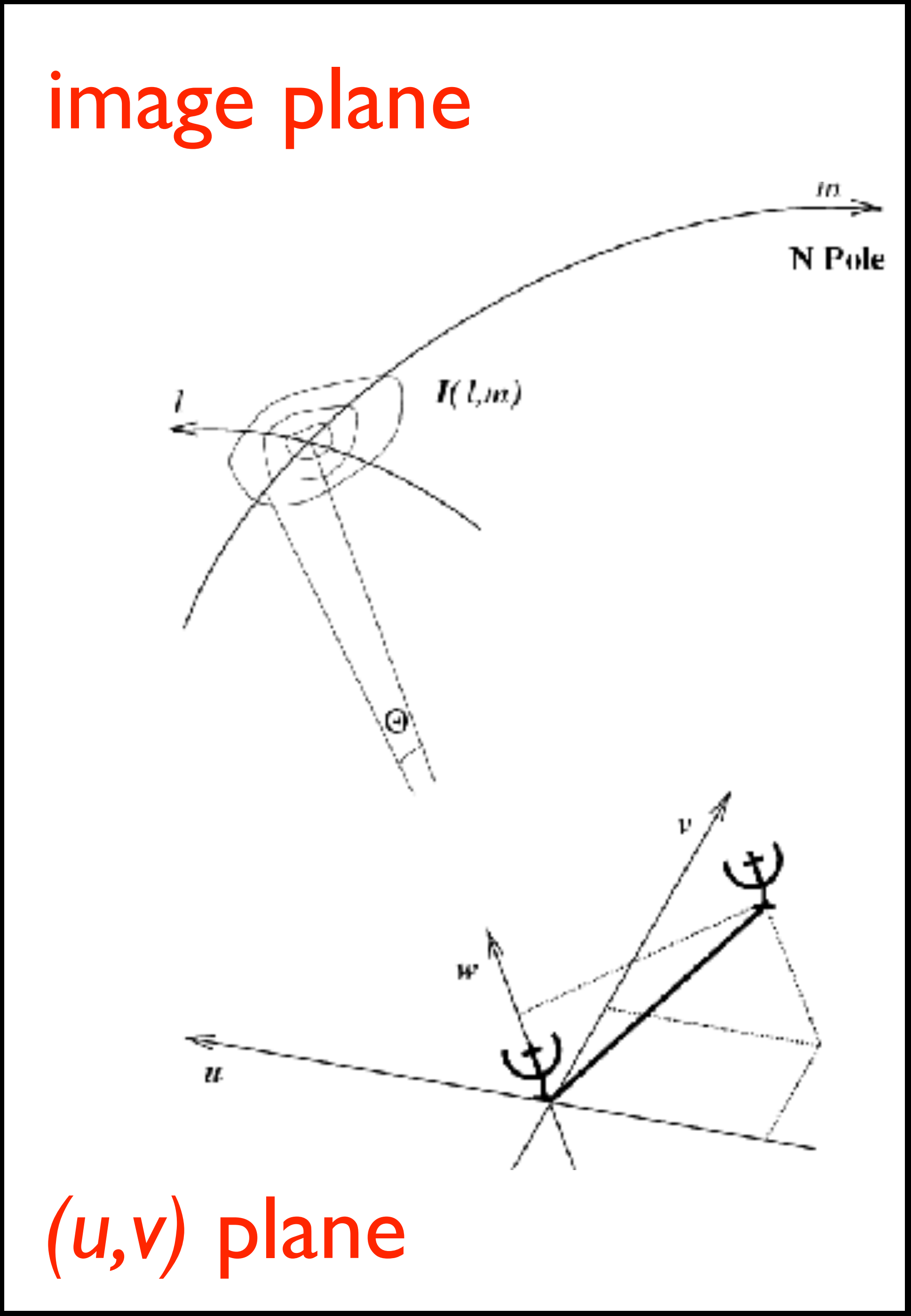

How do we do this in practice?

Observations

$$\mathcal{V}(u,v) = \int\int e^{-2\pi i(ux+vy)} I(x,y)\,dx\,dy$$

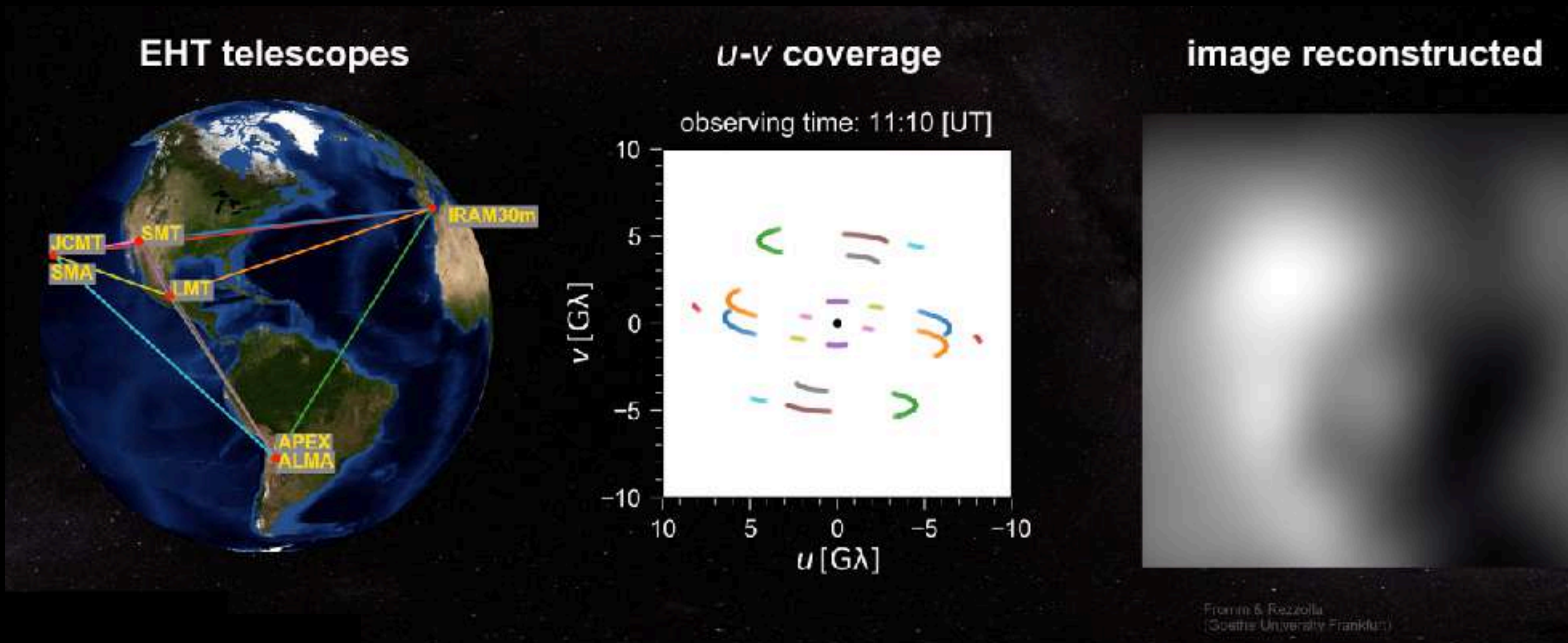

How do we do this in practice?
Observations

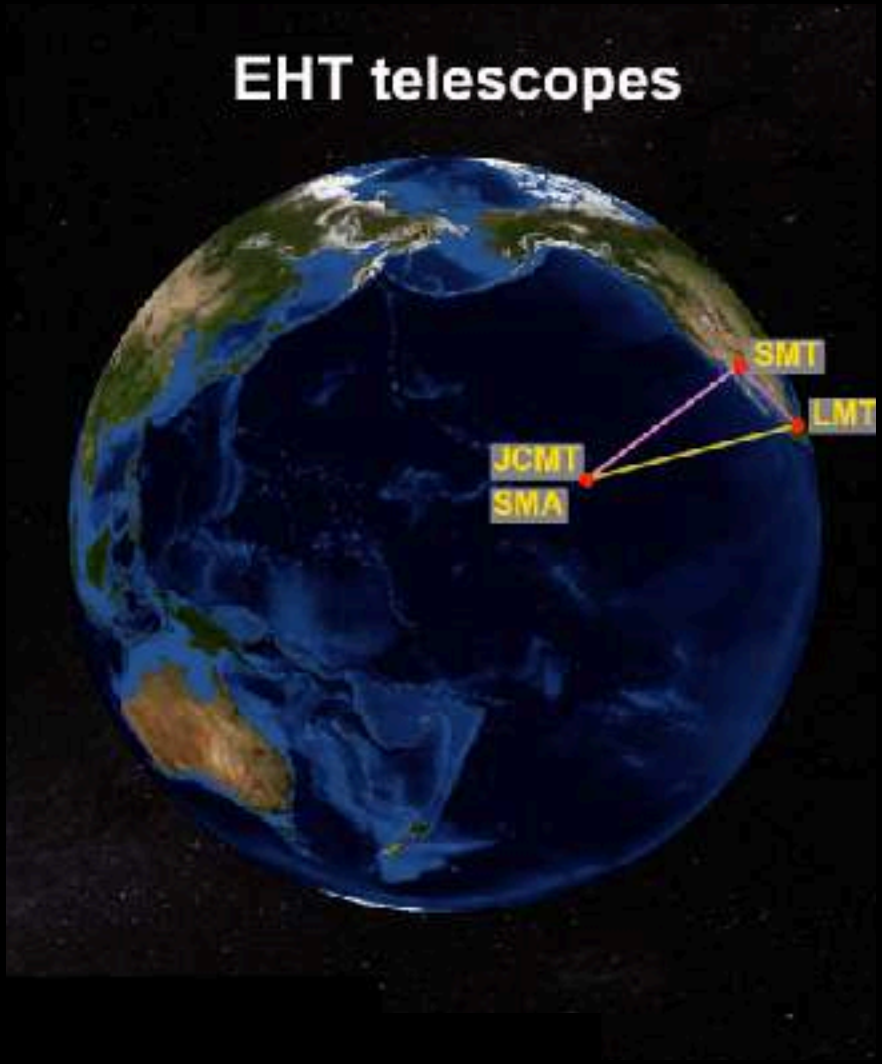

How do we do this in practice?

Observations

As the data was collected, converted and calibrated four different imaging teams were set with the task of computing an image

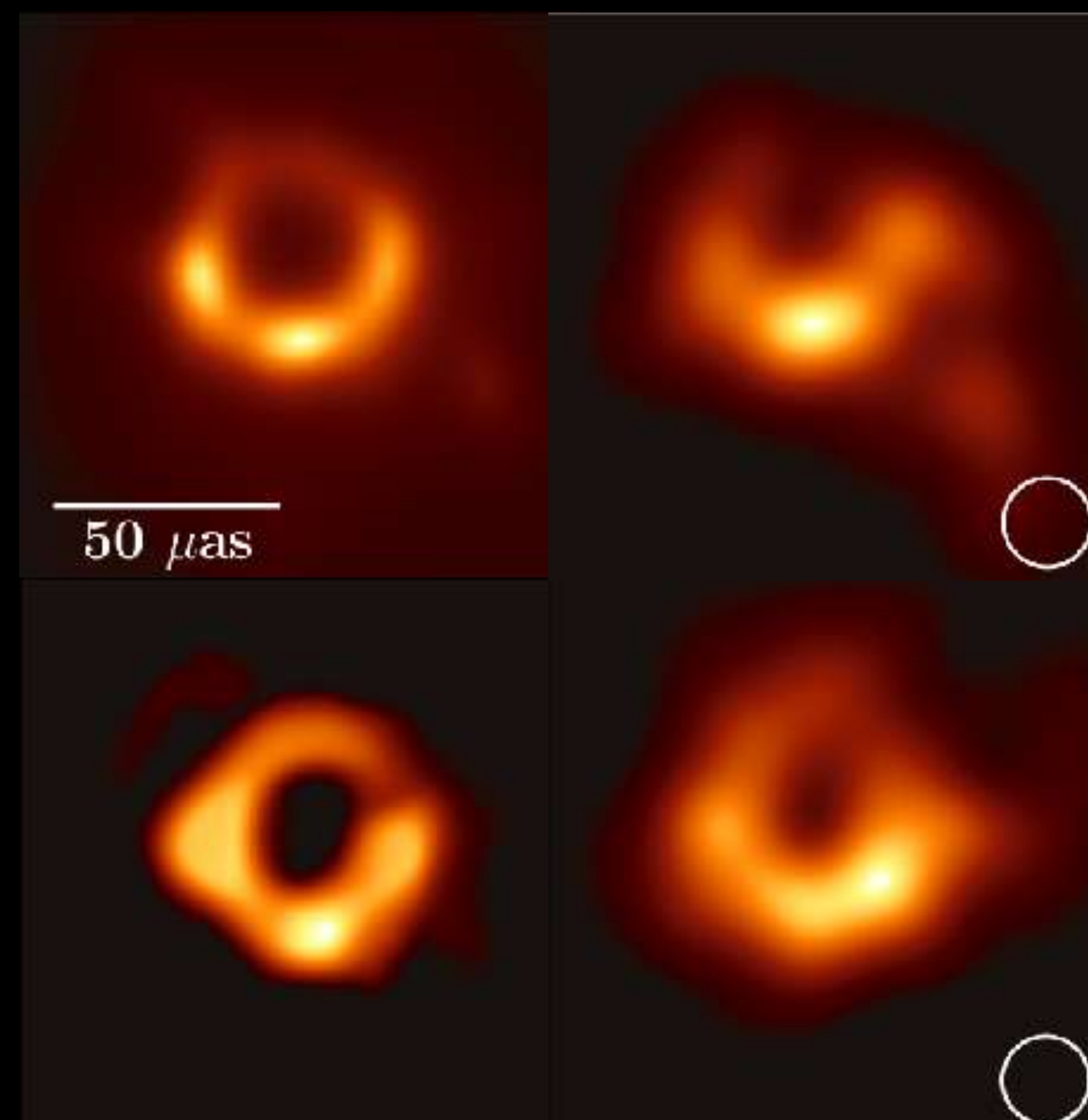

The four teams used multiple software packages and were set to work blindly from each other.

All of the teams recovered a very similar images: asymmetric ring is a robust feature of the image

M87 was observed for several days (eight) and lead to four distinct images.

The images are slightly different but show again that the asymmetric ring emission is stable, as expected on these timescales.

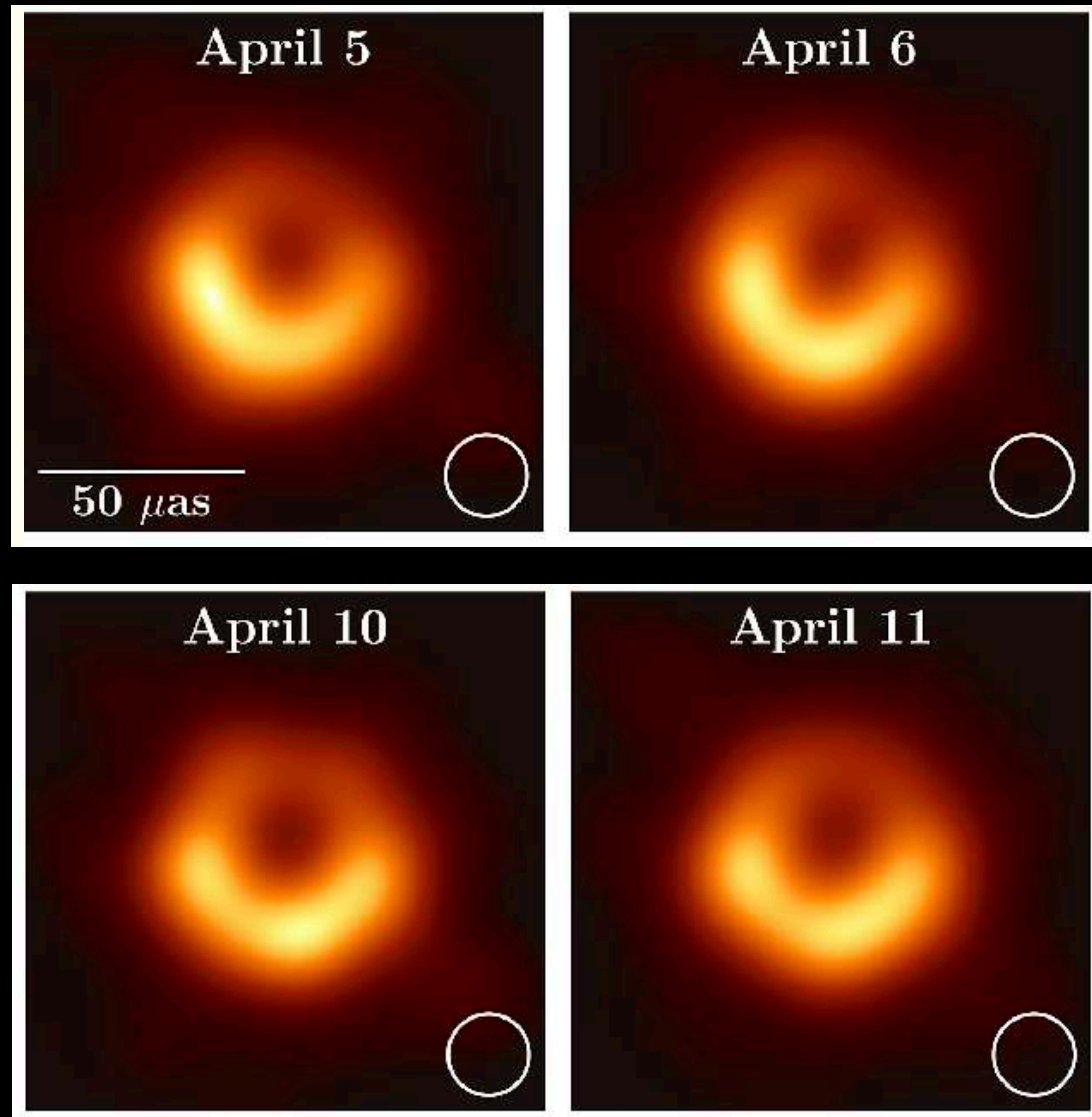

How do we do this in practice?

Theory

BlackHoleCam:
Bonn (Kramer), Frankfurt (LR), Nijmegen (Falcke)

Three basic steps are needed:

(1) **GRMHD simulations** in arbitrary spacetimes

(2) **ray-traced, radiative-transfer**, **deconvolved images**

(3) **comparison** with **observations**.

BlackHoleCam (LR, Falcke, Kramer), has developed a complex and complete computational infrastructure:

BHAC/BHOSS/GENA

C. Fromm

R. Gold

Y. Mizuno

H. Olivares

O. Porth

now UA

Z. Younsi

now UCL

System of equations to solve…

$$\nabla_\mu T^{\mu\nu} = 0\,, \quad \text{(cons. energy/momentum)}$$

$$\nabla_\mu (\rho u^\mu) = 0\,, \quad \text{(cons. rest mass)}$$

$$p = p(\rho, \epsilon, Y_e, \ldots)\,, \quad \text{(equation of state)}$$

$$\nabla_\nu F^{\mu\nu} = I^\mu\,, \qquad \nabla_\nu^* F^{\mu\nu} = 0\,, \quad \text{(Maxwell equations)}$$

$$T_{\mu\nu} = T_{\mu\nu}^{\text{fluid}} + T_{\mu\nu}^{\text{EM}} + \ldots \quad \text{(energy} - \text{momentum tensor)}$$

These GRMHD equations are solved using finite-volume methods with a variety of algorithms in **2D and 3D**.

In addition…

$$\nabla_\mu T^{\mu\nu} = 0\,, \quad \text{(cons. energy/momentum)}$$

$$\nabla_\mu (\rho u^\mu) = 0\,, \quad \text{(cons. rest mass)}$$

$$p = p(\rho, \epsilon, Y_e, \ldots)\,, \quad \text{(equation of state)}$$

$$\nabla_\nu F^{\mu\nu} = I^\mu\,, \qquad \nabla^*_\nu F^{\mu\nu} = 0\,, \quad \text{(Maxwell equations)}$$

$$T_{\mu\nu} = T^{\rm fluid}_{\mu\nu} + T^{\rm EM}_{\mu\nu} + \ldots \quad \text{(energy}-\text{momentum tensor)}$$

The equations of **general-relativistic radiative transfer (GRRT)** need to be solved in the background spacetime.

$$\frac{d\mathcal{I}}{d\lambda} = -k_\mu u^\mu \left(-\alpha_{\nu,0}\,\mathcal{I} + \frac{j_{\nu,0}}{\nu_0^3} \right) \quad \text{(radiative}-\text{transfer eq.)}$$

$$\mathcal{I} := I_\nu / \nu^3 \qquad \tau_\nu\,(\lambda) = -\int_{\lambda_0}^{\lambda} \alpha_{\nu,0}\,(\lambda')\, k_\mu u^\mu \, d\lambda'$$

Which gravity?…

- **Field equations** are not necessary as we are exploiting **equivalence principle:** test-particle motion
- Previous eqs. require background **spacetime metric:** $g_{\mu\nu}(x^\alpha)$
- Testing theory of gravity **not trivial** if hundreds available!
- Opted for **agnostic approach** and built a description able to describe all theories: $g_{\mu\nu}(x^\alpha) \rightarrow g_{\mu\nu}(x^\alpha, a_i, b_i)$
- Derive generic expansion exploiting conformal mapping and rapidly converging Pade' expansion
- GR seen as a possible, reference case: $g_{\mu\nu}(x^\alpha, a_i = 0 = b_i)$

LR, Zhidenko, 2014; Konoplya, LR, Zhidenko, 2016

Tracing photons near a BH is **not easy**...

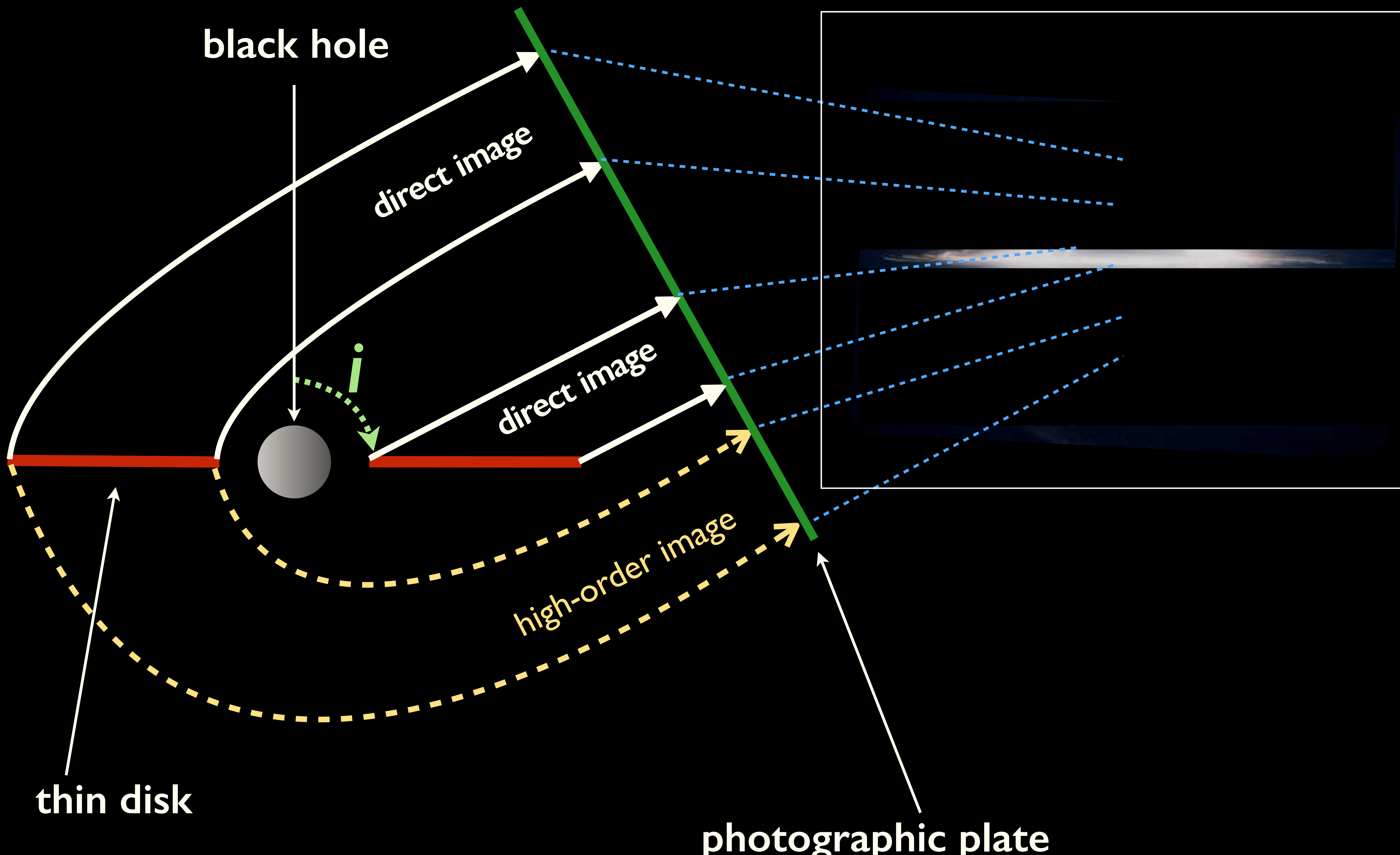

Younsi, LR 2019

To be even clearer…

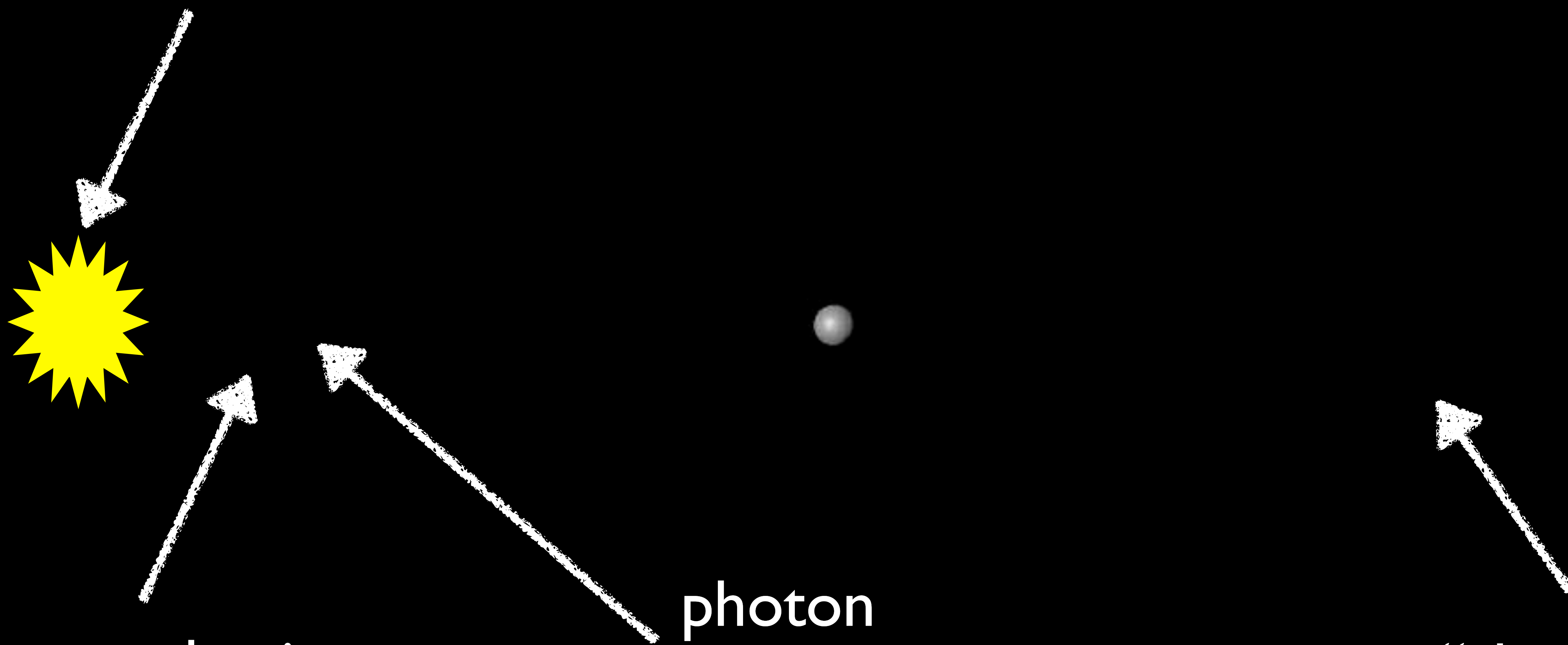

source of light

event horizon

photon circular orbit

“shadow”

$$r_{\mathrm{EH}} = \frac{2GM}{c^2}$$

$$r_{\mathrm{co}} = \frac{3GM}{c^2}; \quad r_{\mathrm{c}} := b_{\mathrm{c}}\big|_{r_{\mathrm{co}}} = \sqrt{27}\left(\frac{GM}{c^2}\right)$$

Müller, Pössel, Weih, LR

The actual shape of the shadow also depends on the spin of the black hole $a := J/M^2$ and on the inclination angle

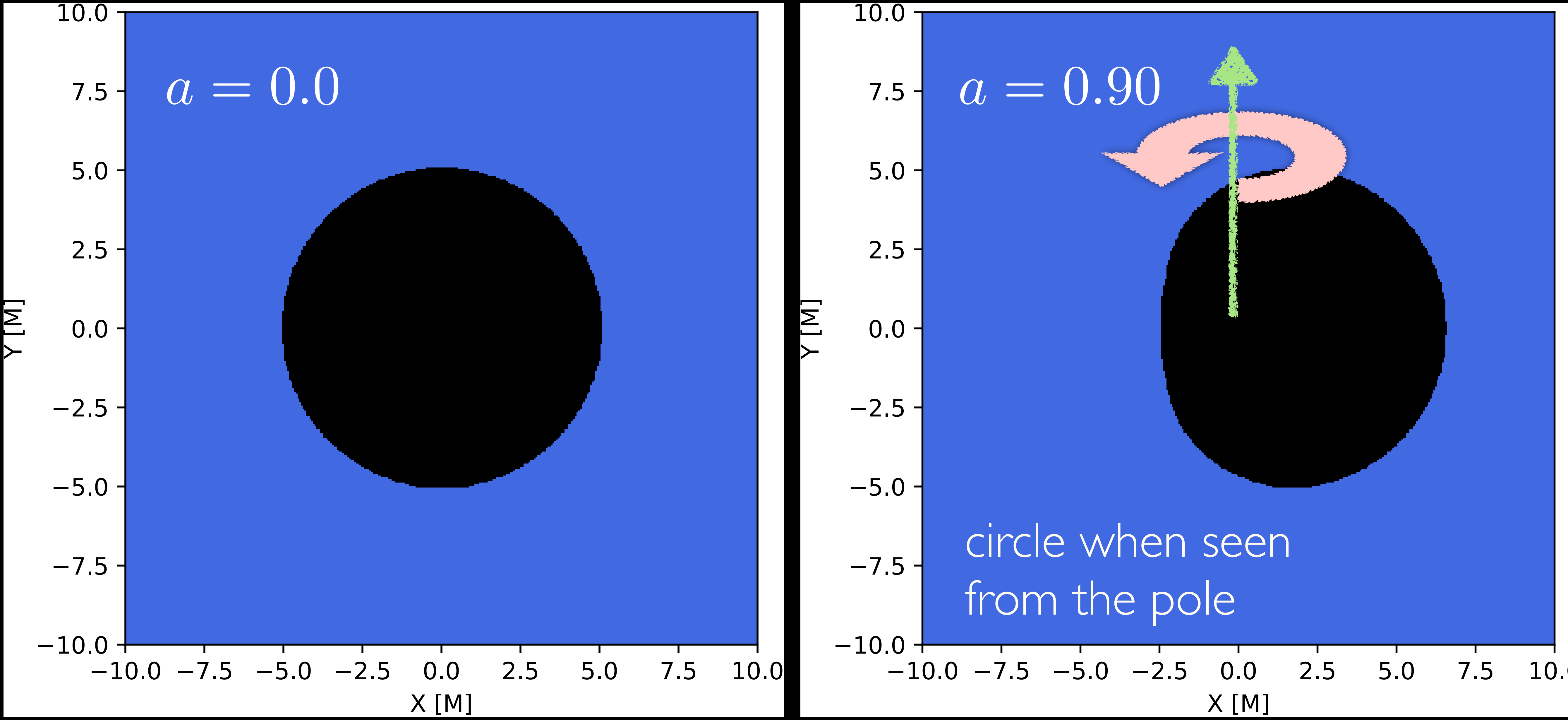

shadow's size depends also on the inclination

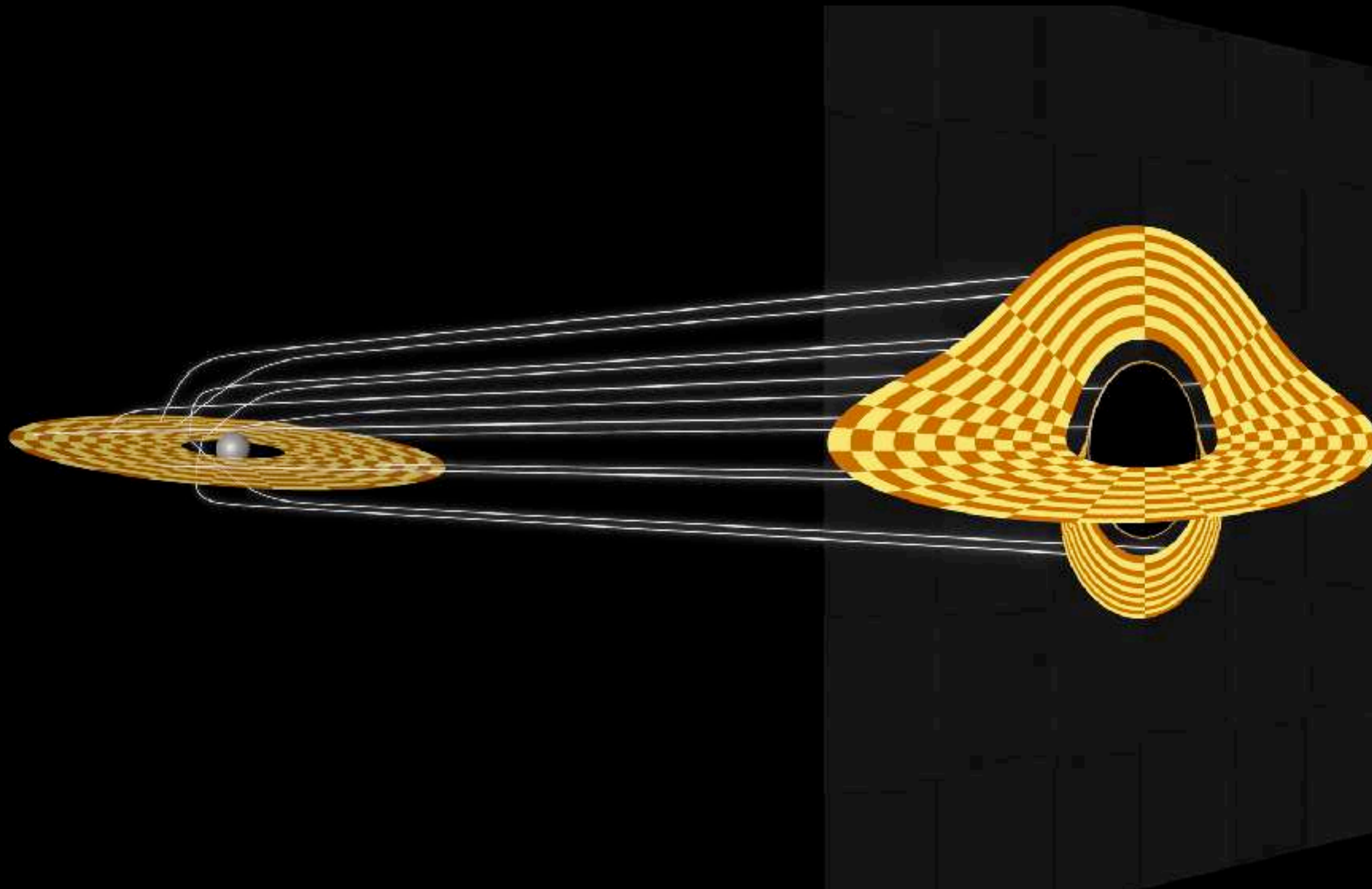

Müller, Pössel, Weih, LR

In reality, the disk is not geometrically thin but geometrically thick, optically thin…

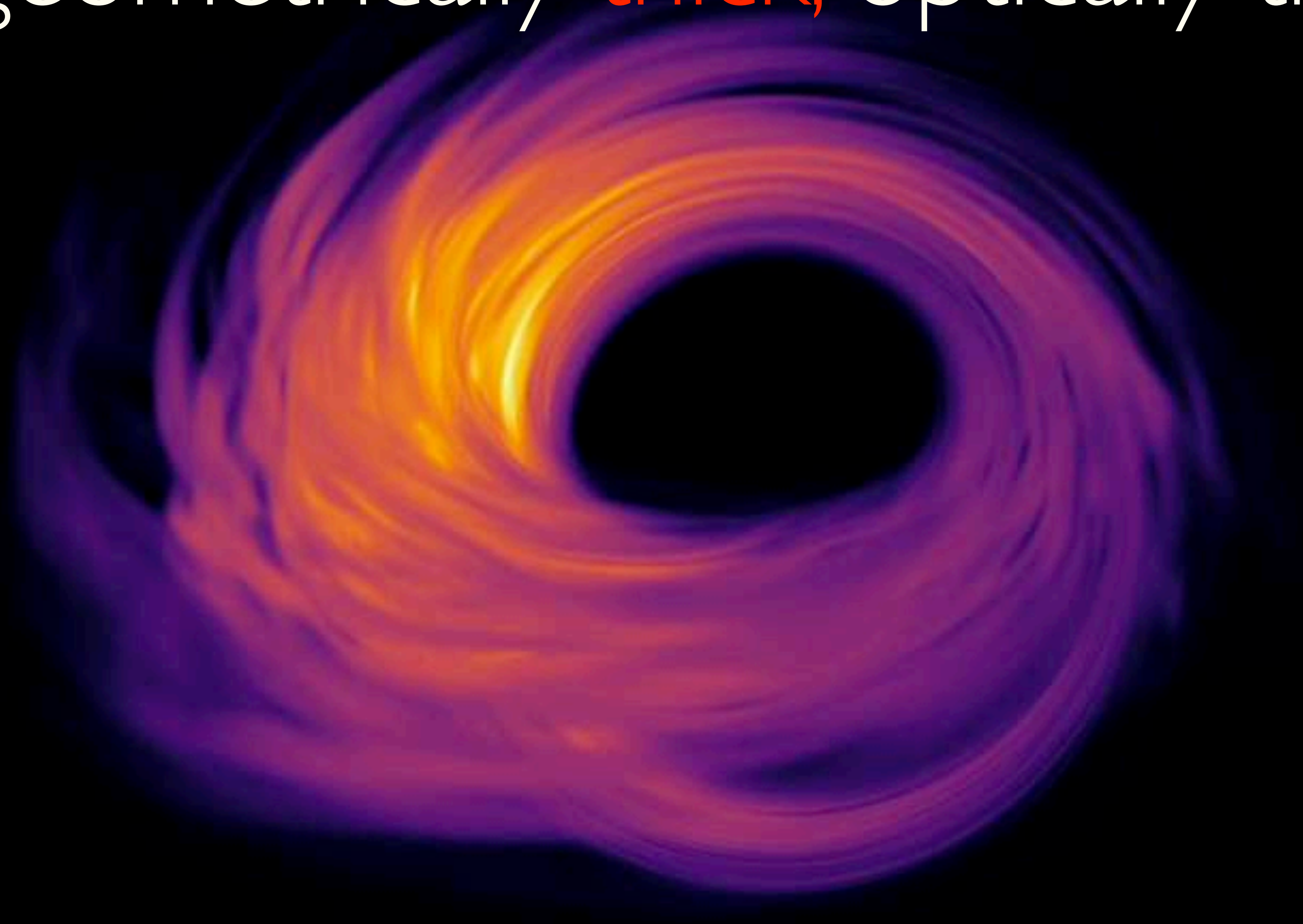

Plasma dynamics:
a typical GRMHD simulation…

A three-dimensional simulation of a Kerr black hole (a=0.9375) in Kerr-Schild coordinates and an MRI unstable torus would produce results of this type…

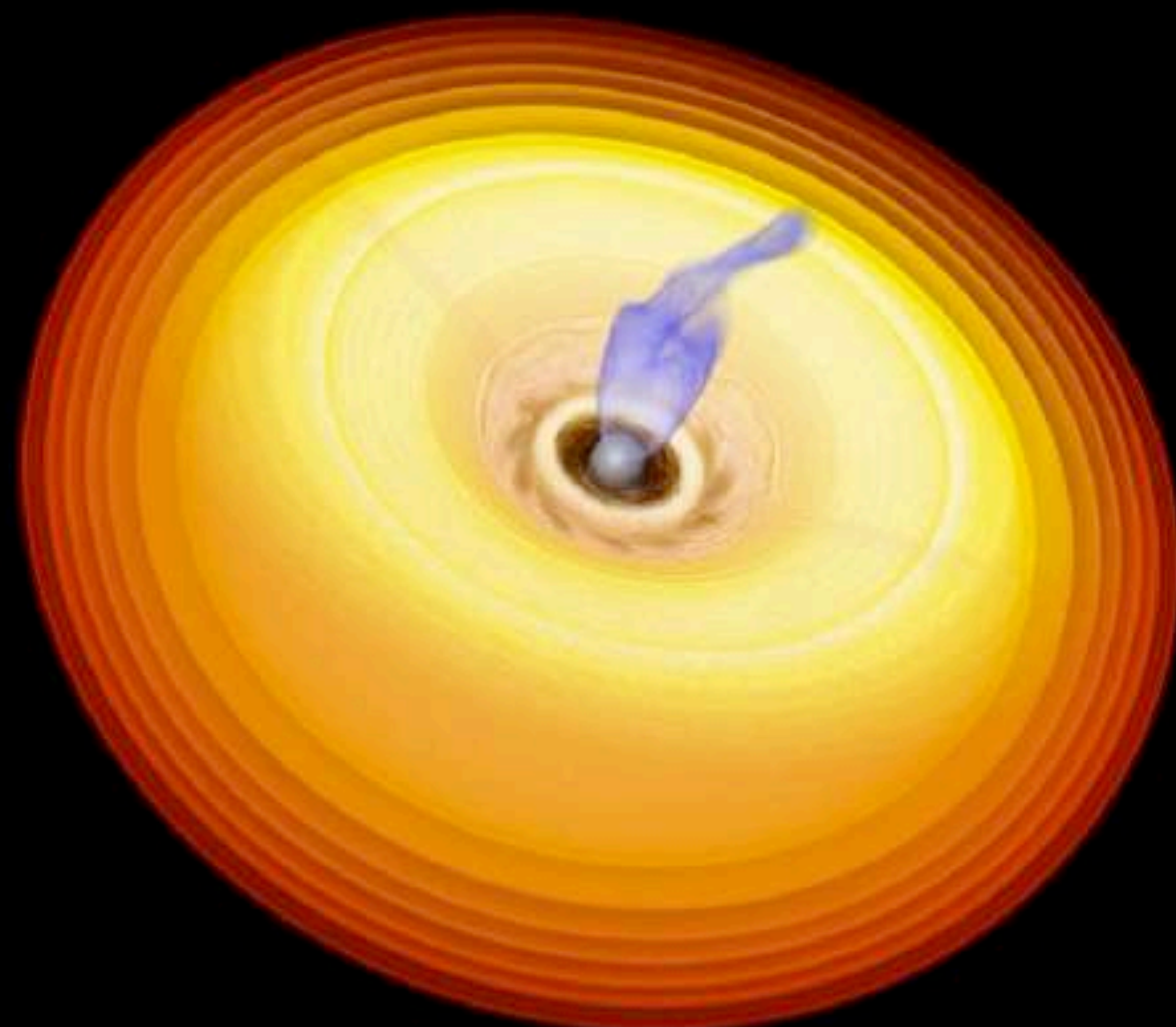

L. R. Weih & L. Rezzolla
(Goethe University Frankfurt)

L. Weih, LR

Space of parameters

✴Plasma dynamics and properties

- black-hole spin (plasma dynamics depends on it): $-1 < a < 1$
- accretion type as regulated by magnetic field (SANE o MAD)

✴Light dynamics and properties

- black-hole mass (sets size of the shadow)
- microphysics of emission (synchrotron emission, disk/jet component)
- orientation wrt to observer (two free angles)

✴Information from previous observations

- black-hole mass: $6.2 \times 10^9\, M_\odot$ (stars) or $3.5 \times 10^9\, M_\odot$ (gas)
- inclination: 17° or 163° , with "position angle" 288°
- X-ray luminosity: $4.4 \times 10^{40}\, \mathrm{erg/s}$
- jet power: $1.0 \times 10^{42}\, \mathrm{erg/s}$

Electron thermodynamics

- Emission of mm-long radiation is expected to be produced from synchrotron radiation processes.
- Simulations evolve temperature of bulk of fluid (ions); electron temperature undetermined.
- Thermal temperature distribution is reasonable approximation.
- T_e deduced from T_i via "plasma parameter": $\beta_p := p_{\mathrm{gas}}/p_{\mathrm{mag}}$

$$\frac{T_i}{T_e} = R_{\mathrm{high}} \frac{\beta_p^2}{1+\beta_p^2} + \frac{1}{1+\beta_p^2}$$

Mościbrodzka+ 2016

- Electrons colder at high plasma beta (i.e., disk), warmer at low plasma beta (i.e., jet).
- $R_{\mathrm{high}} = [1, 10, 20, 40, 80, 160]$: free parameter

- Given physical assumptions (spin, magnetisation), 3D GRMHD simulations were made: ~ *50 high-res simulations*.
- From each simulation several scenarios are constructed by changing the *thermodynamics of the electrons:* ~ *400 scenarios.*

Simulation library (an example…)

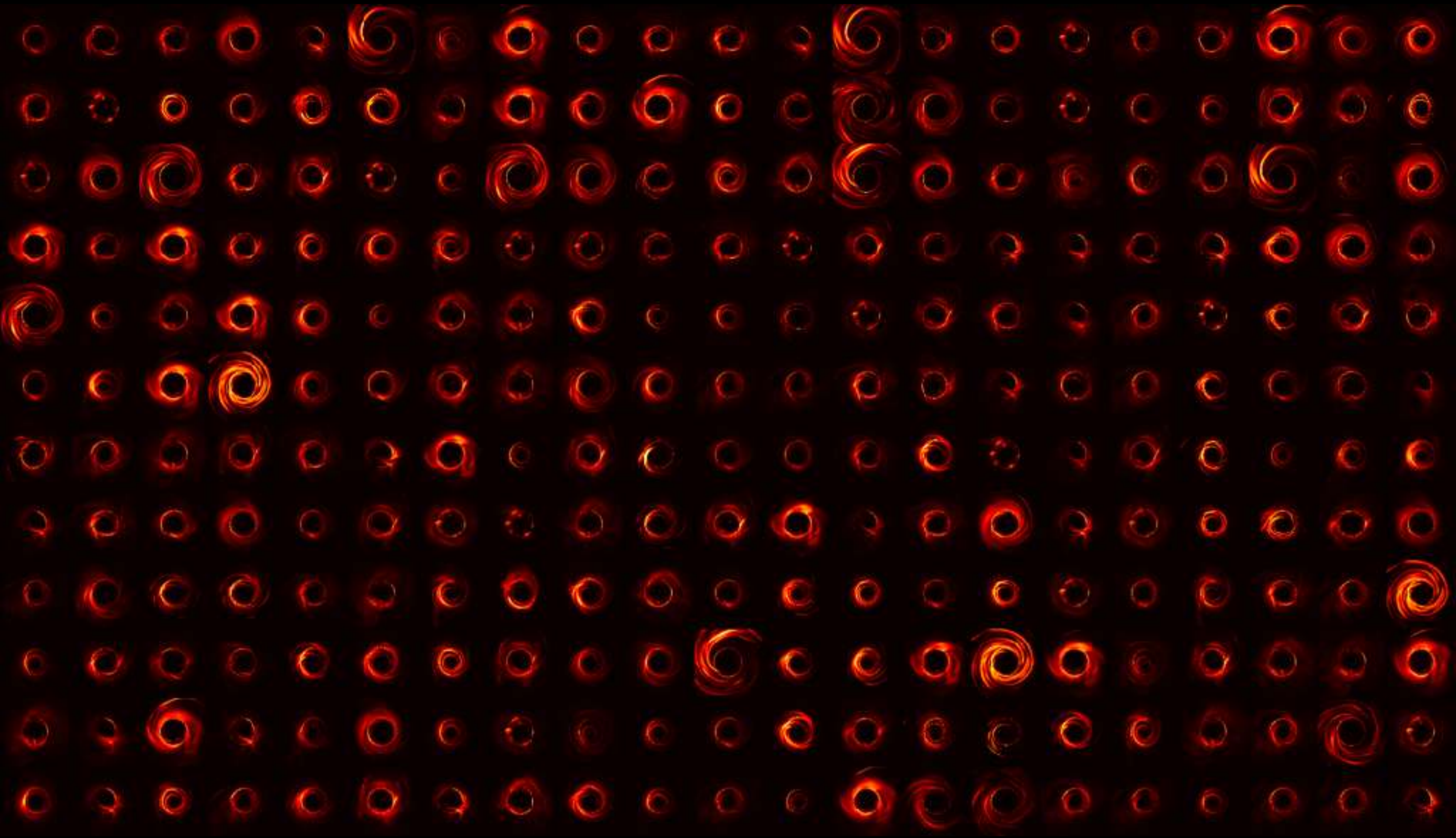

- Given physical assumptions (spin, magnetisation), 3D GRMHD simulations were made: ~ *50 high-res simulations*.
- From each simulation several scenarios are constructed by changing the *thermodynamics of the electrons:* ~ *400 scenarios.*

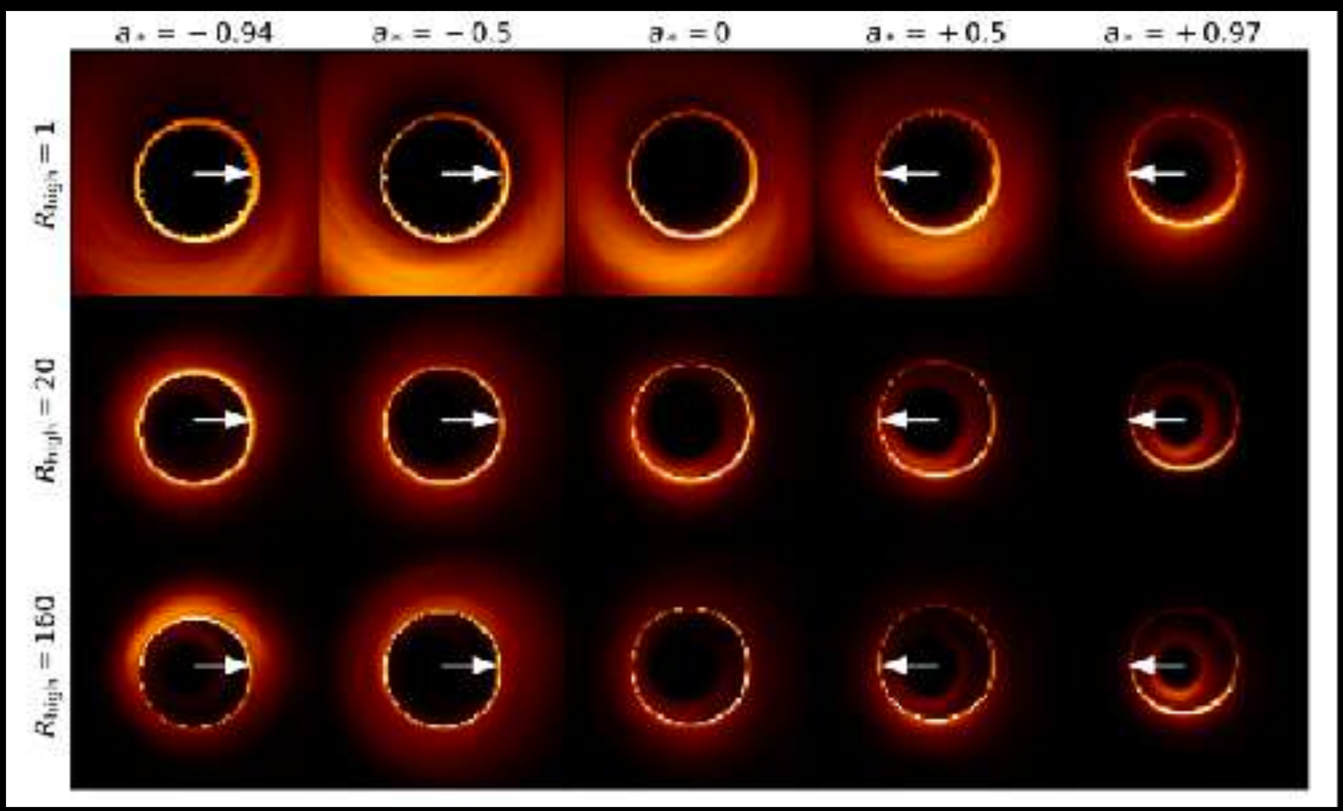

SANE models

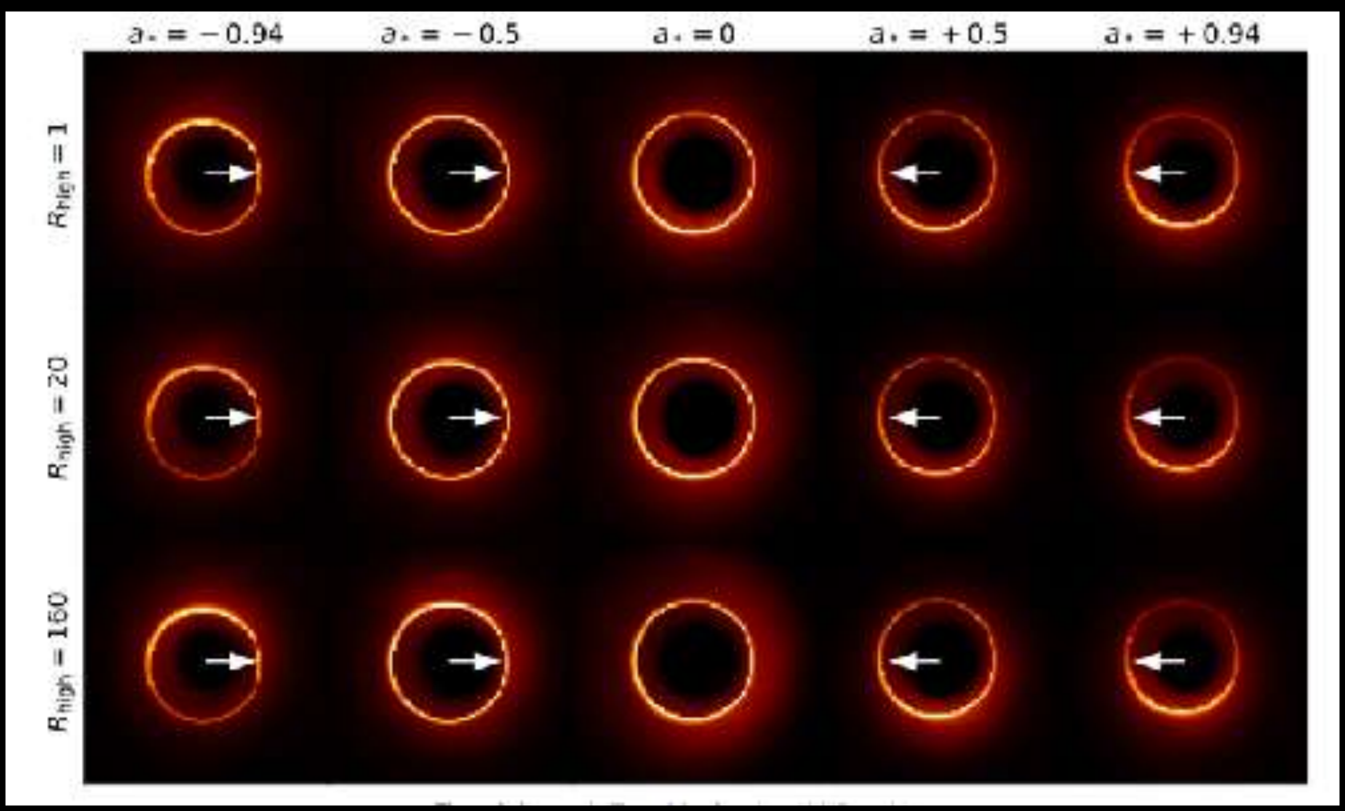

MAD models

black-hole rotation axis

Where do mm-long photons originate?

Kerr black hole, $a_* = 0.94$

MAD: mostly from the equatorial plane

SANE: can switch from equatorial plane to funnel wall

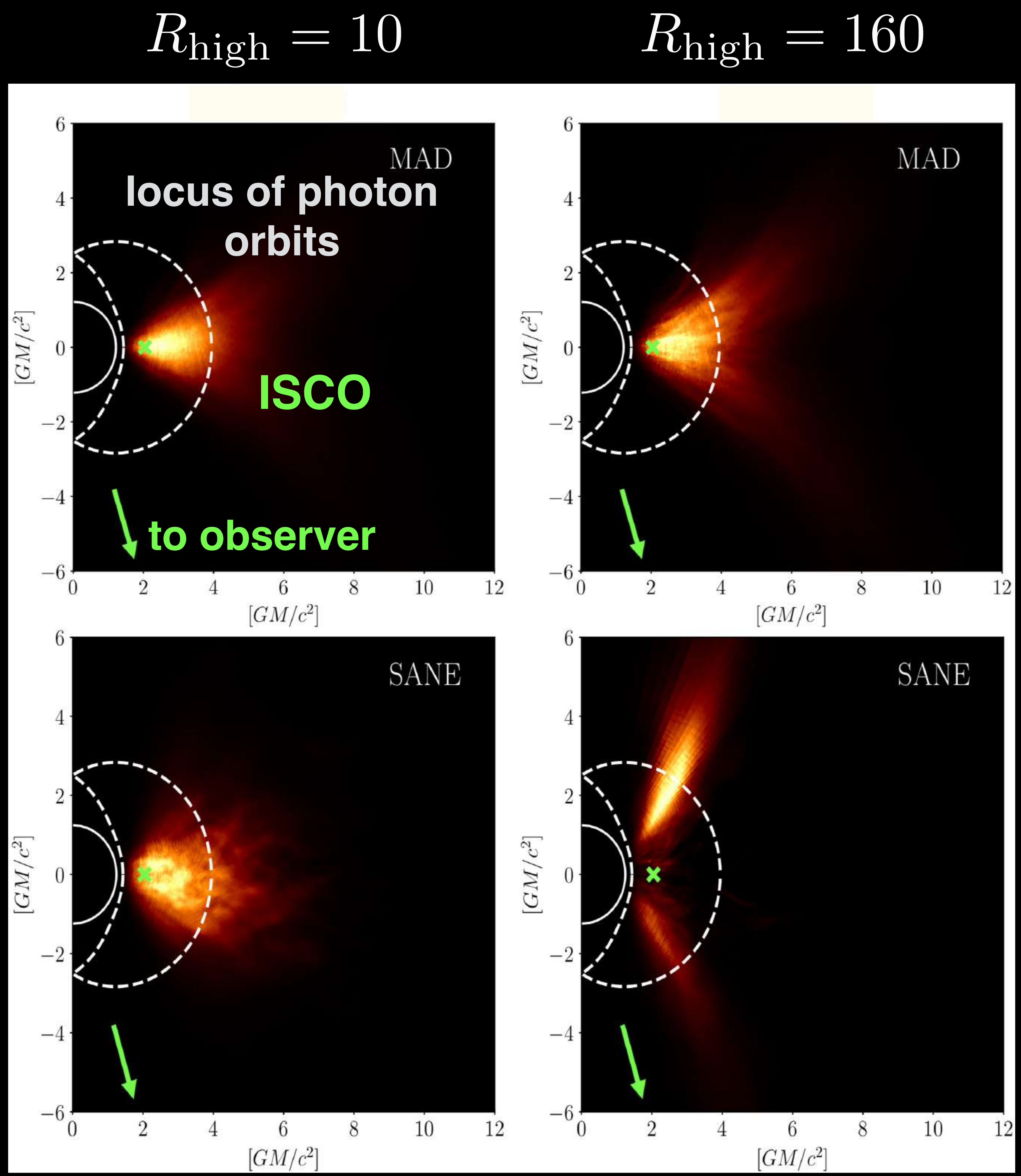

Where do mm-long photons originate?

Kerr black hole, $a_* = -0.94$

MAD: mostly but not only from the equatorial plane

SANE: equatorial plane is essentially depleted

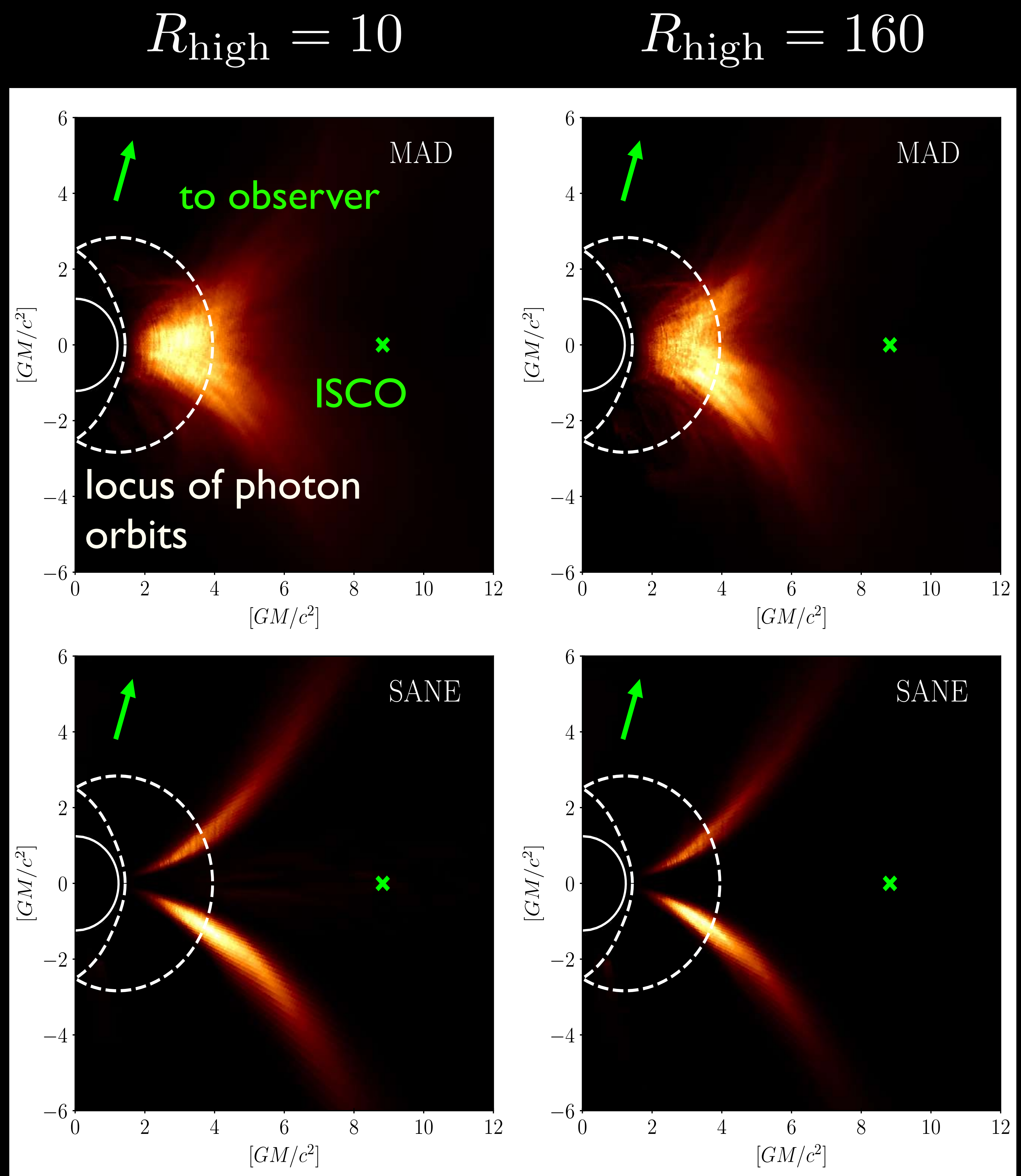

Image is combination of emissions…

- Image decomposed in: midplane, nearside, and farside
- MAD: midplane emission always dominates
- SANE with low R_{high}: midplane emission dominates
- SANE with high R_{high}: farside emission dominates

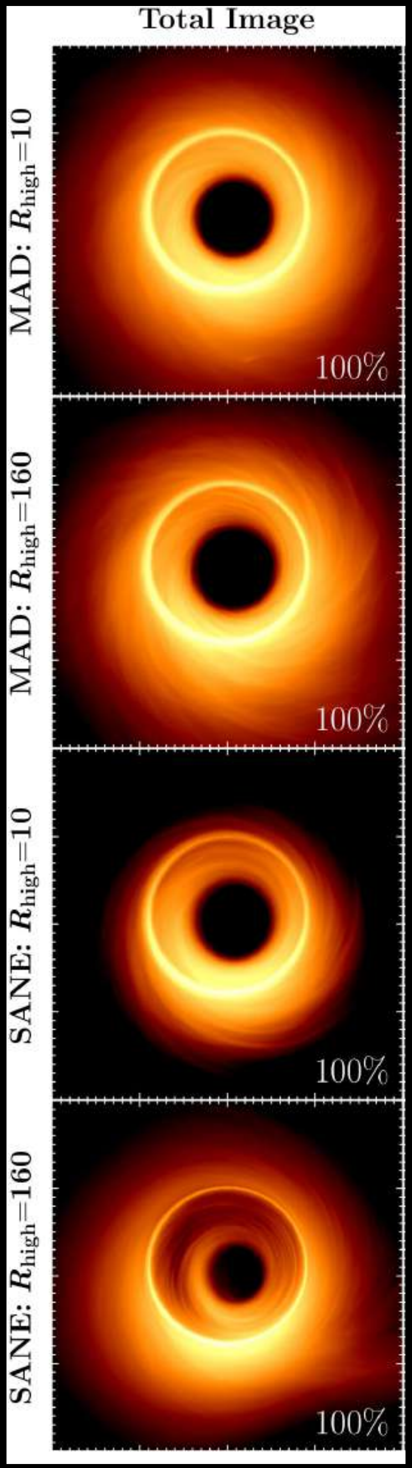

- Given physical assumptions (spin, magnetisation), 3D GRMHD simulations were made: ~ *50 high-res simulations*.
- From each simulation several scenarios are constructed by changing the *thermodynamics of the electrons:* ~ *400* scenarios.

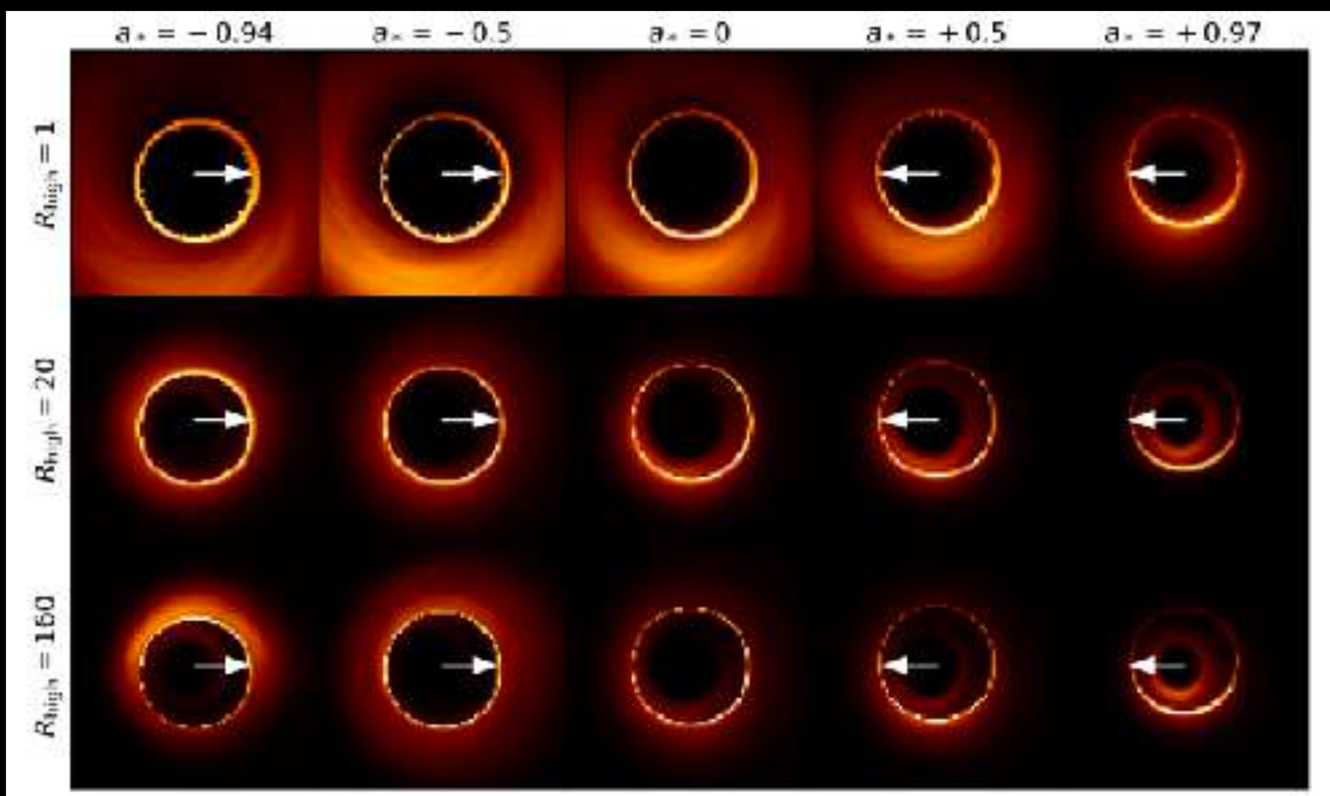

SANE models

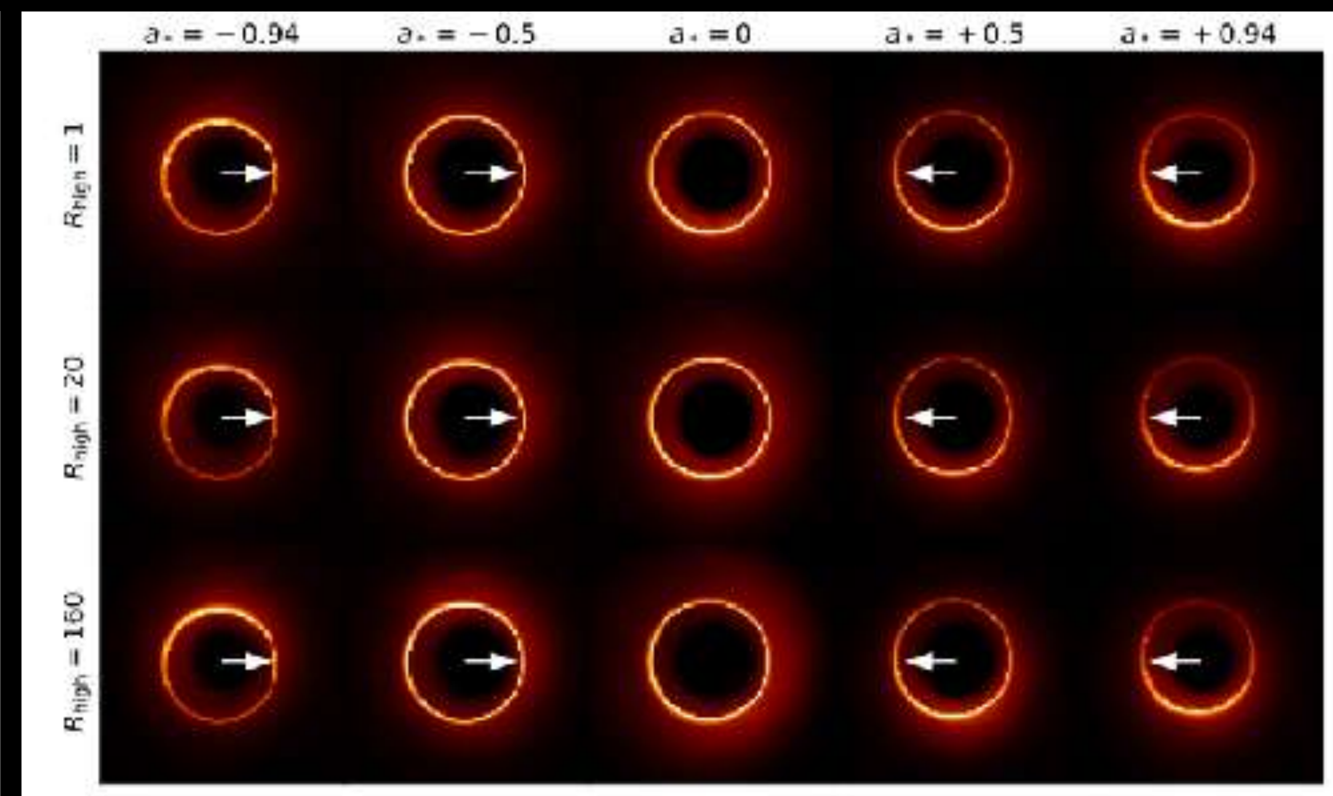

MAD models

- From each scenario synthetic images are constructed after radiative transfer and light bending: ~ *60,000 images*.
- Genetic algorithms and MCMC pipelines find best match.

Fitting the images to the data

visibility amplitude (VA)

Closure phase (CP)

GRMHD image (left) and convolved image (right)

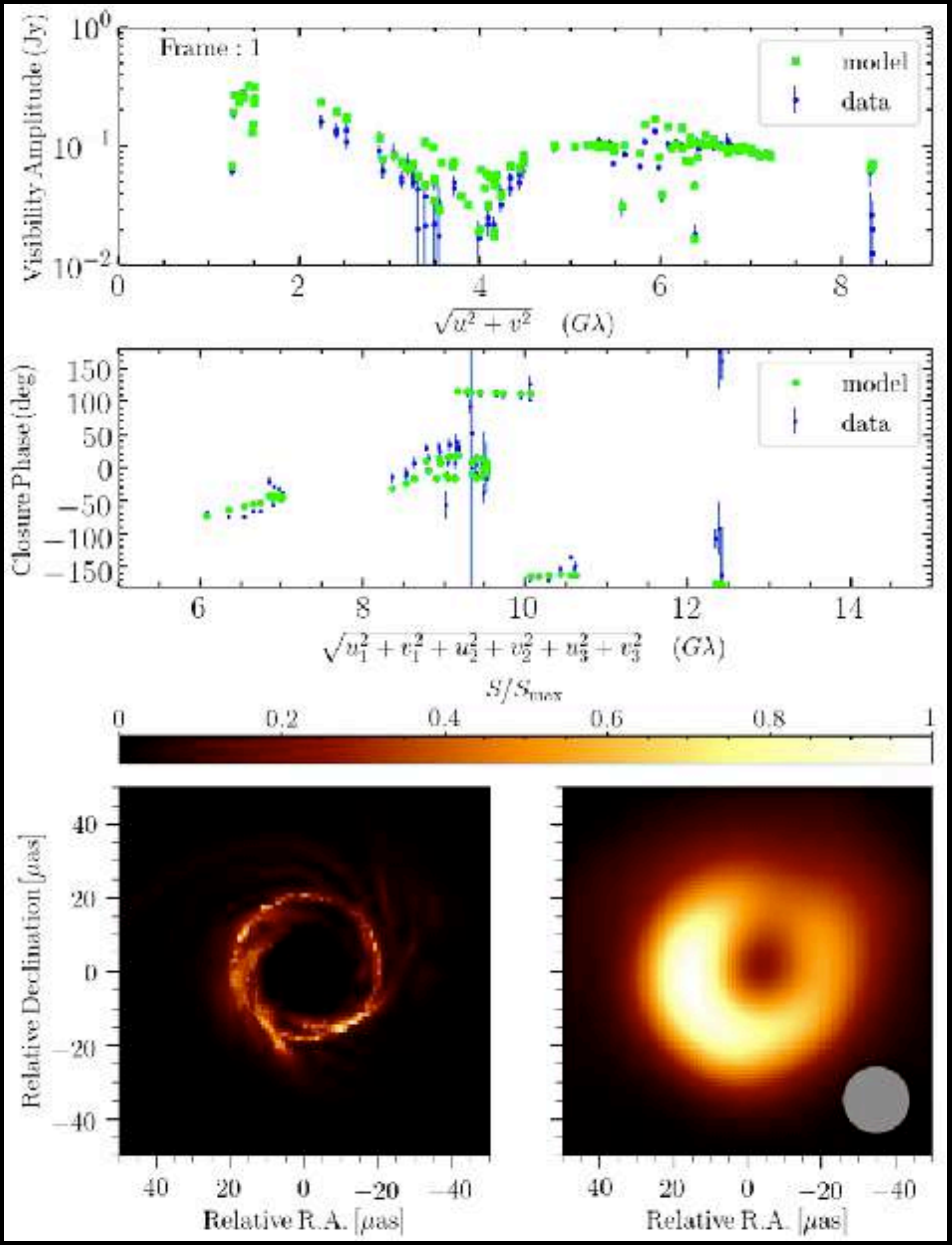

Fromm, Younsi, LR

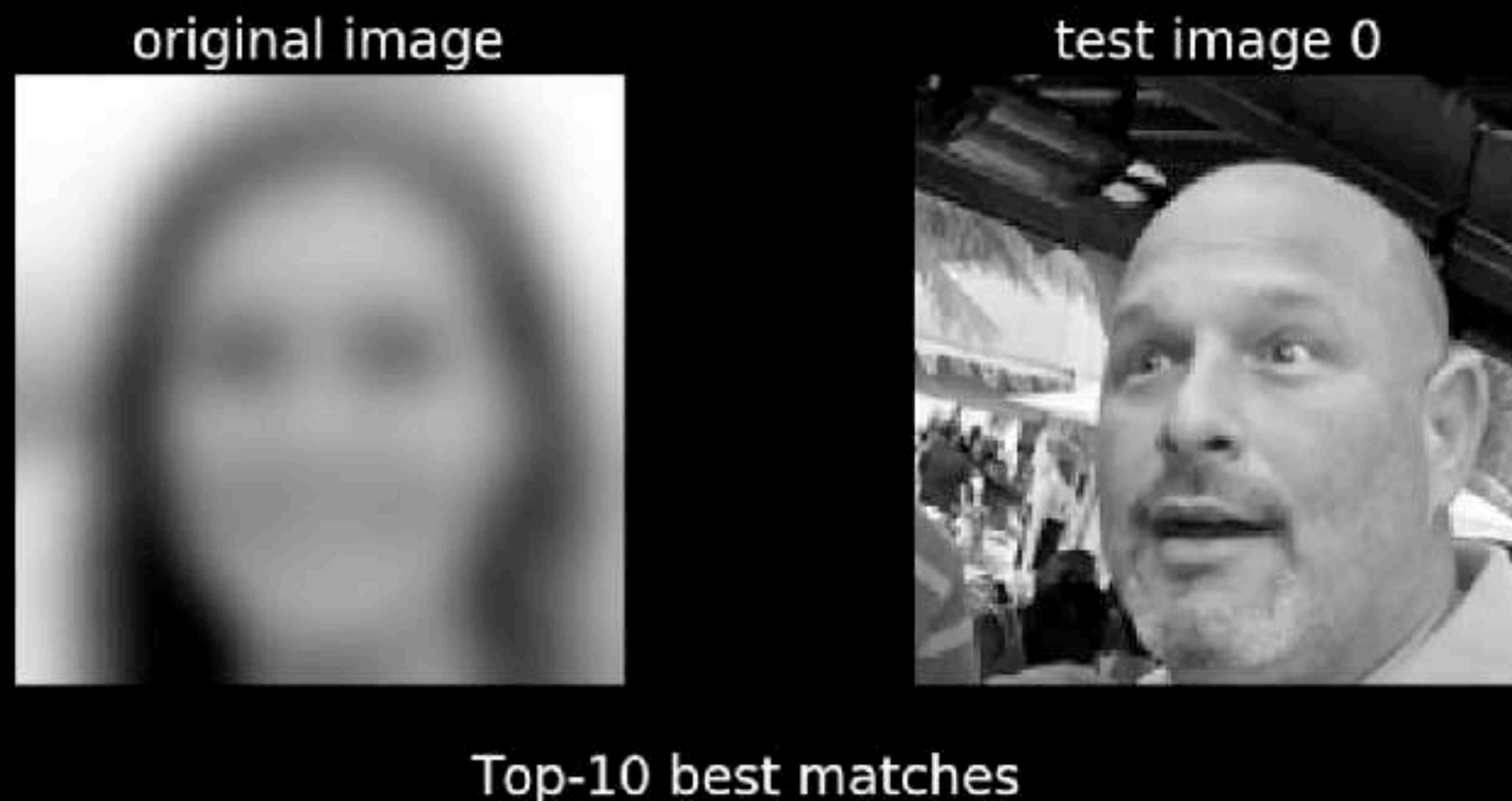

The match is found in the visibility space, but can also be found in image space.

In the image space this would correspond to searching a face in a stadium full of people…

Images:
A Style-Based Generator Architecture for Generative Adversarial Networks
Karras T., Laine S. and Aila T., 2018

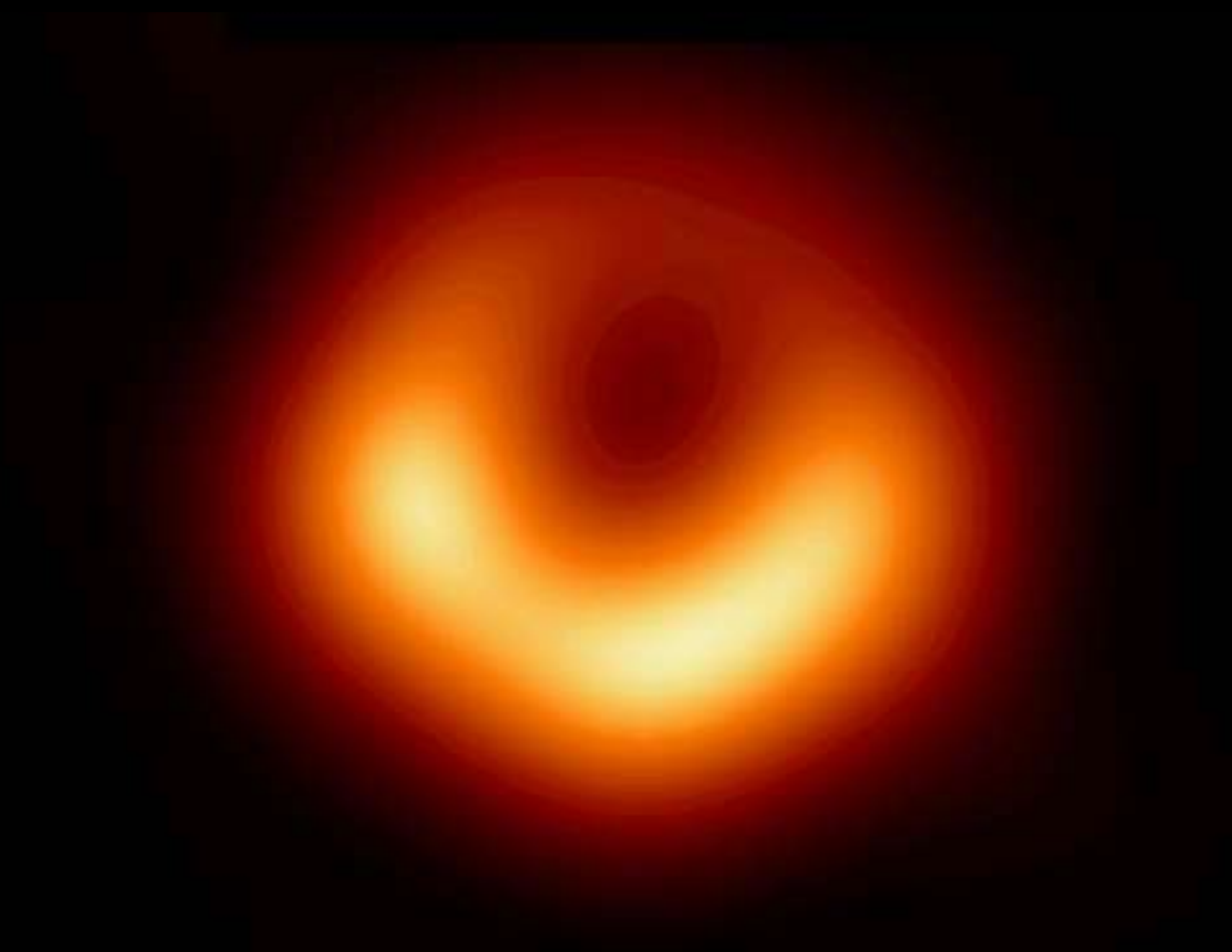

OBSERVATIONS

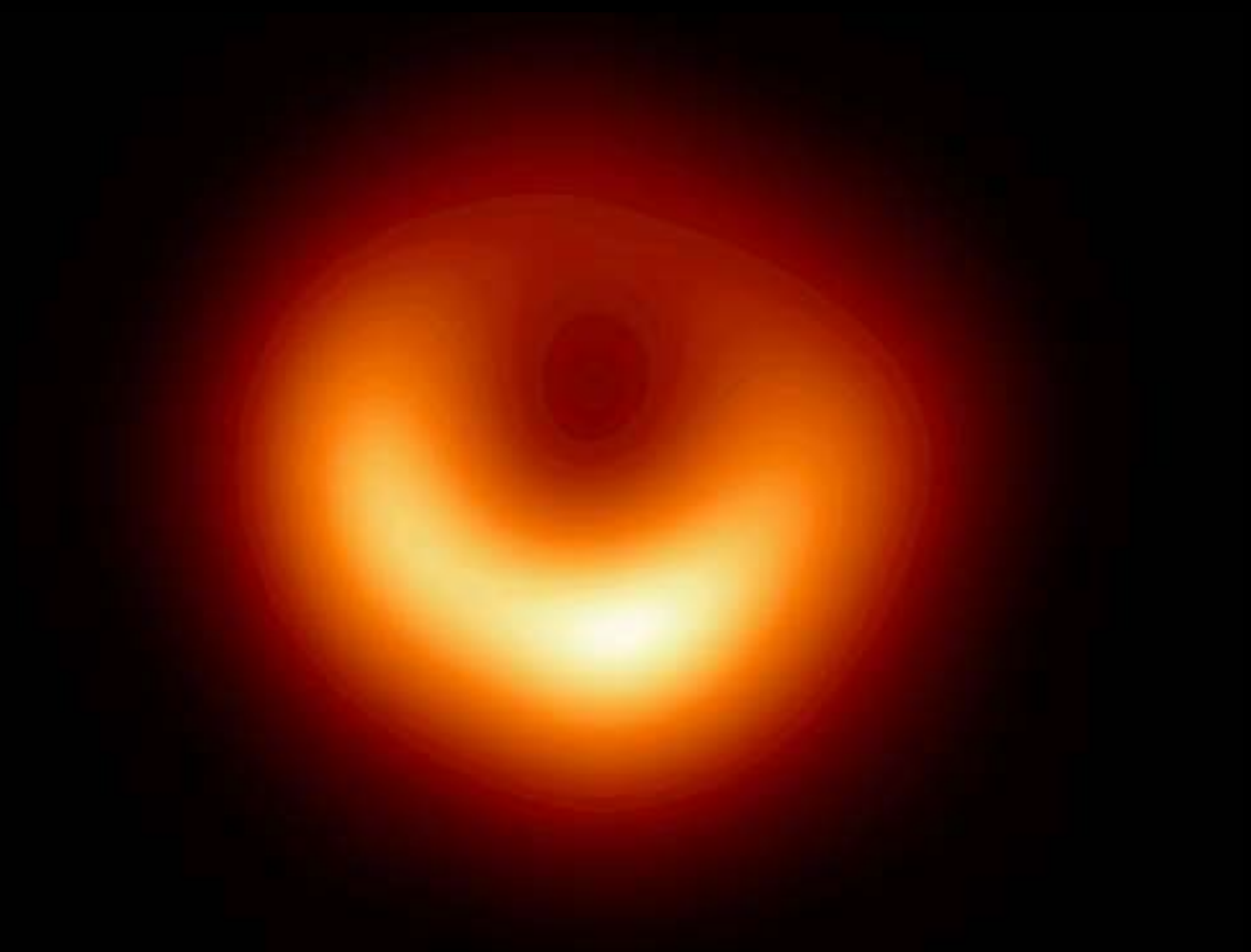

THEORETICAL MODEL

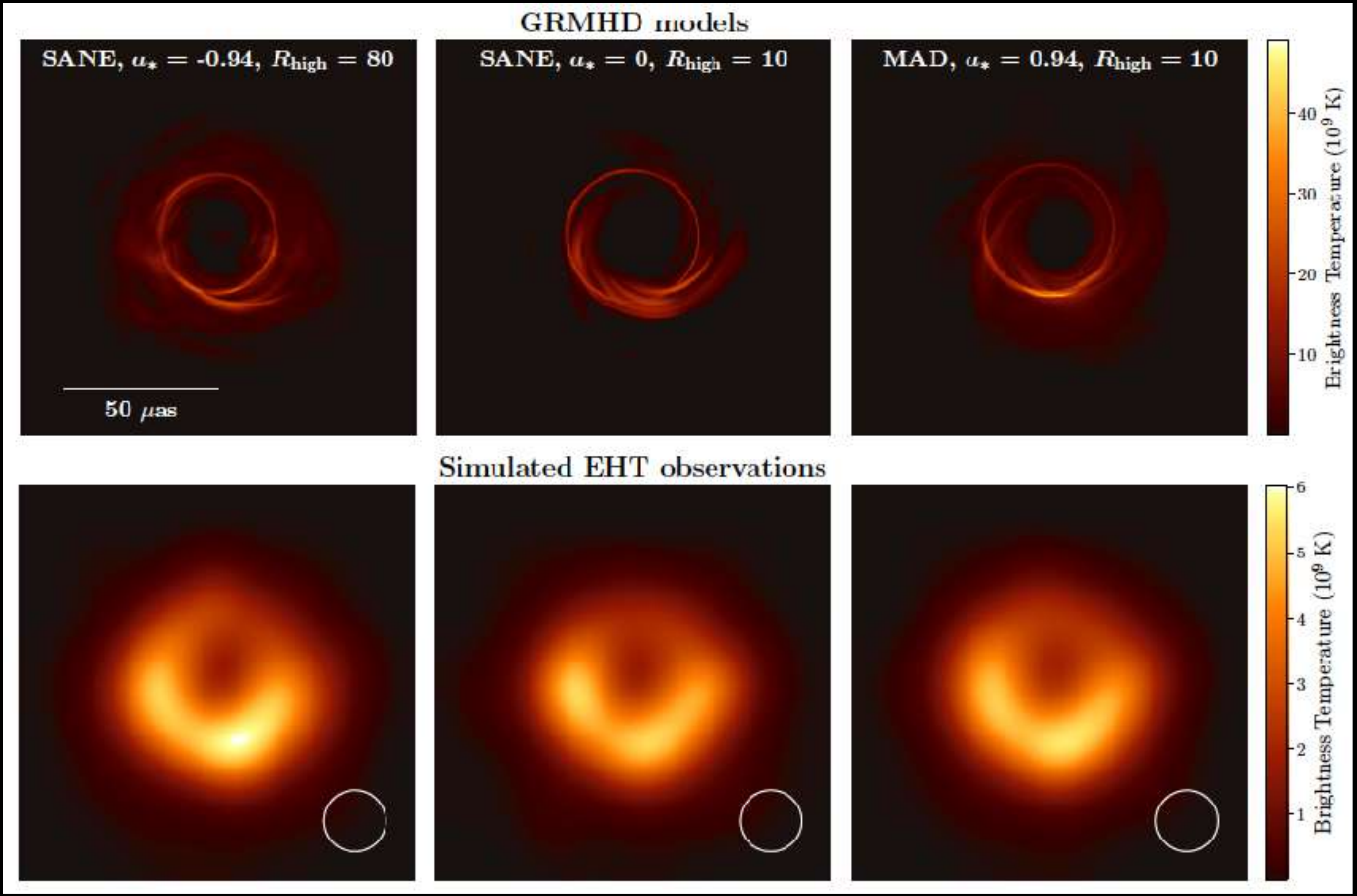

- Degeneracies present in physical conditions and scenarios.

  Good: robustness of conclusions (BHs produce ring)

  Bad: more accurate observations to determine BH spin

What we measured...

Parameter	Estimate
Ring diameter [a] d	$42 \pm 3\ \mu$as
Ring width [a]	$<20\ \mu$as
Crescent contrast [b]	$>10{:}1$
Axial ratio [a]	$<4{:}3$
Orientation PA	150°–200° east of north
$\theta_g = GM/Dc^2$ [c]	$3.8 \pm 0.4\ \mu$as
$\alpha = d/\theta_g$ [d]	$11^{+0.5}_{-0.3}$
M[c]	$(6.5 \pm 0.7) \times 10^9\ M_\odot$
Parameter	**Prior Estimate**
D [e]	(16.8 ± 0.8) Mpc
M(stars) [e]	$6.2^{+1.1}_{-0.6} \times 10^9\ M_\odot$
M(gas) [e]	$3.5^{+0.9}_{-0.3} \times 10^9\ M_\odot$

Ring Asymmetry and Black Hole Spin

Conclusions on the spin can still be drawn if one combines "other" information on jet power and orientation

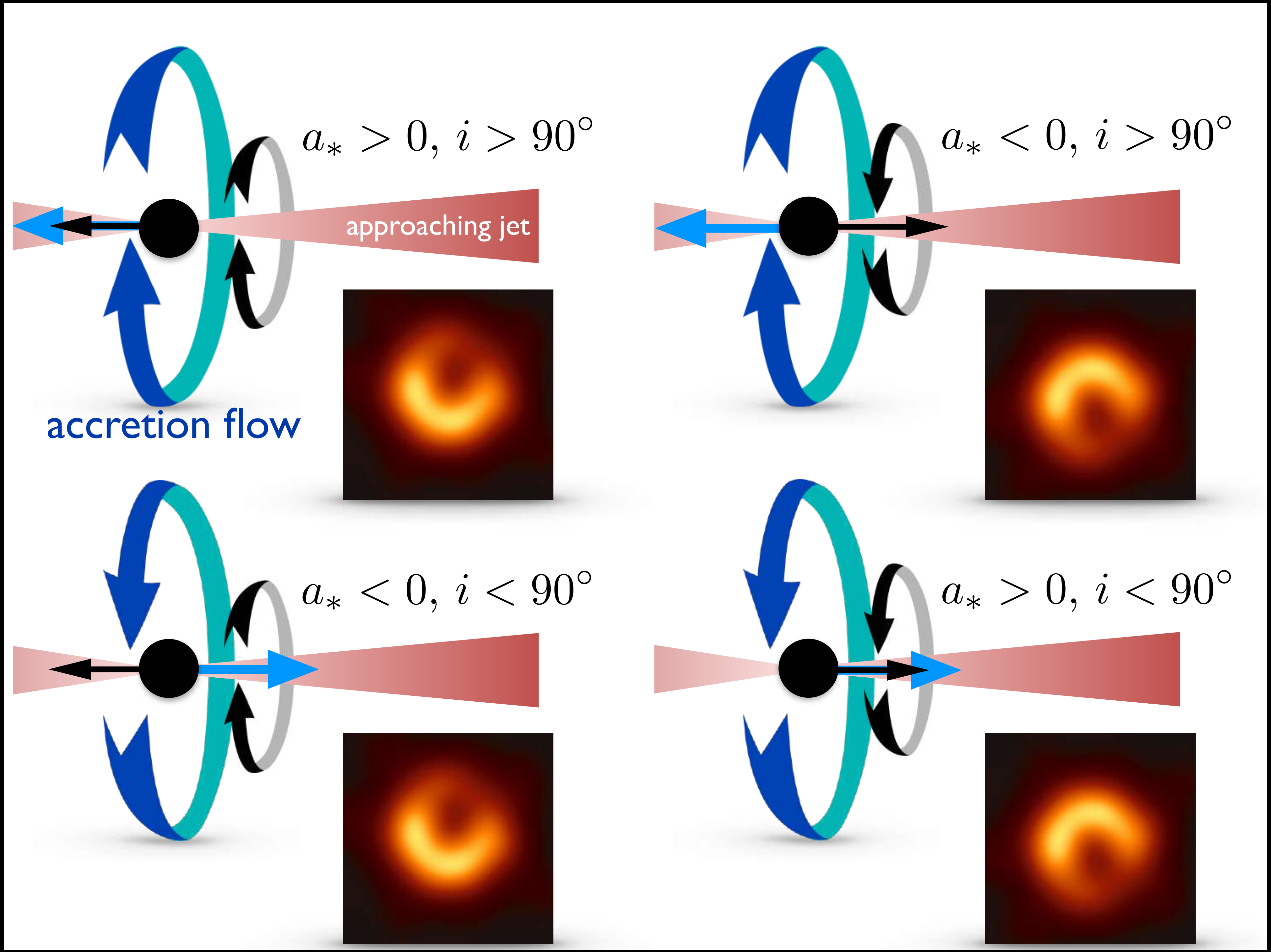

Ring Asymmetry and Black Hole Spin

Conclusions on the spin can still be drawn if one combines "other" information on jet power and orientation

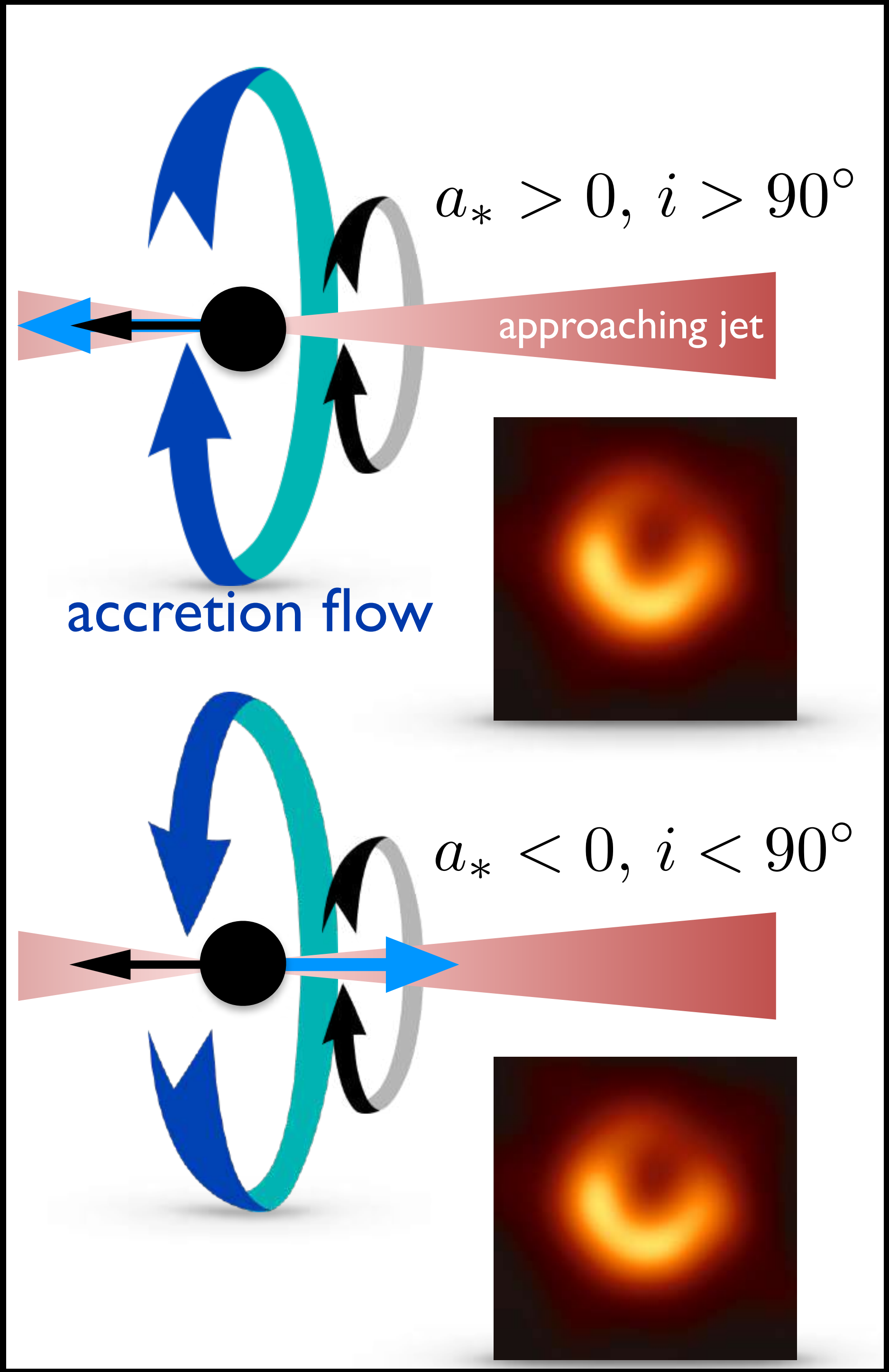

observer

These two degenerate options remain possible

observer

Ring Asymmetry and Black Hole Spin

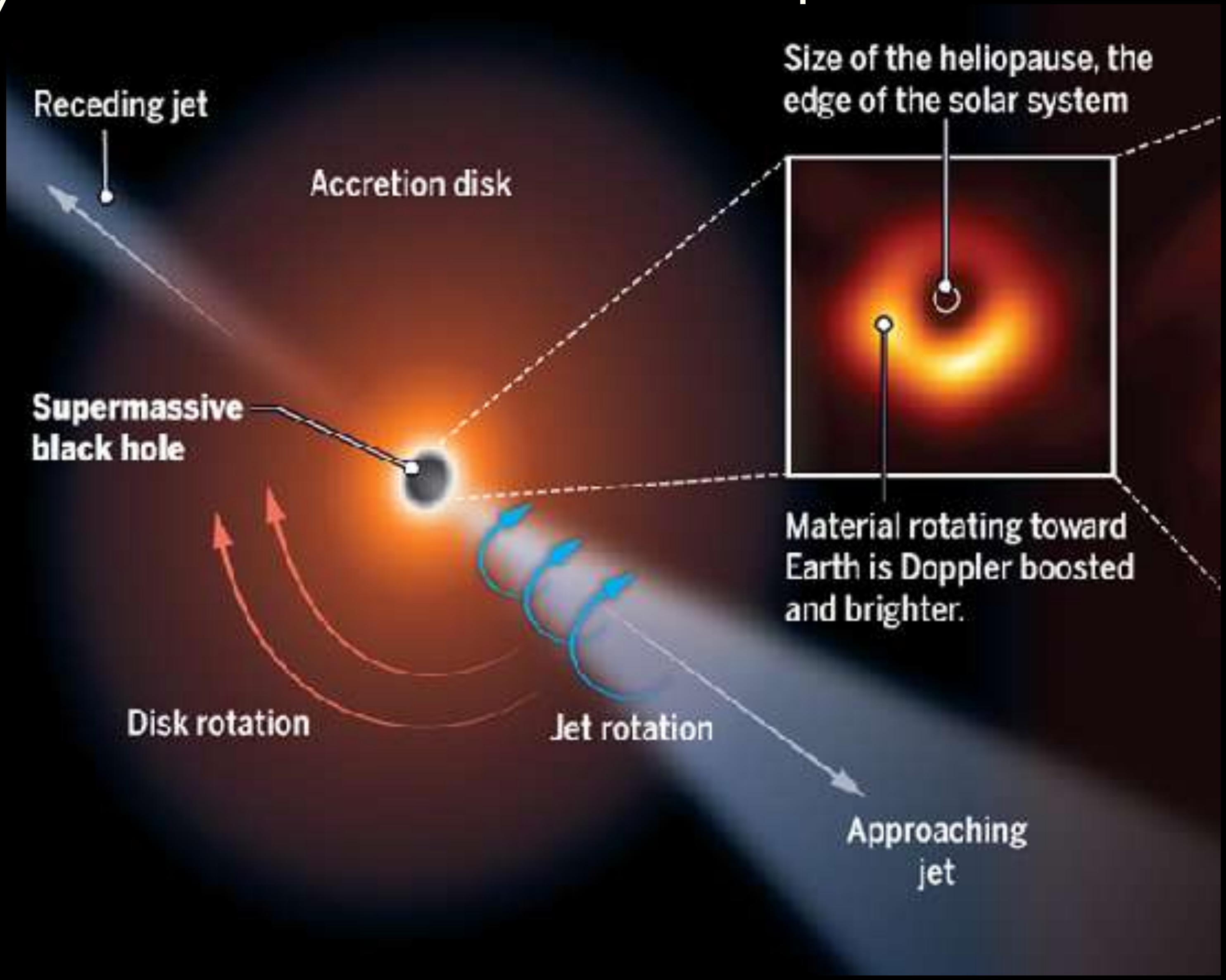

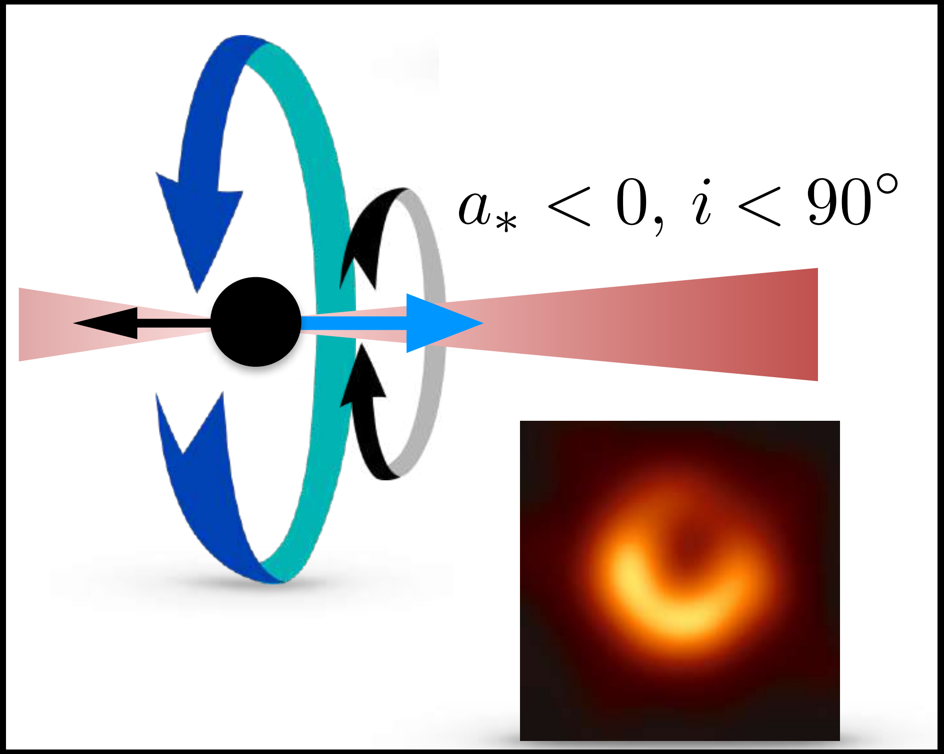

Note that the in the images providing the best match, the emitting material is close to the jet funnel and coronating with the black hole

Moving away from Kerr black holes: accretion onto a **dilaton black hole**

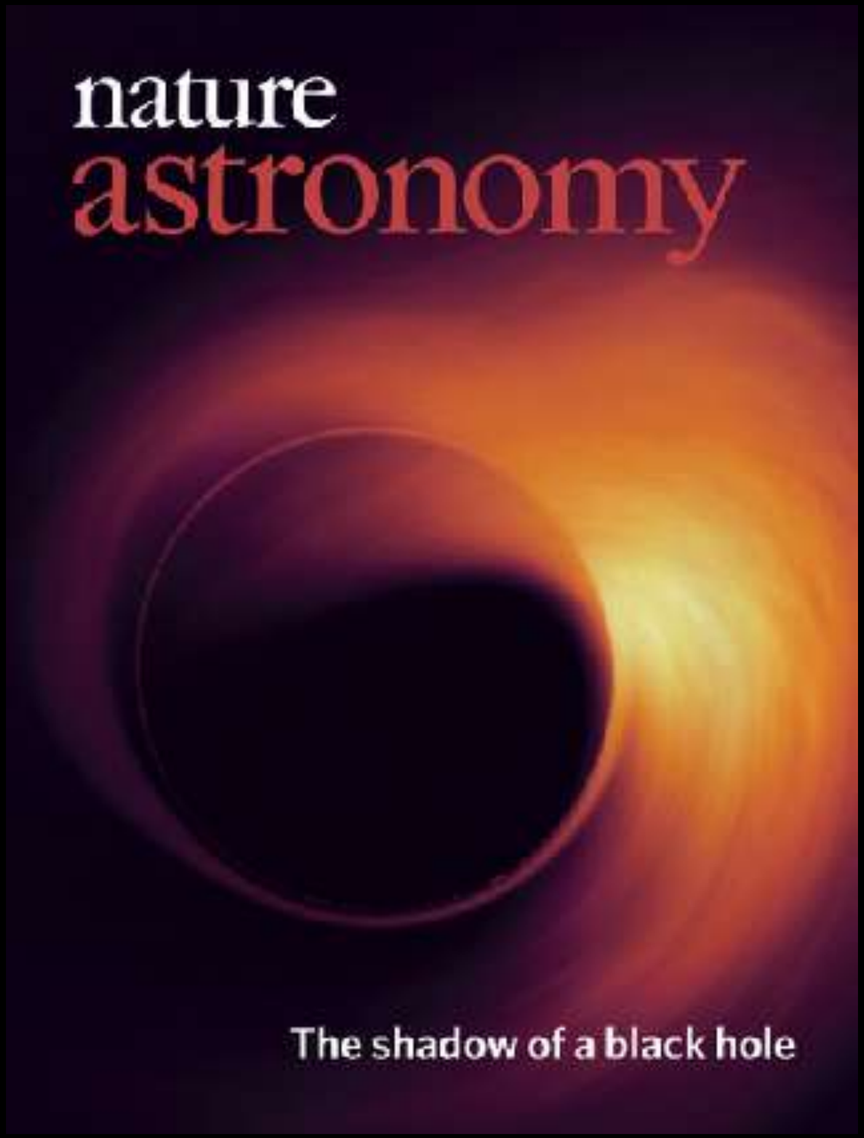

Mizuno+ 2018

Dilaton vs Kerr black hole

- Fair comparison requires that basic features of the flow are matched.
- Three most important are: **horizon radius, photon orbit, ISCO**
- In general, larger dilaton parameter reduces horizon radius, photon orbit, and ISCO (cf. spin in Kerr).

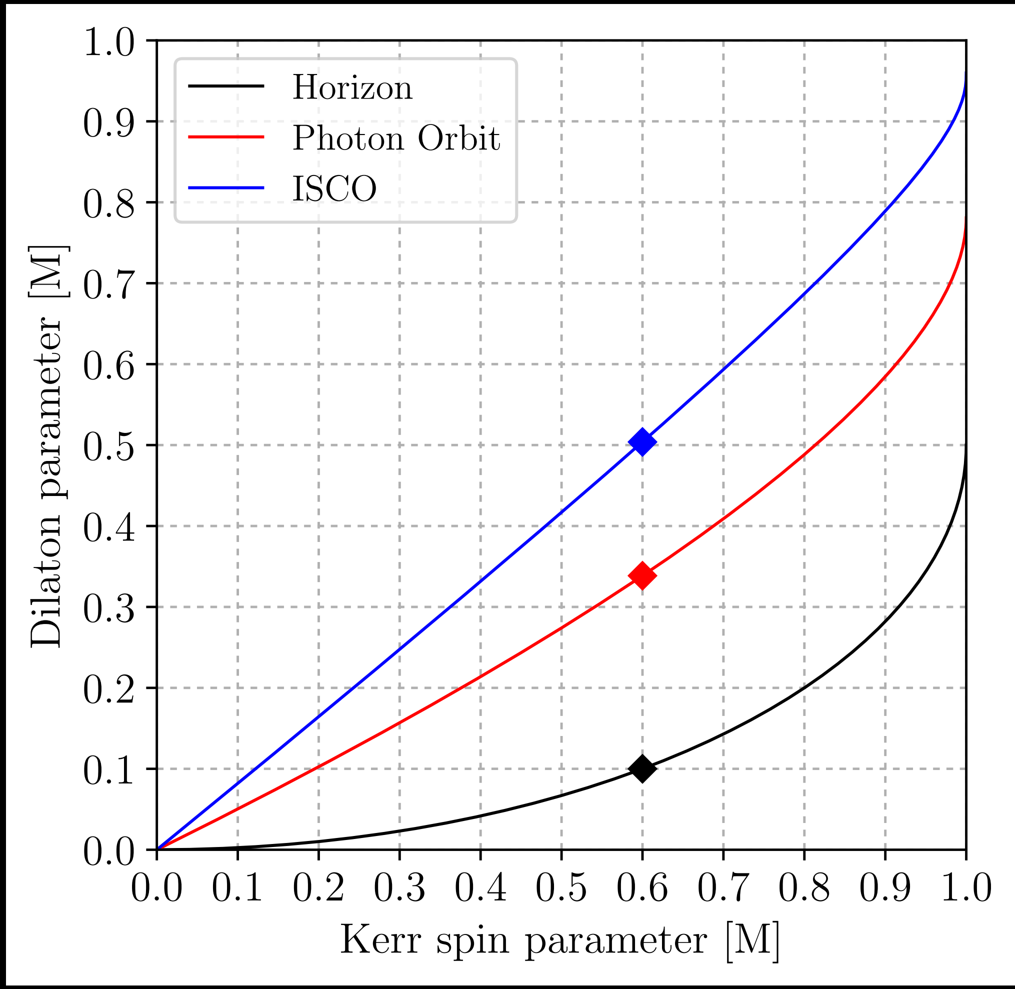

- Different matches possible but ISCO is most critical since most of the emission comes from around ISCO.

GRMHD simulations

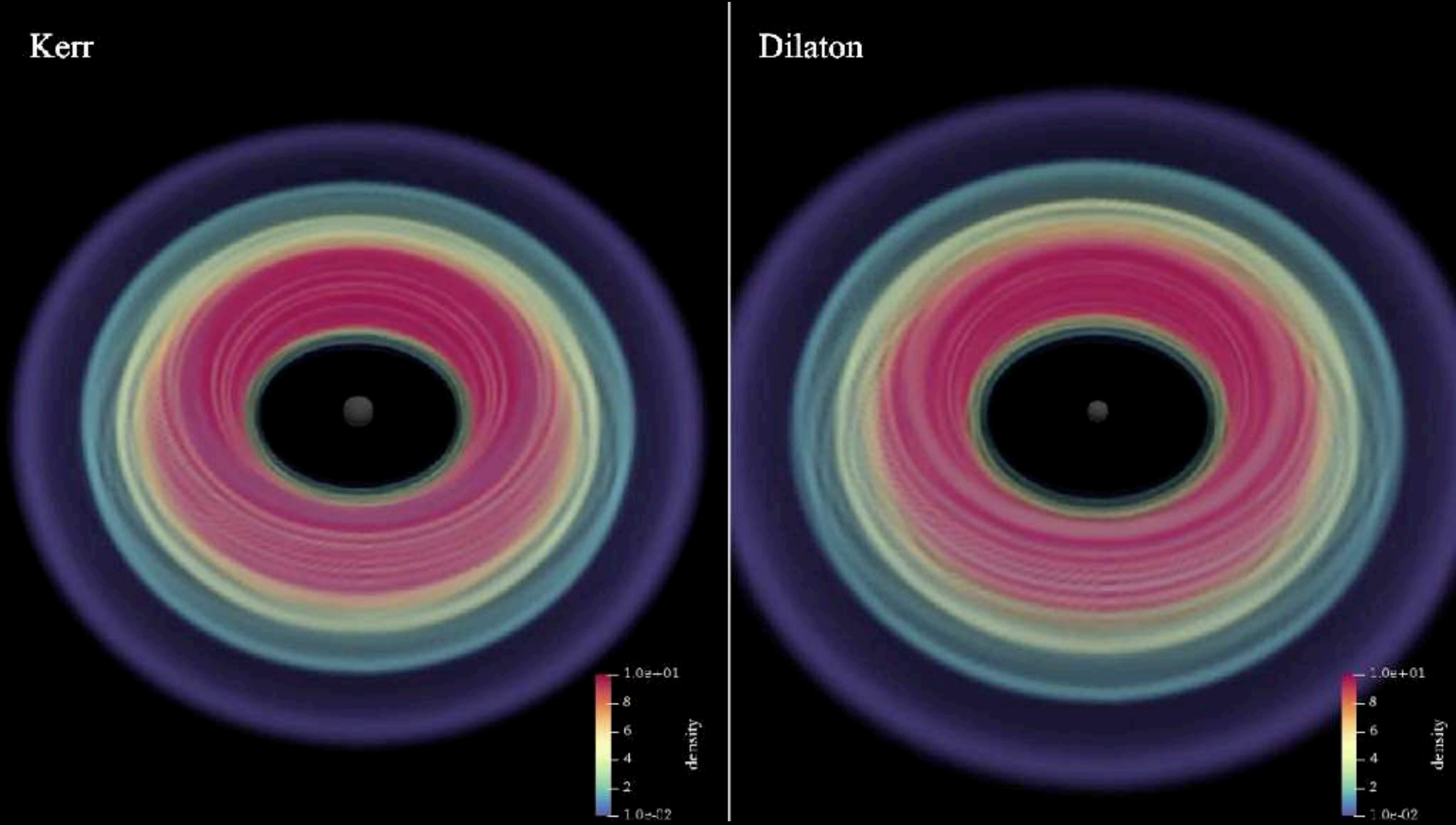

3D GRMHD simulations of magnetized torus with a weak poloidal magnetic field loop accreting onto Kerr BH (*a=0.6*) and ISCO-matched dilaton BH (*b=0.5*) cf. Sgr A*

convolved GRRT images; emission features smeared by beam; crescent reveals presence of BH.

BSMEM reconstructed image with scattering; again, presence of a crescent reveals BH.

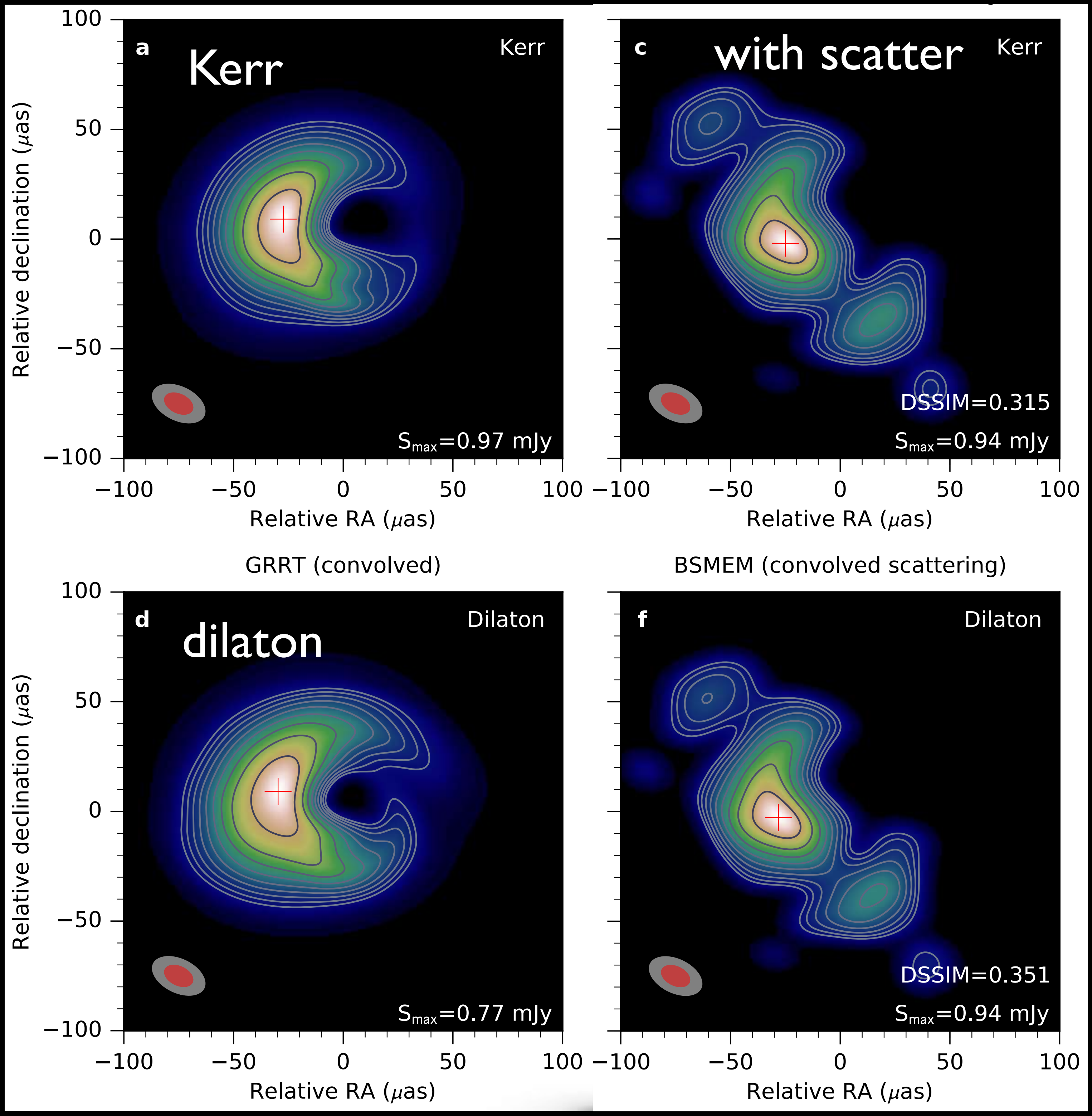

Overall, at present not possible to distinguish the two BHs

Moving away from Kerr black holes: accretion onto a boson star

Olivares+ 2019

Accretion onto a boson star

- Self-gravitating **horizonless** compact objects composed of scalar field (boson stars) have long since been considered potential candidates for Sgr A* (dark-matter cusp).

- Previous work has considered whether emission from boson stars can be distinguished from that of a black hole.
  - Using spectral features: **not possible to distinguish** (Guzman+ 2010)
  - Using shadow image of a boson star surrounded by torus: **not possible to distinguish** (Vincent+ 2016).

- These works did not consider effects of accretion.

- We performed **first GRMHD** simulations of accreting nonrotating boson stars.

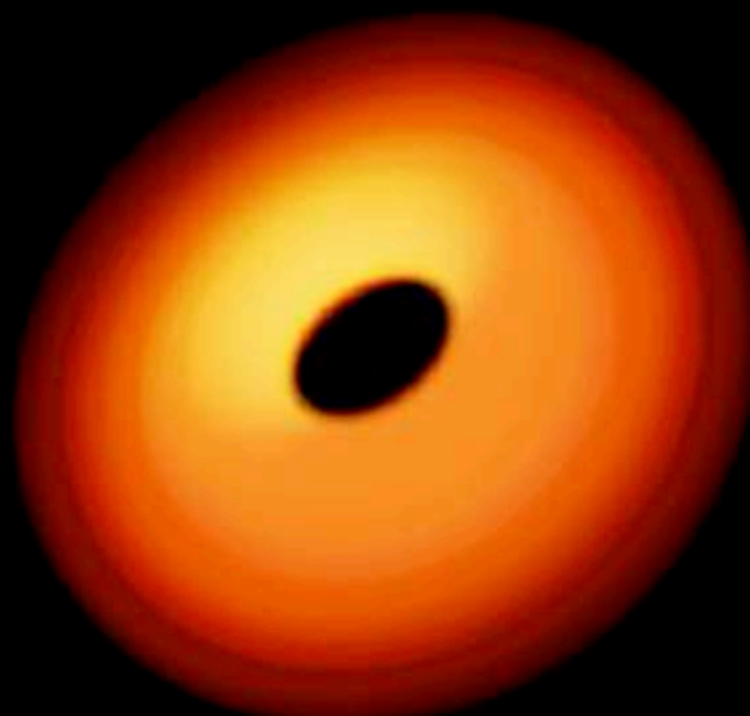

L. Weih, H. Olivares, LR

- Simulations show considerable differences in the dynamics of the accretion flow.
- In the case of the boson star, matter reaches very close to the origin, forming a stalled accretion torus (MRI is quenched).

density *(x,z)* density *(x,y)*

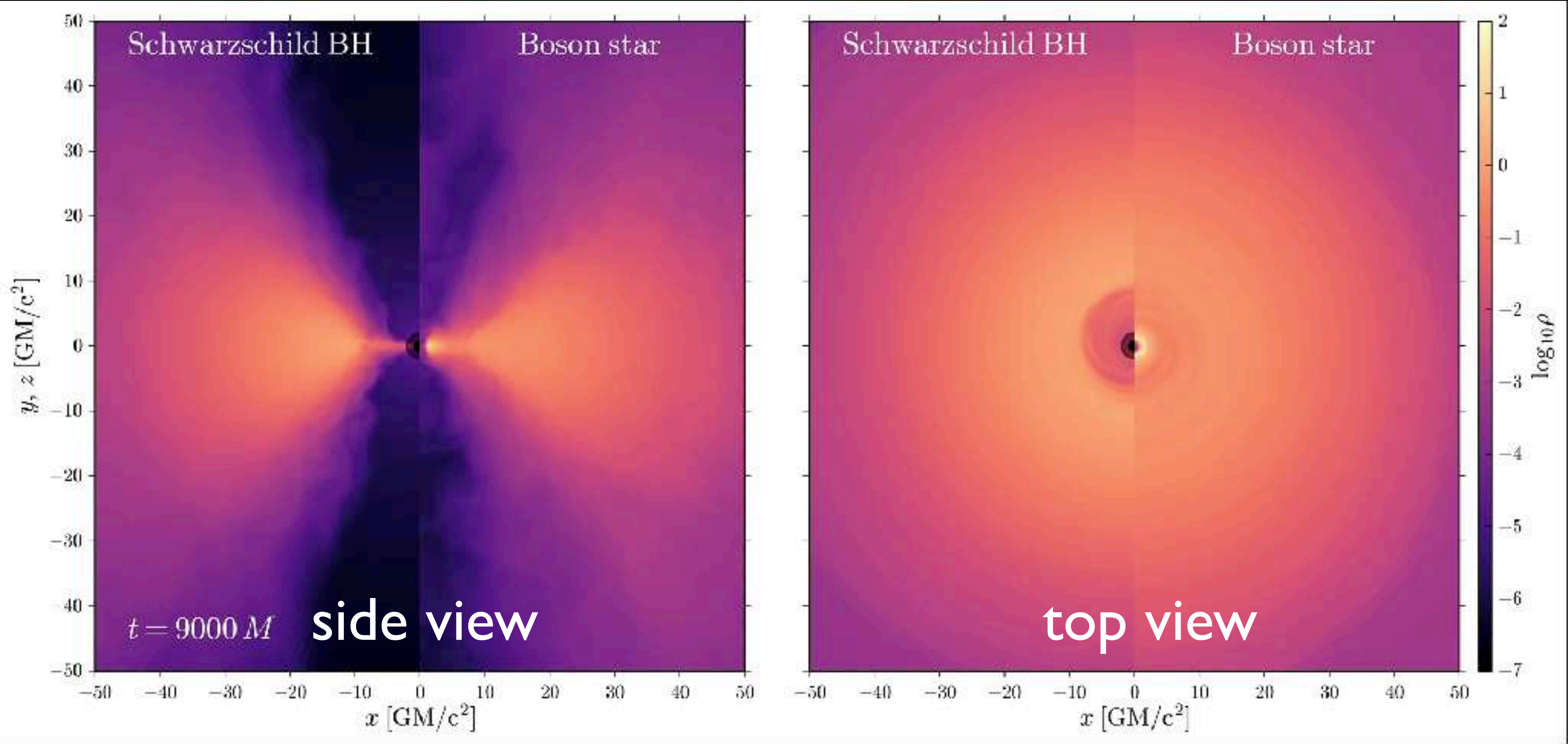

✴compactness is quite high: $\mathcal{C}_{95} := M_{95}/R_{95} = 0.11$

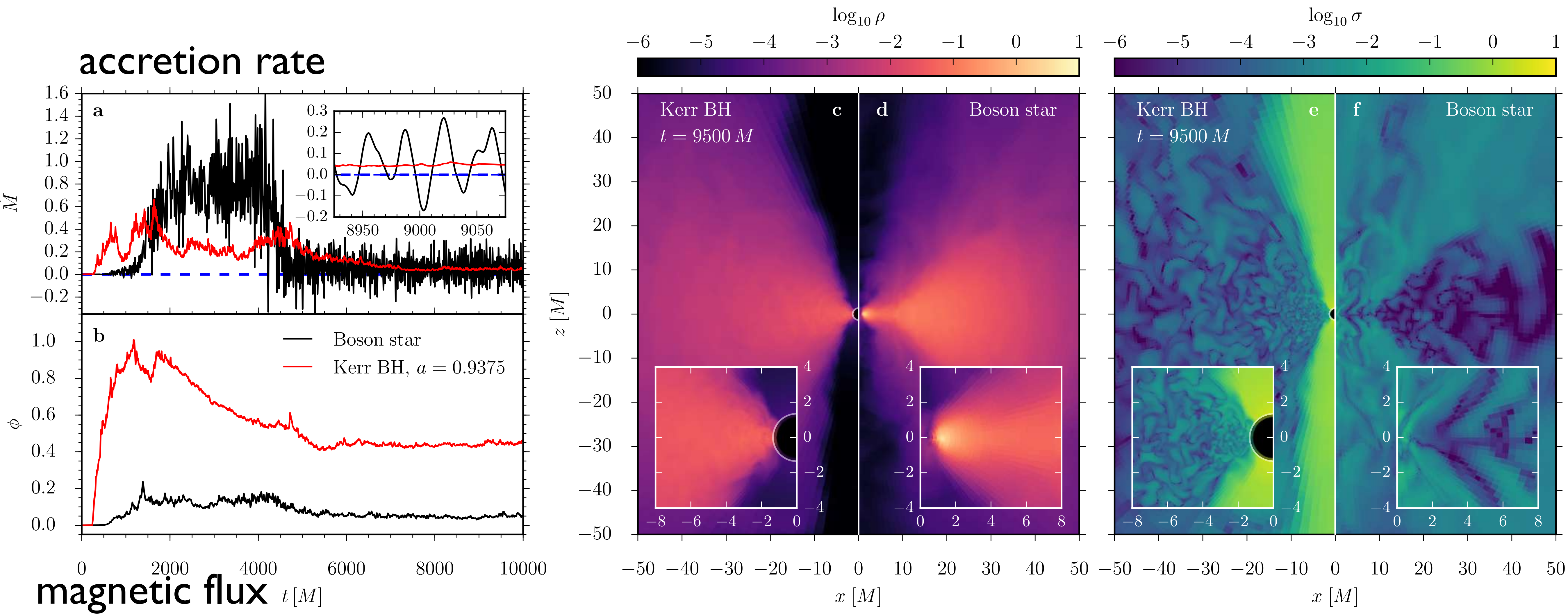

✴Mass-accretion rate: **positive** for black hole but **oscillating** for boson star.

✴Oscillations produced by stalled torus; correspond to epicyclic frequency.

✴No evacuated funnel in polar region in the case of boson star.

✴Slow wind flowing from hot and dense interior: **no jet** from boson star.

- Left: GRRT images; sharp emission from photon ring visible for BH.

- Right: reconstructed image with scattering and conditions of EHT 2017 campaign.

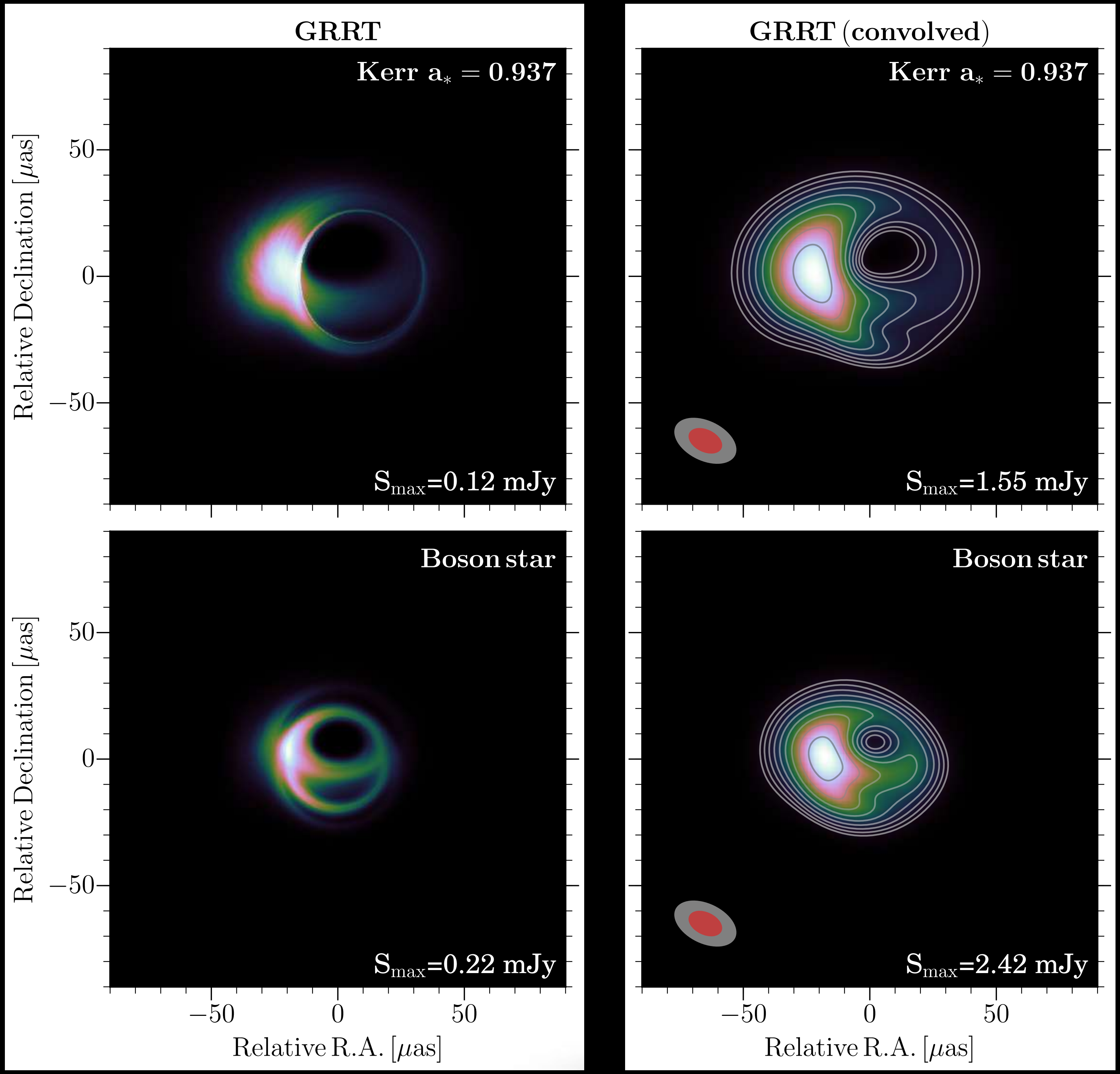

Reconstructed images shows differences, both in size and structure

BH image exhibits crescent; boson star emission from inner regions.

Overall, from images alone it is possible to distinguish them

Conclusions

- ✴ **BlackHoleCam** covered all aspects of these observations, has played a major role in the EHT campaign and analysis.
- ✴ Accretion onto **Kerr black holes** has been explored extensively in various physical and thermodynamical regimes.
- ✴ Exploration of accretion onto **alternatives** to Kerr BHs has started: boson stars can be distinguished, other BHs cannot.
- ✴ EHT has provided first evidence existence of SMBHs and boosted our understanding of accretion in **strong gravity**.

EHT observations of SMBHs is now possible! A new era of astrophysics has started. Much more to come!

EXTRAS

Looking into the future: going into space

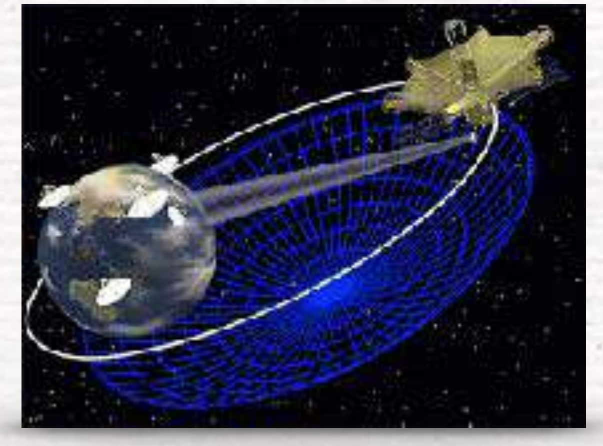

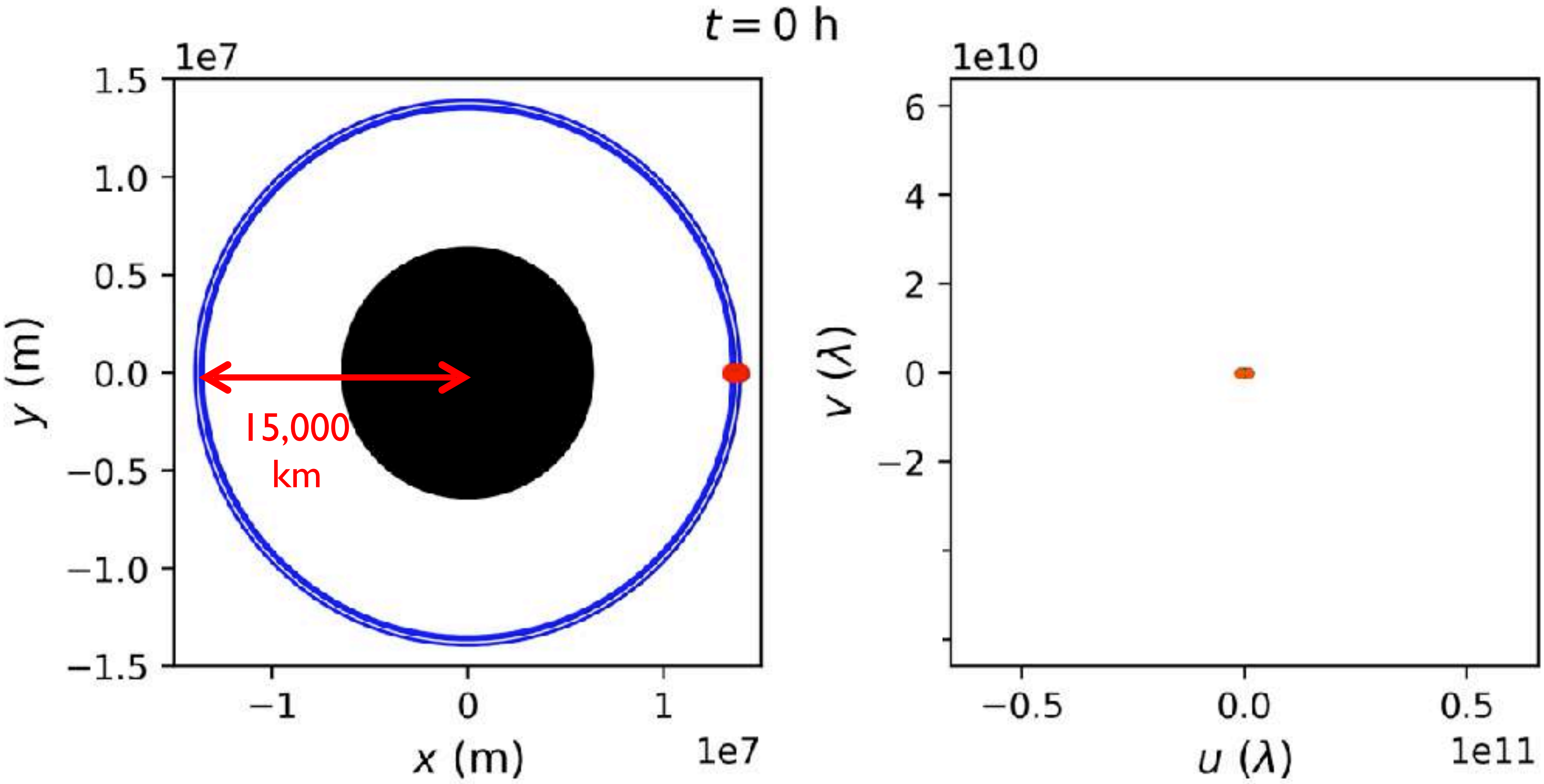

Martin-Neira, V.Kudriashov (ESA) Roelofs+ 2019

Looking into the future: going into space

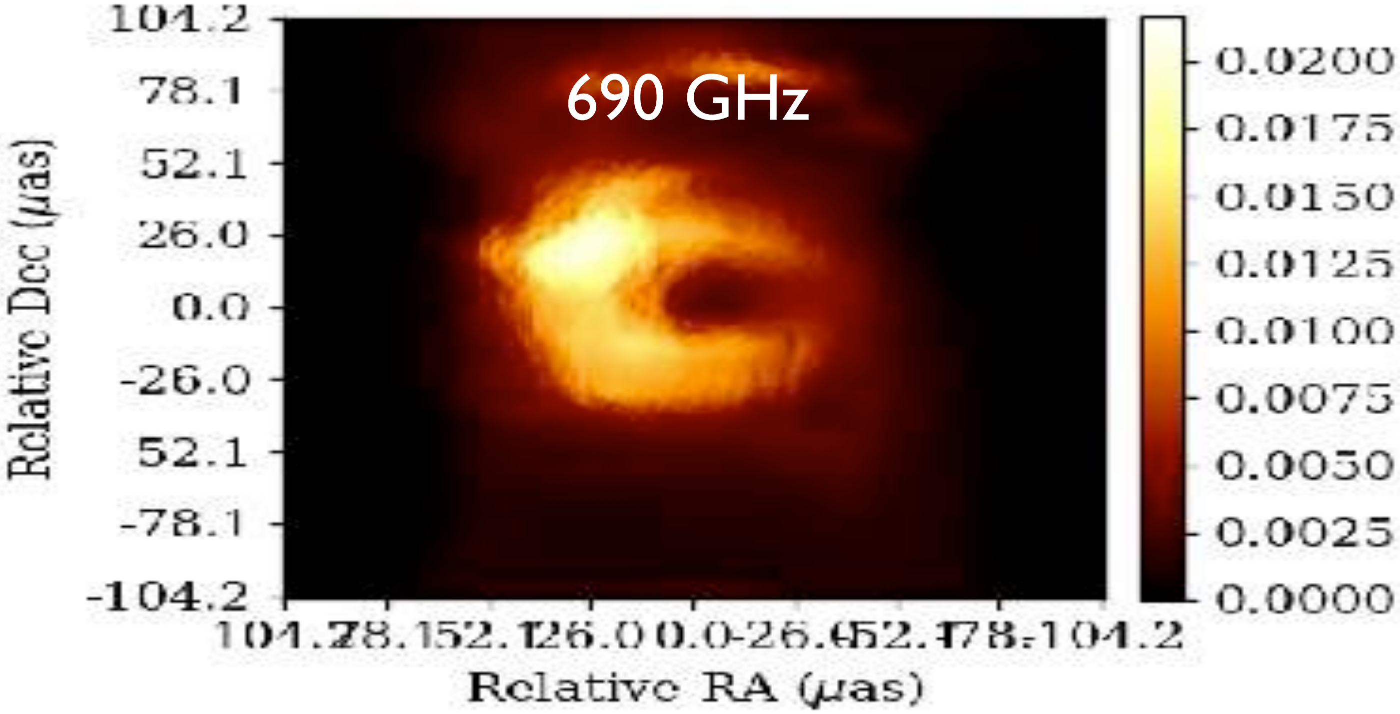

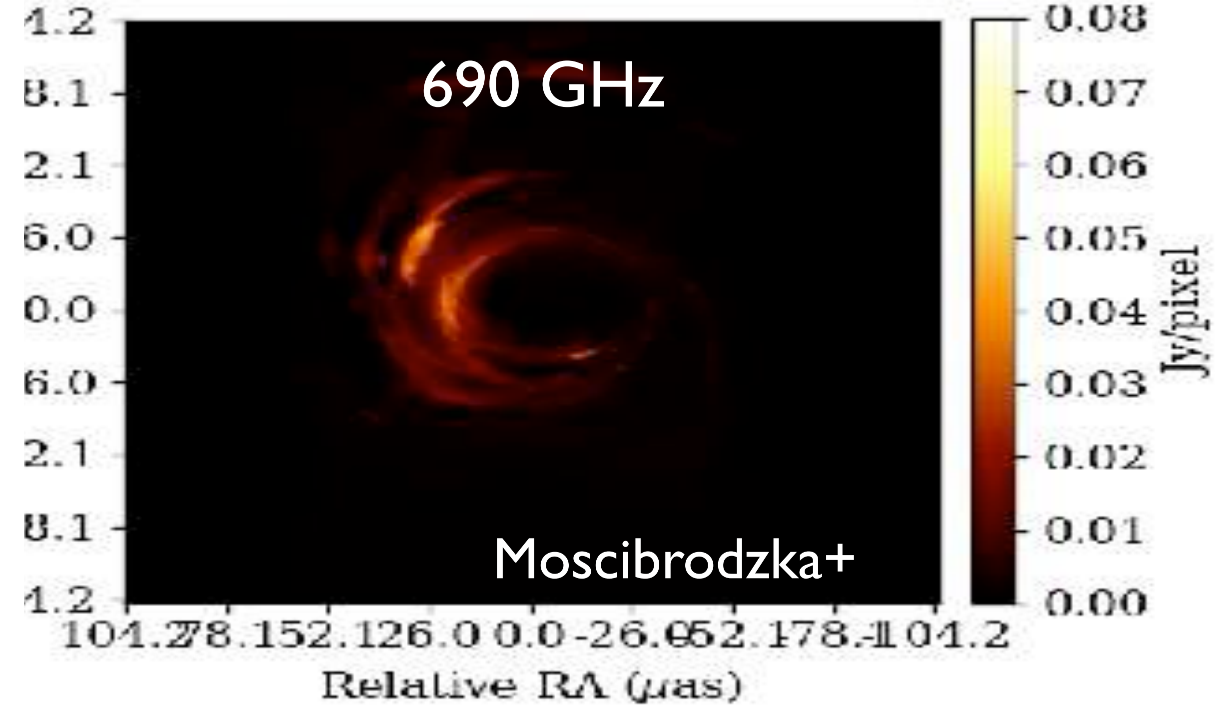

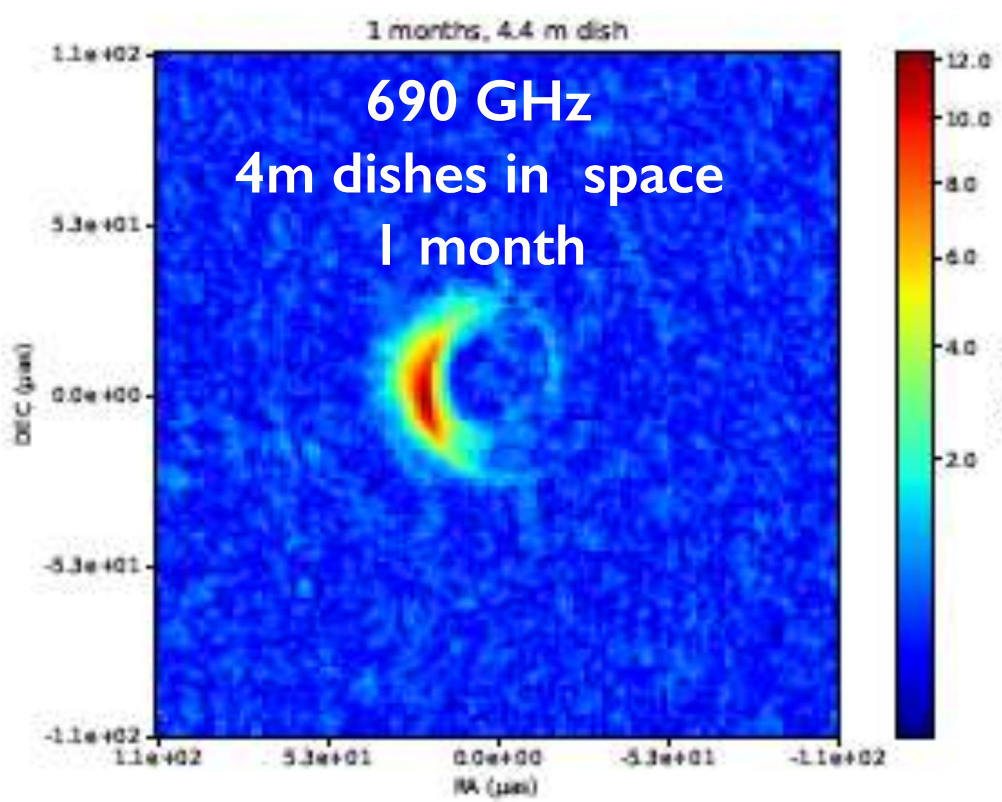

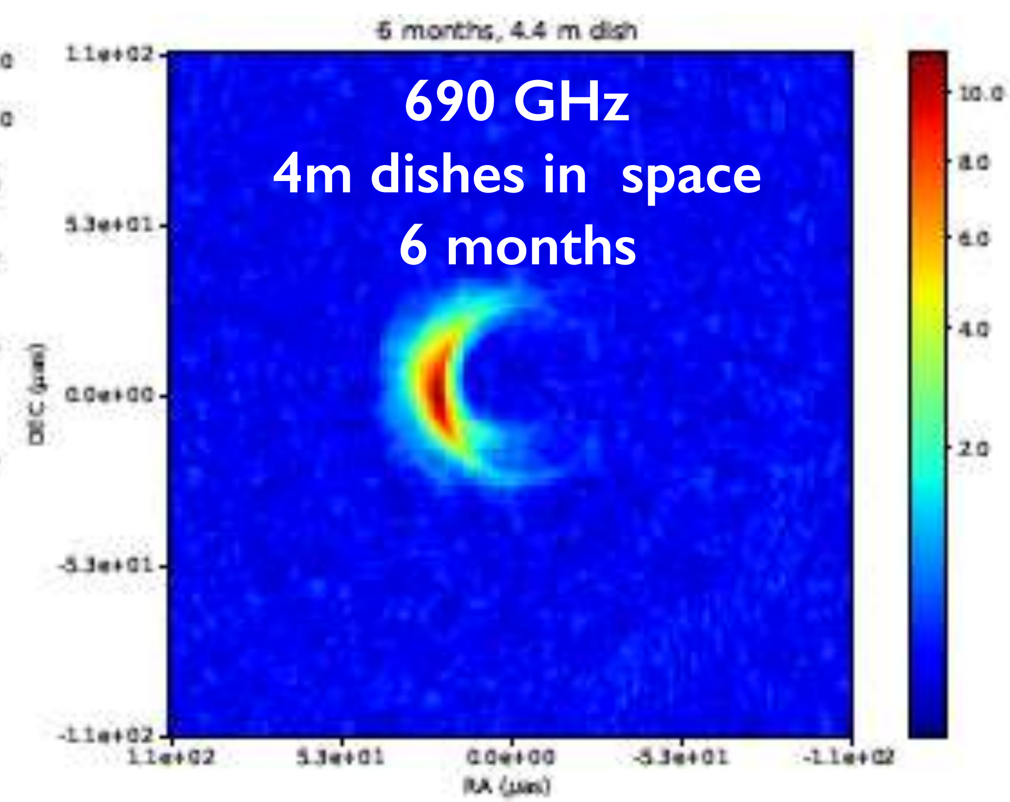

…elofs+ 2019

Accretion onto a gravastar

- Non-rotating gravastar with compactness $\mathcal{C} := M/R = 0.478$
- 3D simulations, logarithmic Kerr-Schild coordinates
- Surface absorbs energy and momentum, but not matter.
- Fluid touching the surface is set at near-zero pressure.

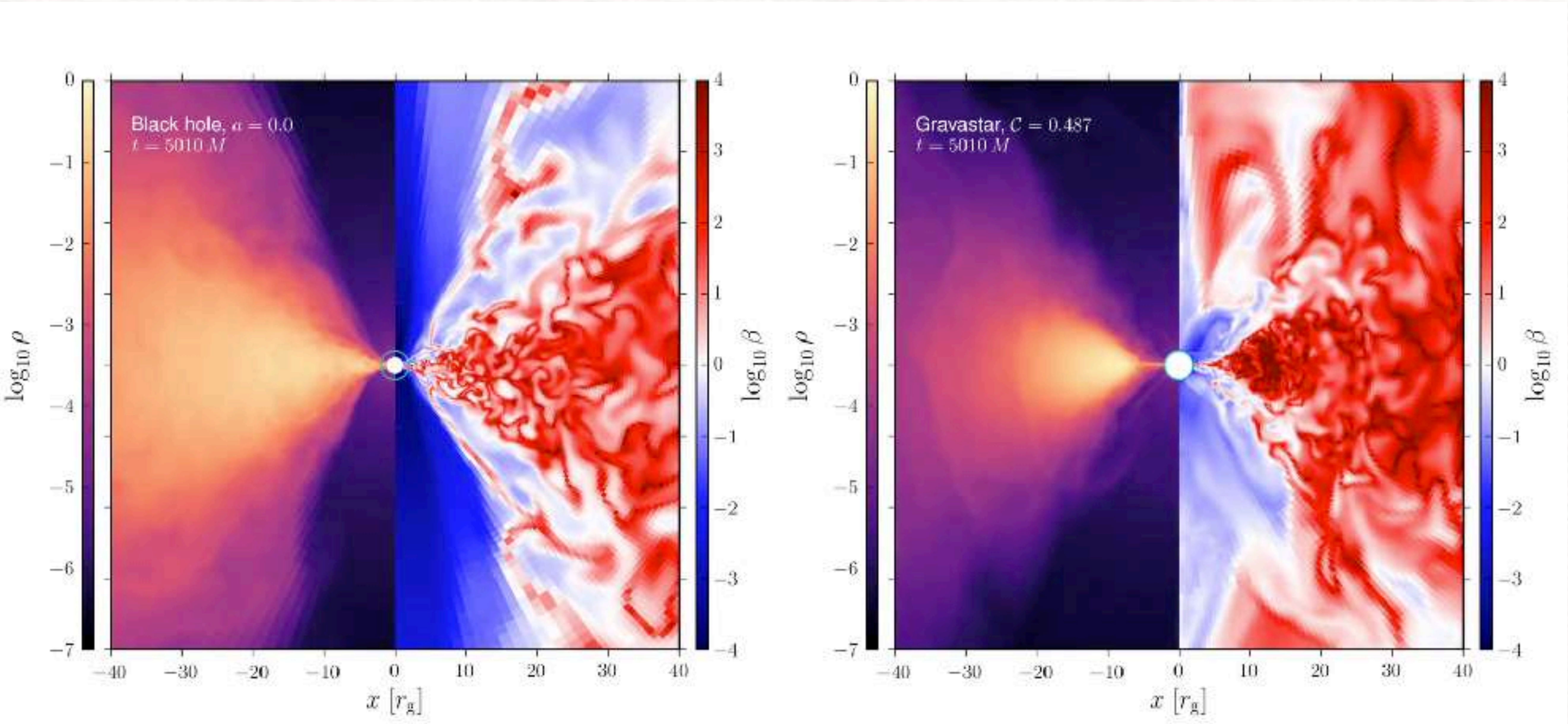

Accretion onto a gravastar: summary

- Also in this case, dynamics of matter very different.
- Mass accretion is reduced by a factor ~ 5 with respect to the Schwarzschild case
- Interaction with surface produces violent outbursts as matter is out of equilibrium once accreted ("nova" bursts).
- Oscillations and outward-moving spiral shocks are sent into the accreting material.
- Although shadow is very similar to black hole, accretion is not. Multi-wavelength observations will tell difference.

Representative GRMHD Model Image of M87

EHT2017 image

Simulated image from GRMHD model

Simulated image convolved with 20 μas beam

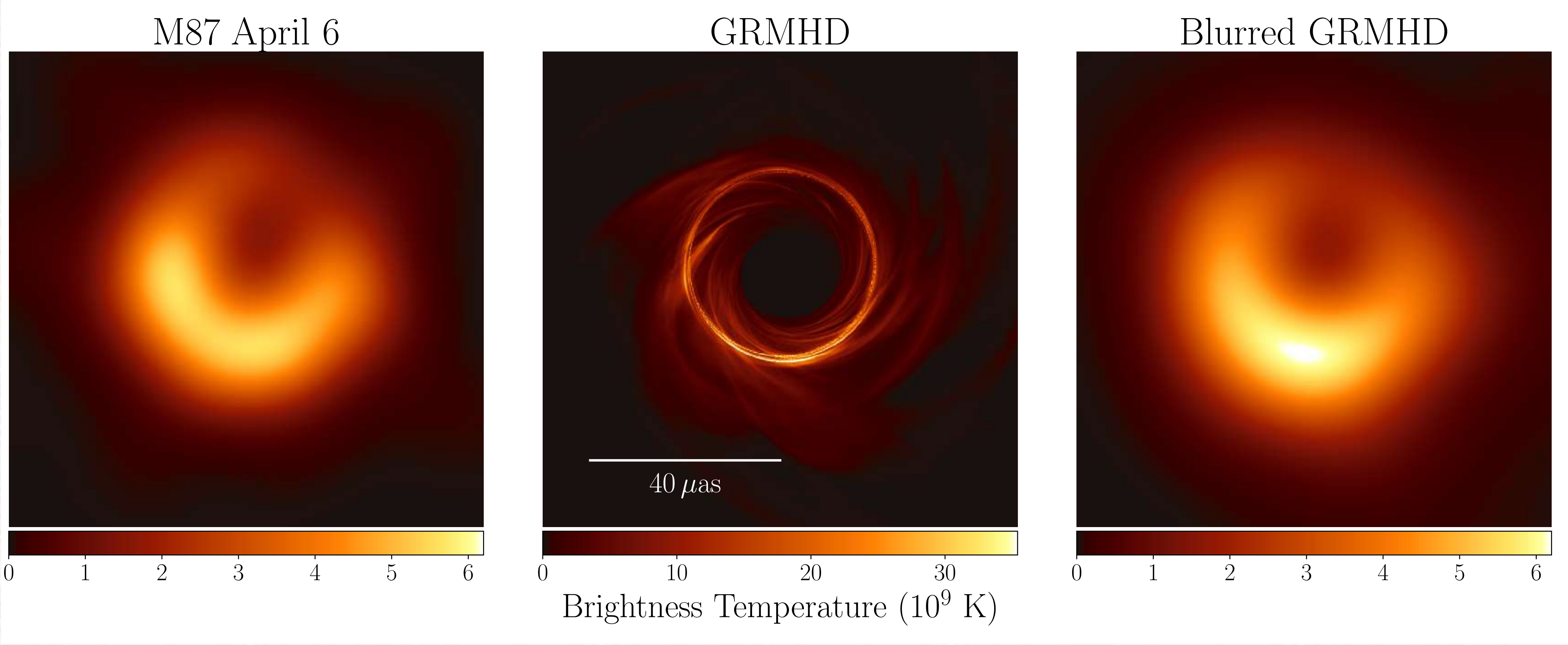

Distribution of Best-Fit Black Hole Angular Size

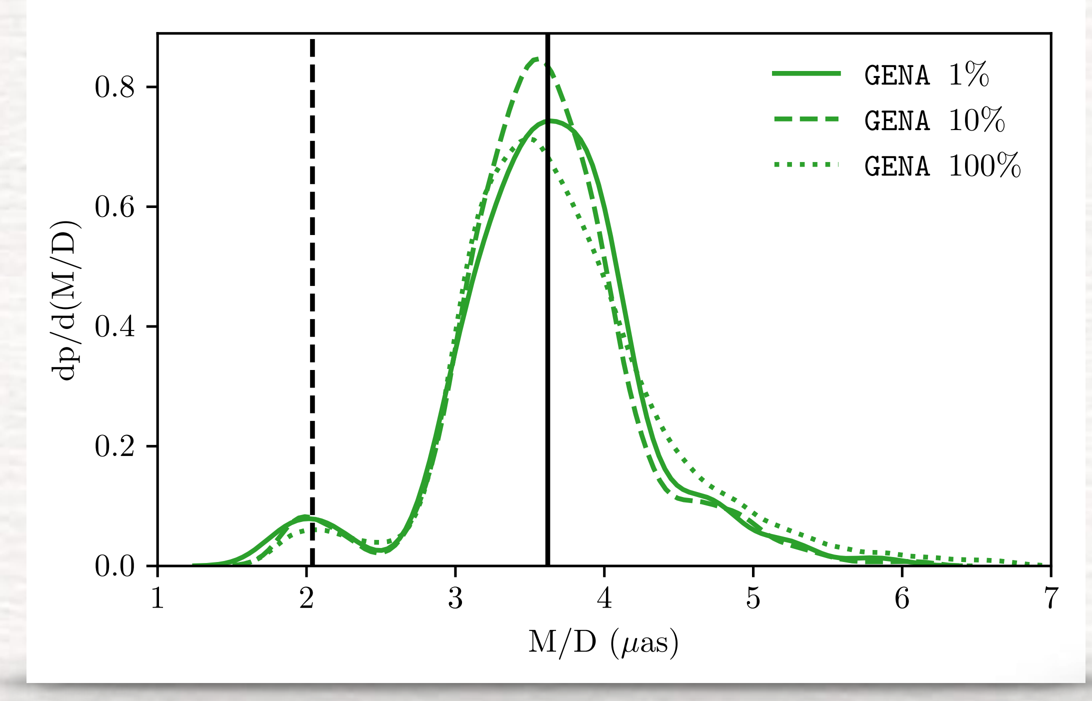

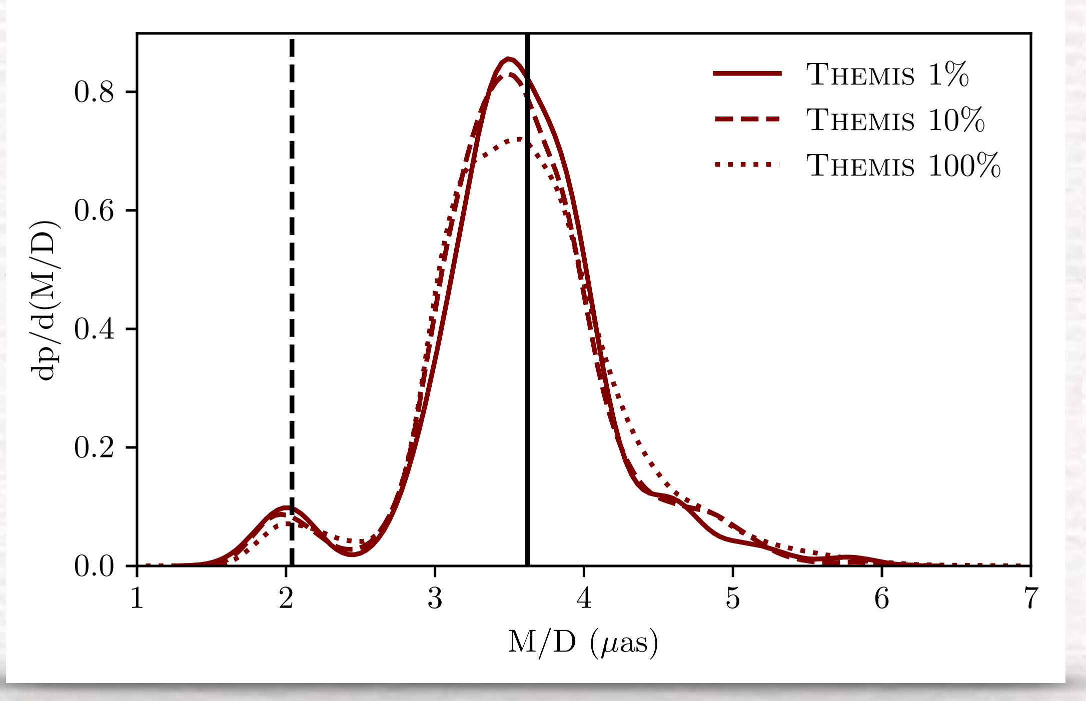

- Distribution of M/D from fitting Image Library snapshots to 2017 April 6th EHT data
- Results by Themis & GENA pipelines are qualitatively similar
- The distribution peaks close to M/D ~ 3.6 μas with a width of ~0.5 μas
- The models are broadly consistent with stellar mass estimate

Distribution of *M/D*

- Distribution of M/D of different BH spin and R_{high} for SANE & MAD models
- BH mass is calculated with D=16.9 Mpc
- Most individual models favour M/D close to 3.6 μas
- a < 0, SANE, R_{high}=1 model favours M/D ~ 2 μas due to outer ring at scale of counterrotating disk ISCO
- a =0.94, SANE favors M/D > 3.6 μas due to secondary inner ring

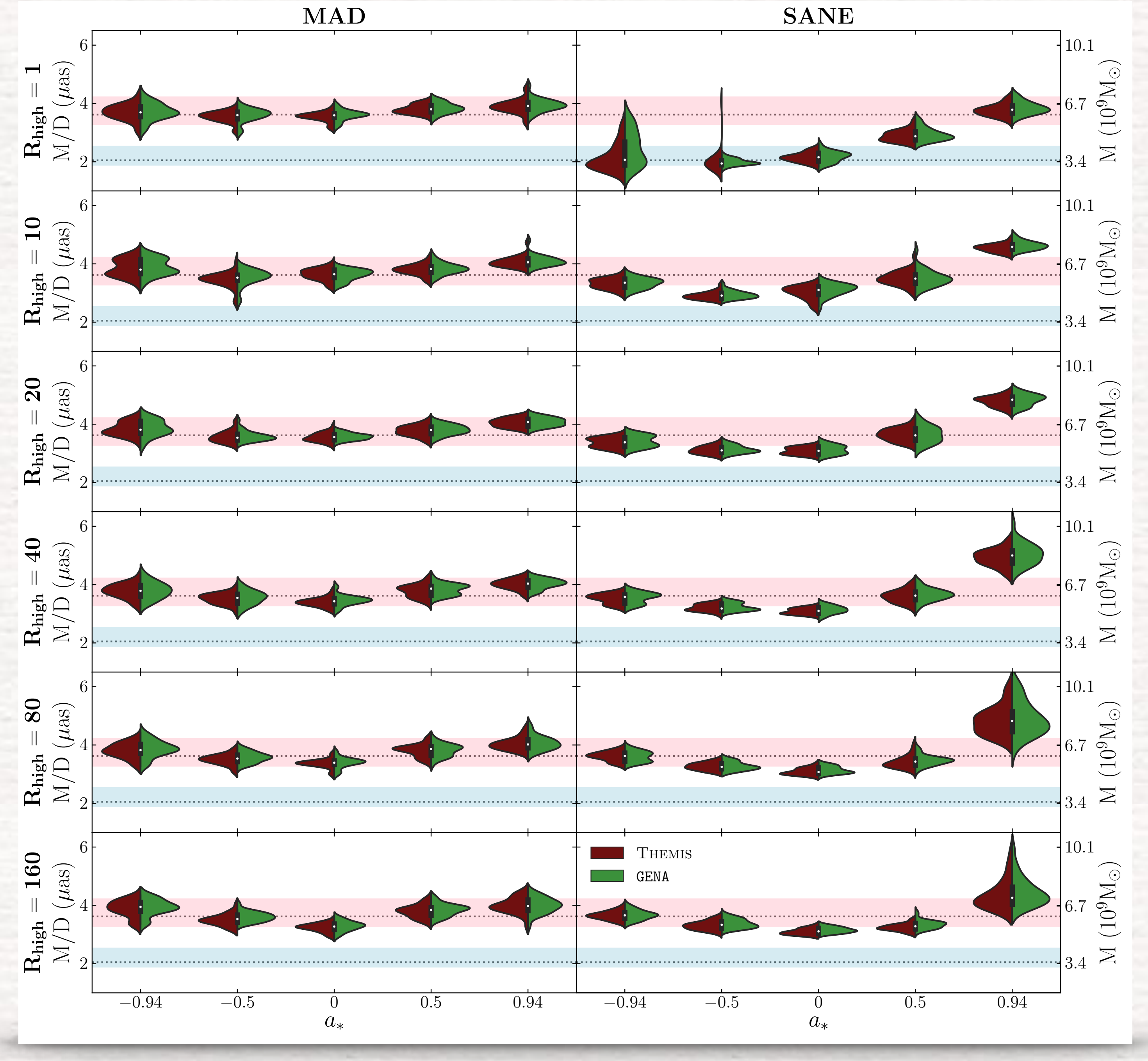

Distribution of Model Best-Fit Position Angle

BH spin vector pointing away from Earth

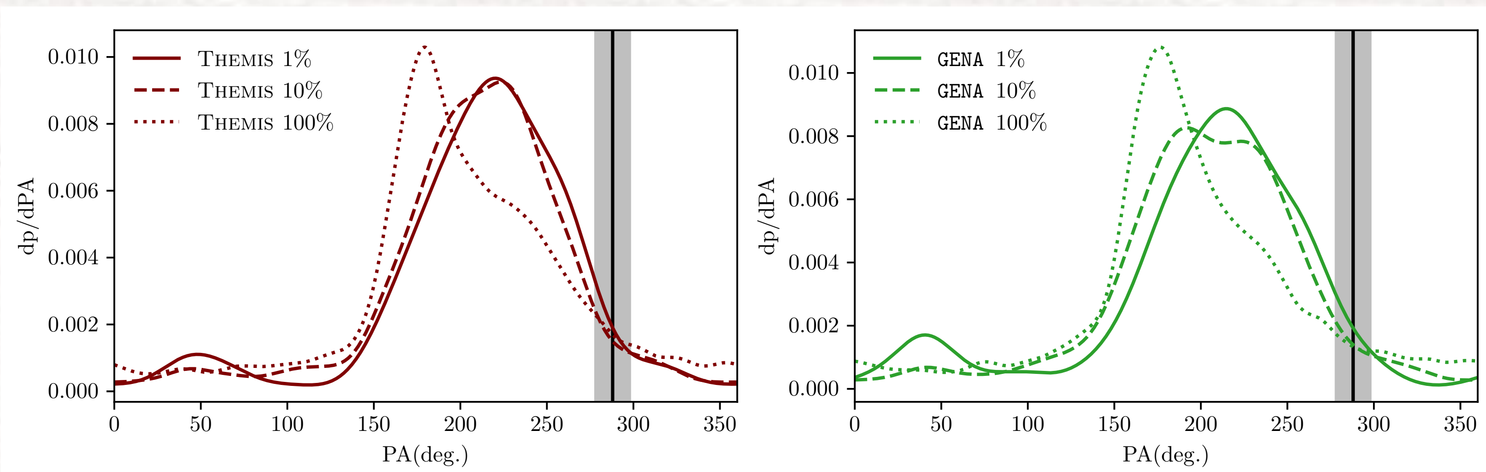

BH spin vector pointing toward Earth

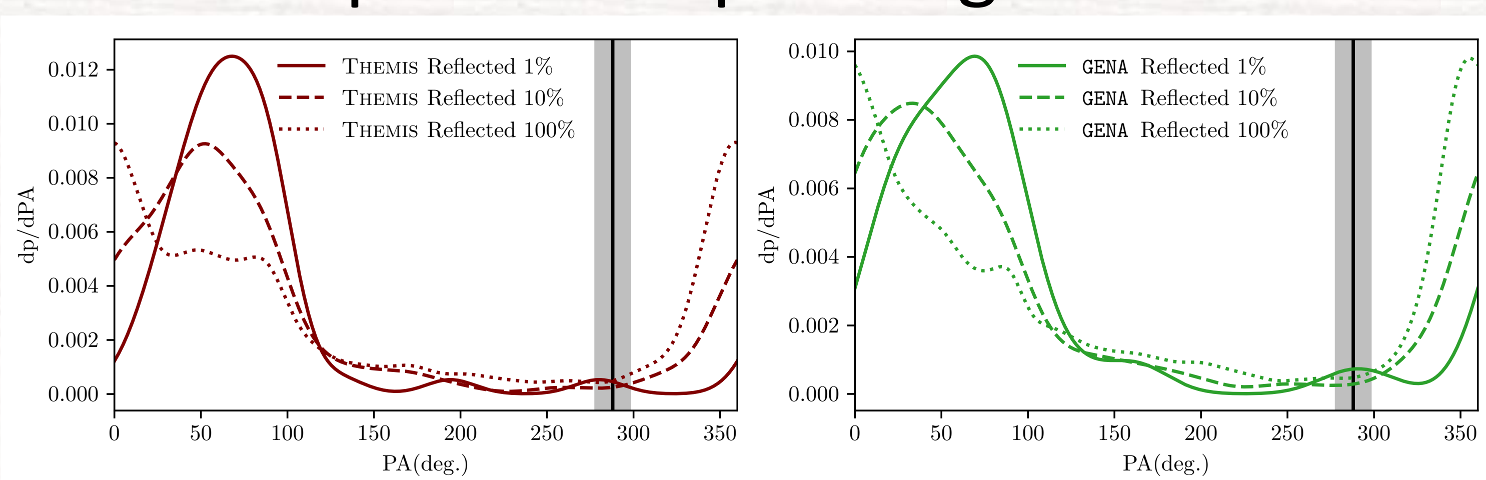

- Large scale jet orientation lies on the shoulder of the spin-away models ($\langle PA \rangle \sim 200$ deg, $\sigma_{PA} \sim 55$ deg)
- Large scale jet orientation lies off the shoulder of the spin-toward models
- BH spin-away models are strongly favored
- Width of distributions arises from brightness fluctuations in the ring

Average Image Scoring Summary

Flux[b]	a_*[c]	$\langle p \rangle$[d]	$N_{\rm model}$[e]	MIN(p)[f]	MAX(p)[g]
SANE	−0.94	0.33	24	0.01	0.88
SANE	−0.5	0.19	24	0.01	0.73
SANE	0	0.23	24	0.01	0.92
SANE	0.5	0.51	30	0.02	0.97
SANE	0.75	0.74	6	0.48	0.98
SANE	0.88	0.65	6	0.26	0.94
SANE	0.94	0.49	24	0.01	0.92
SANE	0.97	0.12	6	0.06	0.40
MAD	−0.94	0.01	18	0.01	0.04
MAD	−0.5	0.75	18	0.34	0.98
MAD	0	0.22	18	0.01	0.62
MAD	0.5	0.17	18	0.02	0.54
MAD	0.75	0.28	18	0.01	0.72
MAD	0.94	0.21	18	0.02	0.50

- Compare:
  data - ⟨model⟩
  model - ⟨model⟩
  using Themis-AIS
- Rejects a = -0.94 MAD models
- This model exhibit highest morphological variability

Other Constraints

Apply three additional constraints:

1. Close to radiative equilibrium
2. Must not overproduce X-rays
3. Must produce jet power > minimal jet power = 10^{42} erg/sec

Radiative Equilibrium

- Calculate radiative efficiency, $\epsilon \equiv L_{\rm bol}/(\dot{M} c^2)$
- Reject model if $\varepsilon > \varepsilon$(classical thin disk model); inconsistent; would cool quickly
- L_{bol}: calculated by Monte Carlo code grmonty
- Rejects MAD models with $a \geq 0$ and $R_{high} = 1$ (hot midplane electrons)

X-ray Constraint

- X-ray data: simultaneously Chandra, NuSTAR observations during EHT2017 Campaign
  - 2-10 keV luminosity: $L_x = 4.4 \pm 0.1 \times 10^{40}$ erg/s
- Compare data to SEDs generated from simulations
  - X-ray flux is produced by inverse Compton scattering of synchrotron photons
- Reject models that consistently *overproduce* X-ray
- Overluminous model: mostly SANE with $R_{high} <= 20$.
- L_X is sensitive to R_{high}, very low values of R_{high} are disfavored.

Jet Power

- M87's jet power (P_{jet}) estimates range from 10^{42} to 10^{45} erg/s
- Adopt conservative lower limit on jet power, $P_{jet,min} = 10^{42}$ erg/s
- P_{jet} defined as total energy flux in polar regions where $\beta\gamma > 1$
- P_{out} defined as energy flux in all polar outflow regions (includes wide-angle, low velocity wind)
- P_{out} is maximal definition of jet power

Jet Power

- Constraint $P_{jet} > P_{jet,min} = 10^{42}$ erg/s rejects all a=0 models (P_{jet} =0). These models also have $P_{out} < 10^{42}$ erg/s
- SANE models with $|a| < 0.5$ rejected
- Most $|a| > 0$ MAD models acceptable
- P_{jet} dominated by Poynting flux; driven by extraction of black hole spin energy through Blandford-Znajek process

Constraint Summary

- Applied AIS, consistency of radiative equilibrium, max X-ray luminosity, and minimum jet power
- Most SANE models fail, except a=-0.94 and a=0.94 models with large R_{high}
- Large fraction of MAD model pass, except a = 0 models and small R_{high} models

SANE

flux[1]	a_*[2]	$R_{\rm high}$[3]	AIS[4]	ϵ[5]	L_X[6]	$P_{\rm jet}$[7]	
SANE	-0.94	1	Fail	Pass	Pass	Pass	Fail
SANE	-0.94	10	Pass	Pass	Pass	Pass	**Pass**
SANE	-0.94	20	Pass	Pass	Pass	Pass	**Pass**
SANE	-0.94	40	Pass	Pass	Pass	Pass	**Pass**
SANE	-0.94	80	Pass	Pass	Pass	Pass	**Pass**
SANE	-0.94	160	Fail	Pass	Pass	Pass	Fail
SANE	-0.5	1	Pass	Pass	Fail	Fail	Fail
SANE	-0.5	10	Pass	Pass	Fail	Fail	Fail
SANE	-0.5	20	Pass	Pass	Pass	Fail	Fail
SANE	-0.5	40	Pass	Pass	Pass	Fail	Fail
SANE	-0.5	80	Fail	Pass	Pass	Fail	Fail
SANE	-0.5	160	Pass	Pass	Pass	Fail	Fail
SANE	0	1	Pass	Pass	Pass	Fail	Fail
SANE	0	10	Pass	Pass	Pass	Fail	Fail
SANE	0	20	Pass	Pass	Fail	Fail	Fail
SANE	0	40	Pass	Pass	Pass	Fail	Fail
SANE	0	80	Pass	Pass	Pass	Fail	Fail
SANE	0	160	Pass	Pass	Pass	Fail	Fail
SANE	+0.5	1	Pass	Pass	Pass	Fail	Fail
SANE	+0.5	10	Pass	Pass	Pass	Fail	Fail
SANE	+0.5	20	Pass	Pass	Pass	Fail	Fail
SANE	+0.5	40	Pass	Pass	Pass	Fail	Fail
SANE	+0.5	80	Pass	Pass	Pass	Fail	Fail
SANE	+0.5	160	Pass	Pass	Pass	Fail	Fail
SANE	+0.94	1	Pass	Fail	Pass	Fail	Fail
SANE	+0.94	10	Pass	Fail	Pass	Fail	Fail
SANE	+0.94	20	Pass	Pass	Pass	Fail	Fail
SANE	+0.94	40	Pass	Pass	Pass	Fail	Fail
SANE	+0.94	80	Pass	Pass	Pass	Pass	**Pass**
SANE	+0.94	160	Pass	Pass	Pass	Pass	**Pass**

MAD

flux[1]	a_*[2]	$R_{\rm high}$[3]	AIS[4]	ϵ[5]	L_X[6]	$P_{\rm jet}$[7]	
MAD	-0.94	1	Fail	Fail	Pass	Pass	Fail
MAD	-0.94	10	Fail	Pass	Pass	Pass	Fail
MAD	-0.94	20	Fail	Pass	Pass	Pass	Fail
MAD	-0.94	40	Fail	Pass	Pass	Pass	Fail
MAD	-0.94	80	Fail	Pass	Pass	Pass	Fail
MAD	-0.94	160	Fail	Pass	Pass	Pass	Fail
MAD	-0.5	1	Pass	Fail	Pass	Fail	Fail
MAD	-0.5	10	Pass	Pass	Pass	Fail	Fail
MAD	-0.5	20	Pass	Pass	Pass	Pass	**Pass**
MAD	-0.5	40	Pass	Pass	Pass	Pass	**Pass**
MAD	-0.5	80	Pass	Pass	Pass	Pass	**Pass**
MAD	-0.5	160	Pass	Pass	Pass	Pass	**Pass**
MAD	0	1	Pass	Fail	Pass	Fail	Fail
MAD	0	10	Pass	Pass	Pass	Fail	Fail
MAD	0	20	Pass	Pass	Pass	Fail	Fail
MAD	0	40	Pass	Pass	Pass	Fail	Fail
MAD	0	80	Pass	Pass	Pass	Fail	Fail
MAD	0	160	Pass	Pass	Pass	Fail	Fail
MAD	+0.5	1	Pass	Fail	Pass	Fail	Fail
MAD	+0.5	10	Pass	Pass	Pass	Pass	**Pass**
MAD	+0.5	20	Pass	Pass	Pass	Pass	**Pass**
MAD	+0.5	40	Pass	Pass	Pass	Pass	**Pass**
MAD	+0.5	80	Pass	Pass	Pass	Pass	**Pass**
MAD	+0.5	160	Pass	Pass	Pass	Pass	**Pass**
MAD	+0.94	1	Pass	Fail	Fail	Pass	Fail
MAD	+0.94	10	Pass	Fail	Pass	Pass	Fail
MAD	+0.94	20	Pass	Pass	Pass	Pass	**Pass**
MAD	+0.94	40	Pass	Pass	Pass	Pass	**Pass**
MAD	+0.94	80	Pass	Pass	Pass	Pass	**Pass**
MAD	+0.94	160	Pass	Pass	Pass	Pass	**Pass**

P_{jet}/P_{out} vs $\beta\gamma_{cut}$

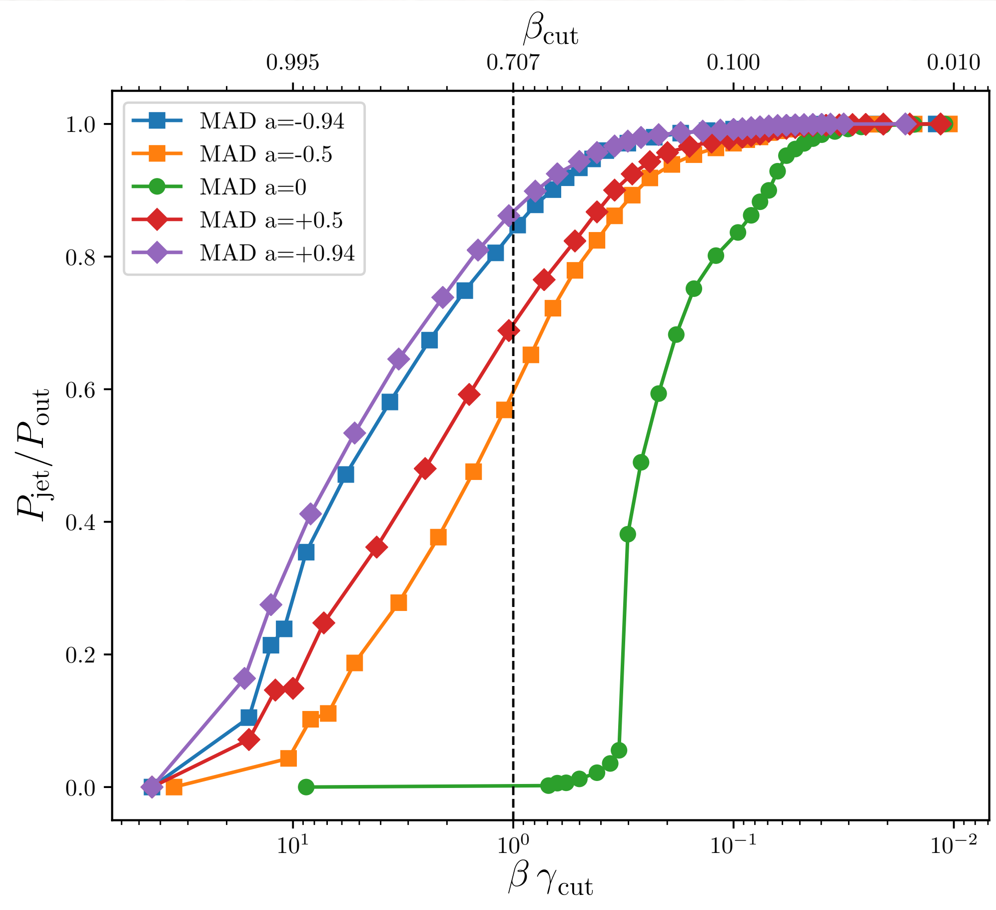

MAD

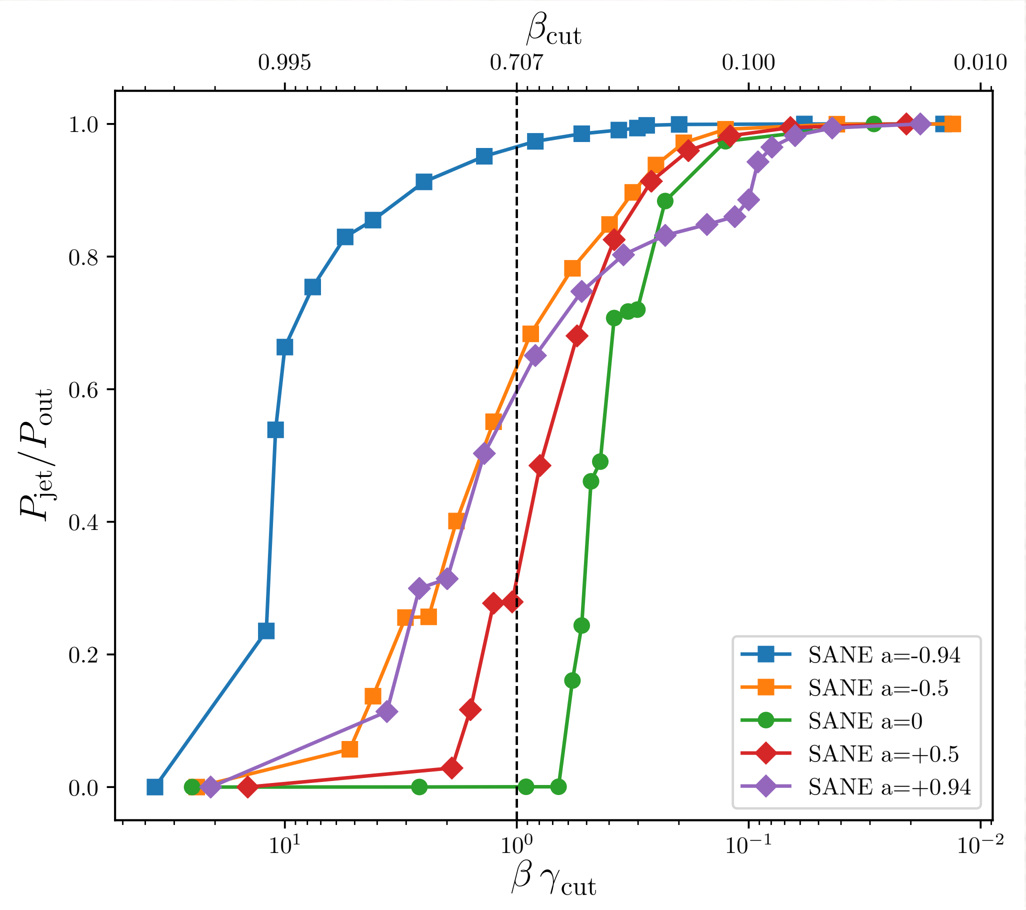

SANE

- P_{jet} depends on βγ cutoff used in definition
- P_{jet} small for a = 0 because energy flux in relativistic outflow is small

Source	BH Mass (M_{solar})	Distance (Mpc)	1 R_s (μas)
Sgr A*	4×10^6	0,008	10
M87	~~**3.3 - 6.2 x**~~ ~~$\mathbf{10^9}$~~	**16,8**	~~**3.6 - 7.3**~~ **7.6**
M104	1×10^9	10	2
Cen A	5×10^7	4	0,25

Event Horizon Telescope

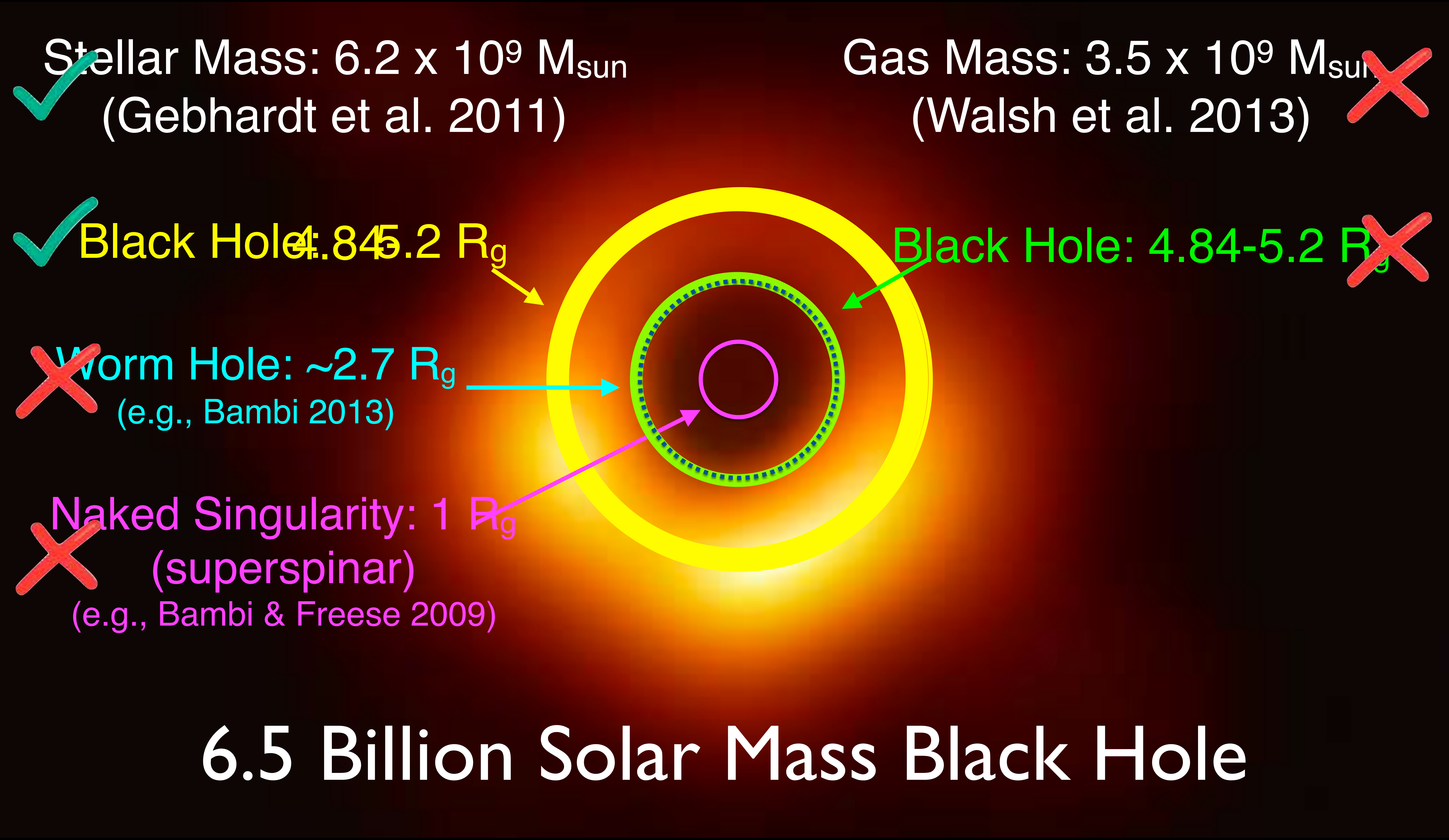
Stellar Mass: 6.2 x 10^{9} M$_{sun}$
(Gebhardt et al. 2011)
Gas Mass: 3.5 x 10^{9} M$_{sun}$
(Walsh et al. 2013)
Black Hole: 4.84-5.2 R$_g$
Black Hole: 4.84-5.2 R$_g$
Worm Hole: ~2.7 R$_g$
(e.g., Bambi 2013)
Naked Singularity: 1 R$_g$
(superspinar)
(e.g., Bambi & Freese 2009)
6.5 Billion Solar Mass Black Hole

MAD vs SANE (GRMHD Simulations)

AF model, two extreme situation

3D GRMHD simulations with a=0.94

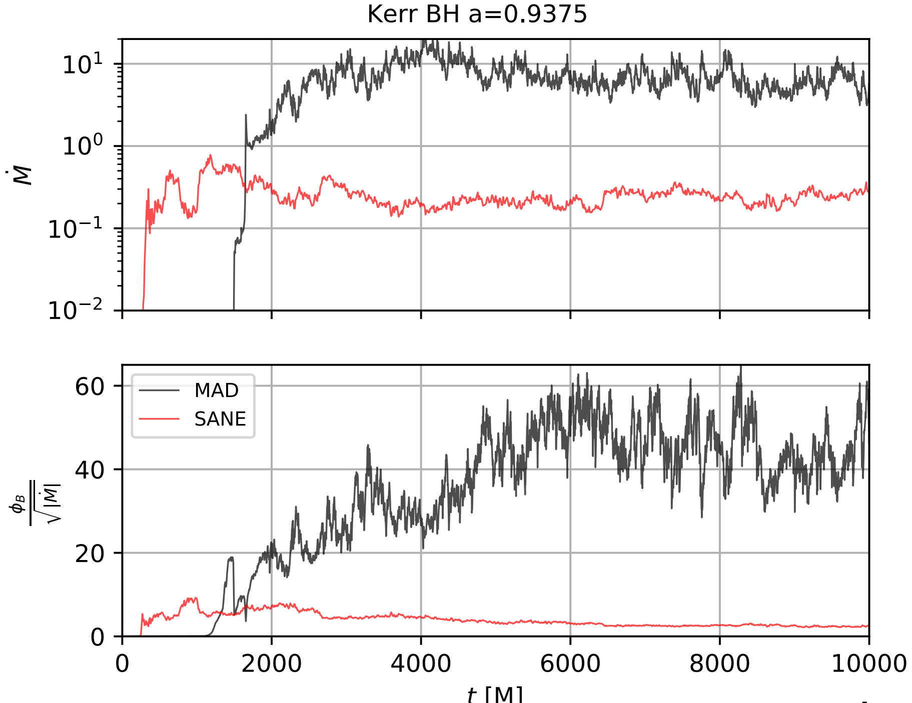

side view

top view

density

plasma beta

magnetisation

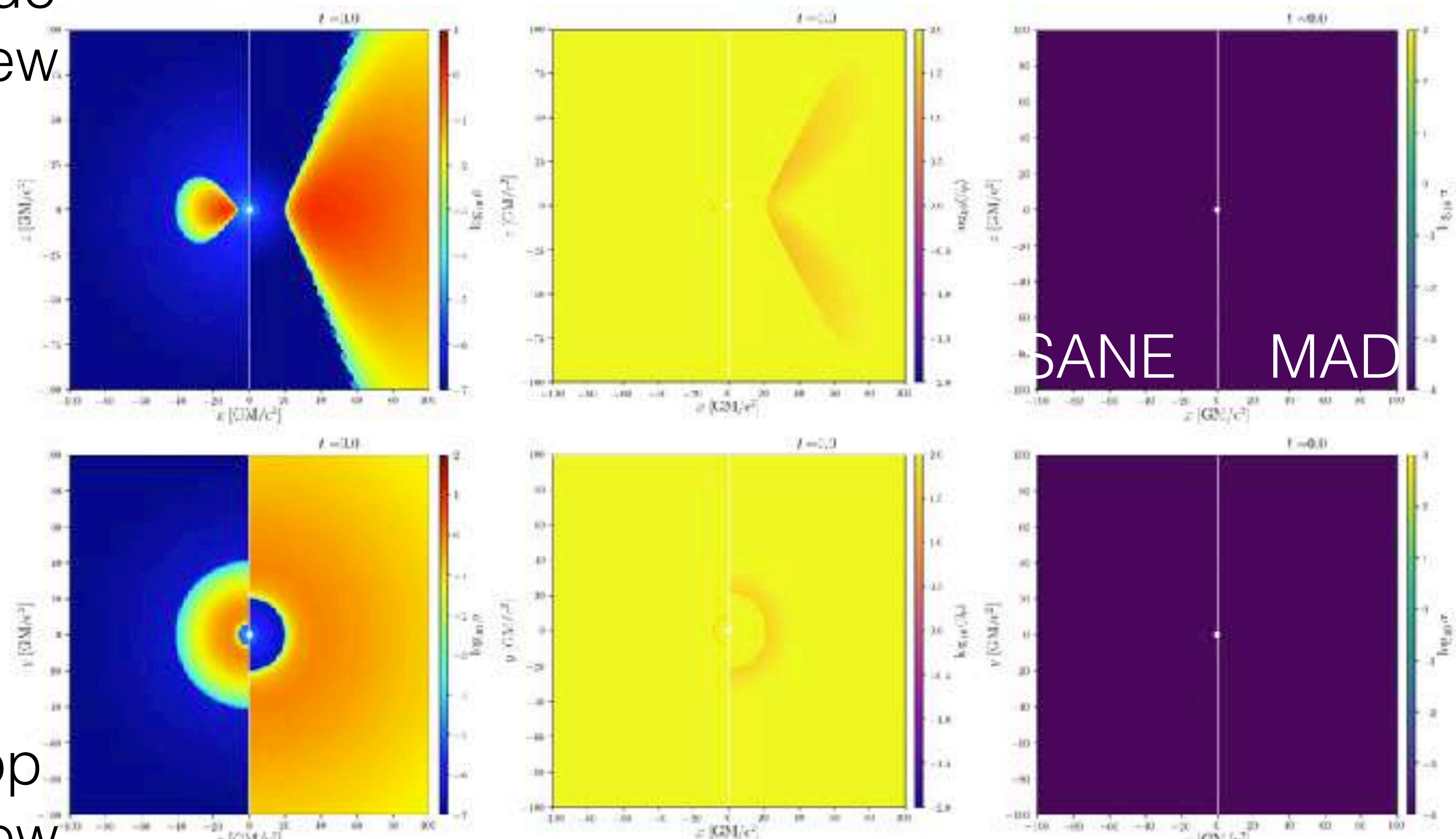

Event Horizon Telescope

GRRT Image at 230 GHz

- MAD, a=+0.94, R_{high}=160
- i=163 deg
- each frame corresponds to 1M (~0.35 day)

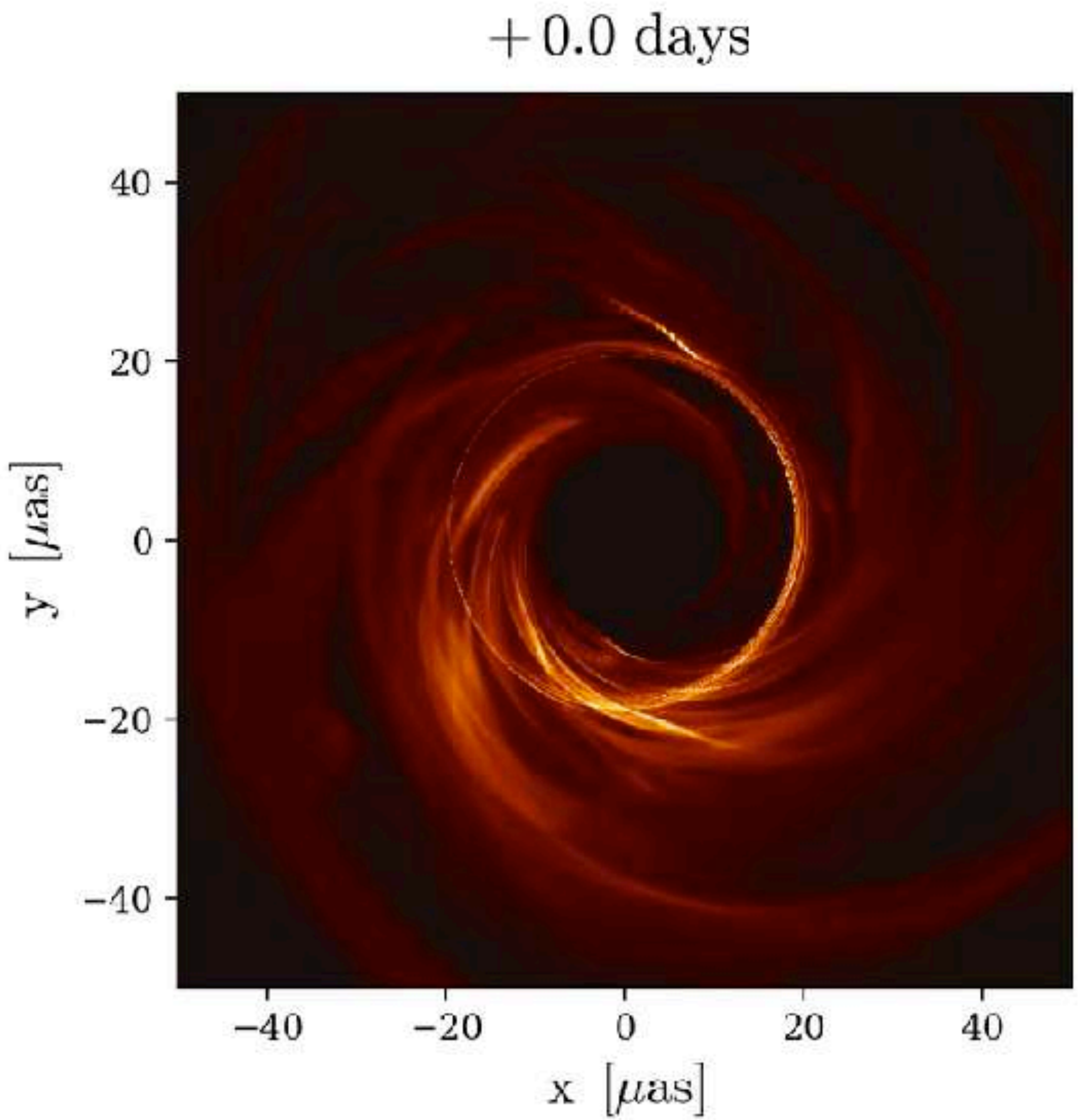

(Paper V)

Event Horizon Telescope

SANE averaged GRRT images

i=163 deg

black hole
rotational axis

the forward jet is pointed to the right in all panels

(Paper V)

Event Horizon Telesco

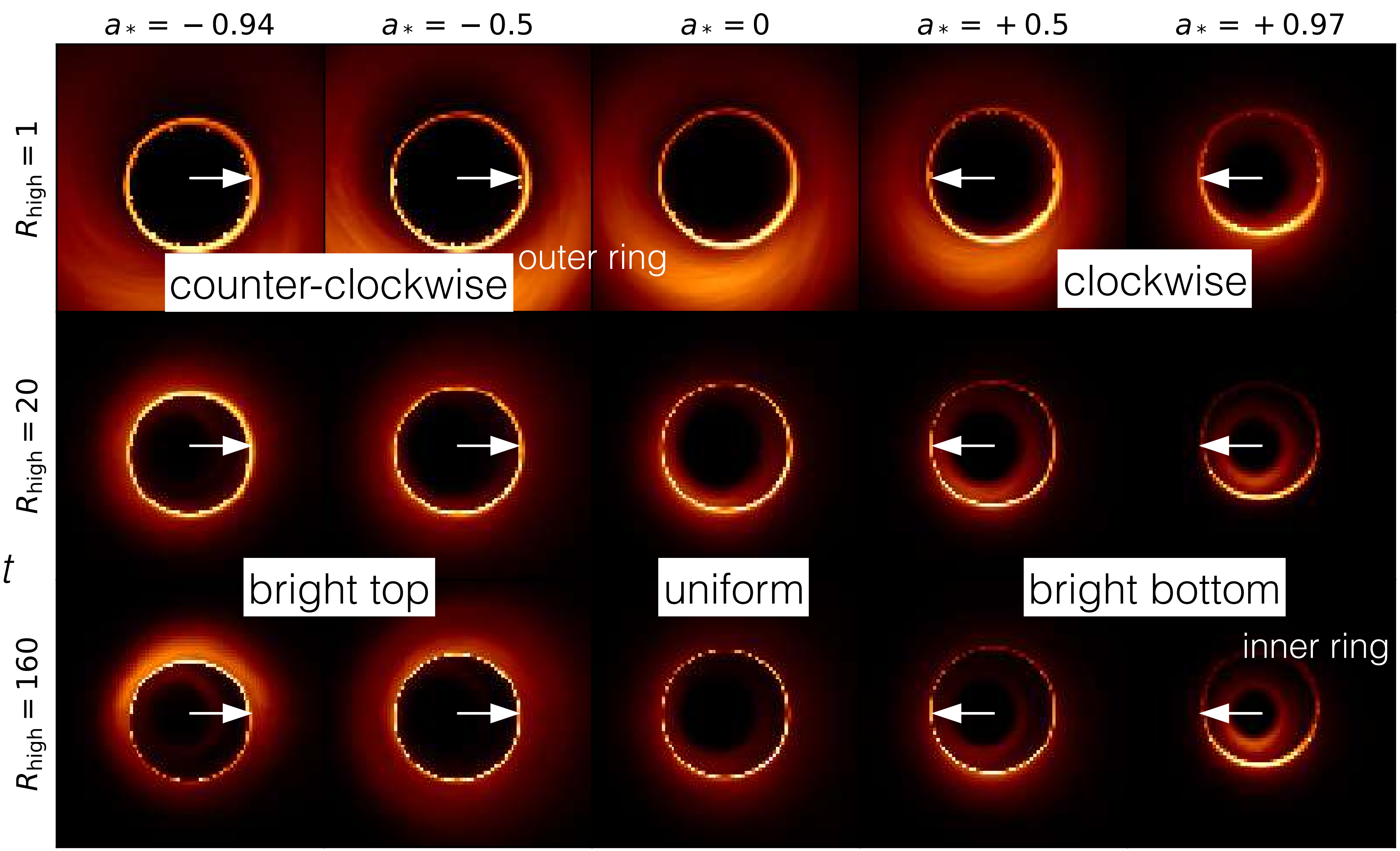

M87 Polarization

- EHT observed polarization in 2017 (Sgr A*, M87, + AGN sources)
- Polarization map (linear & circular), rotation measure, total polarization degree
- Given additional constraint for theoretical model

GRMHD simulation
(SANE, i=20 deg, R_{high}=40)

Semi-analytic force-free jet model (Broderick & Loeb 09)

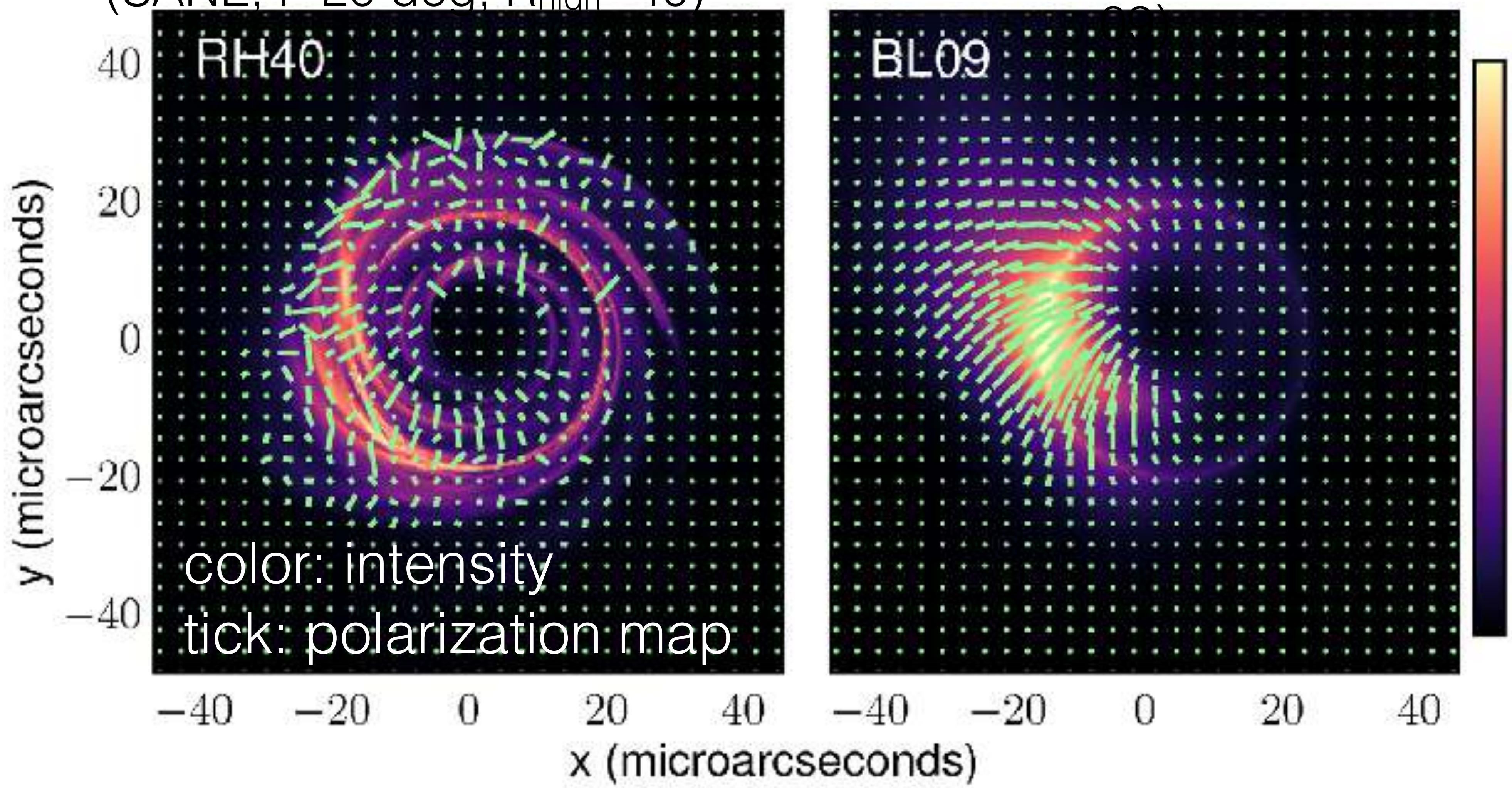

Event Horizon Telescope

Moscibrodzka et al. (17)

Movie of Sgr A*

- Sgr A* is more complicated due to time variability & scattering during EHT observation period (~6h)
- Image snapshot => Movie

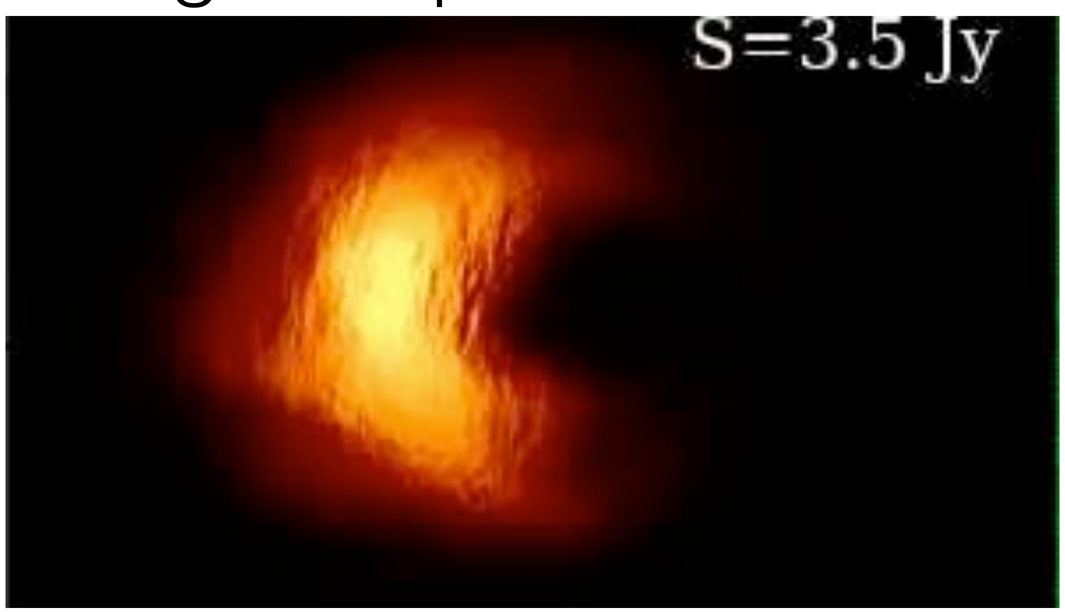

GRMHD + GRRT + scattering (SANE, a=0.6, i=60 deg)

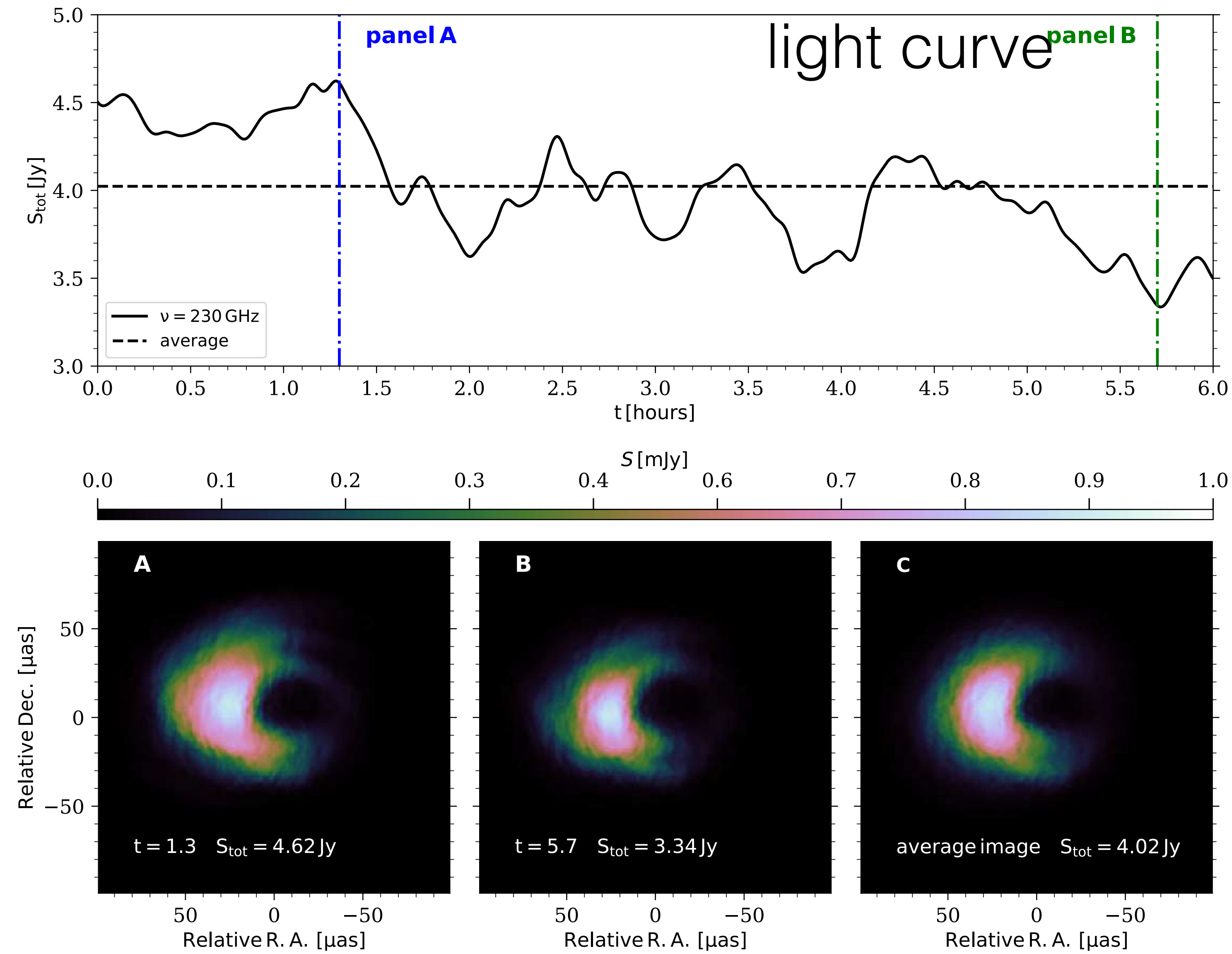

Event Horizon Telescope

Extend EHT: space VLBI (EHT+satellite)

- Consider EHT ground VLBI array + 1 orbiting satellite ⇒ increase resolution

Fromm et al. (2019)

- Question: which orbit to use?
- 6 orbital elements

semi major axis: a, eccentricity: e, inclination: i, right ascension of the ascending node: Ω, argument of perigee: ω, true anomaly: θ

Stellar orbit

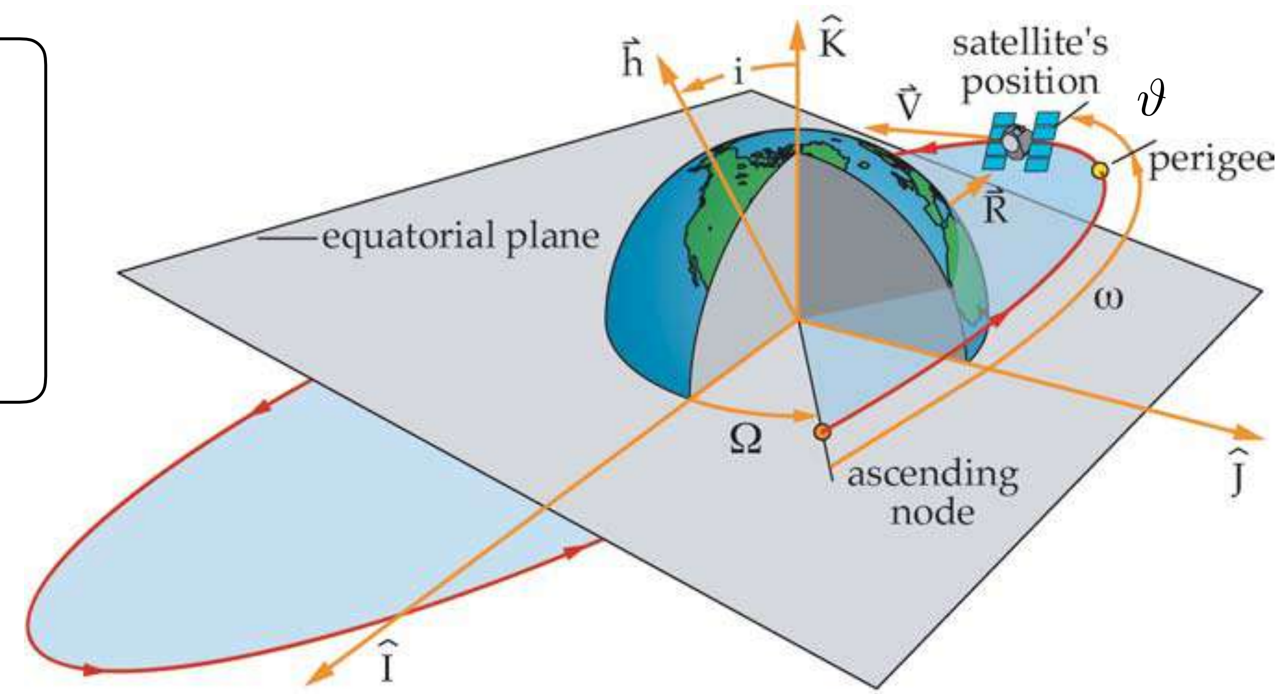

- Set constraints:
  - keep beam nearly circular
  - fill uv-plane within 24 hours
  - optimise orbit for Sgr A* observations

⇒ constrained non-linear optimisation by using Genetic Algo (GA)

GA Results for Satellite Orbit

number of individuals: 1000   number of generations: 10

Calculated by C. Fror

animation: iteration until best orbit (last frame)

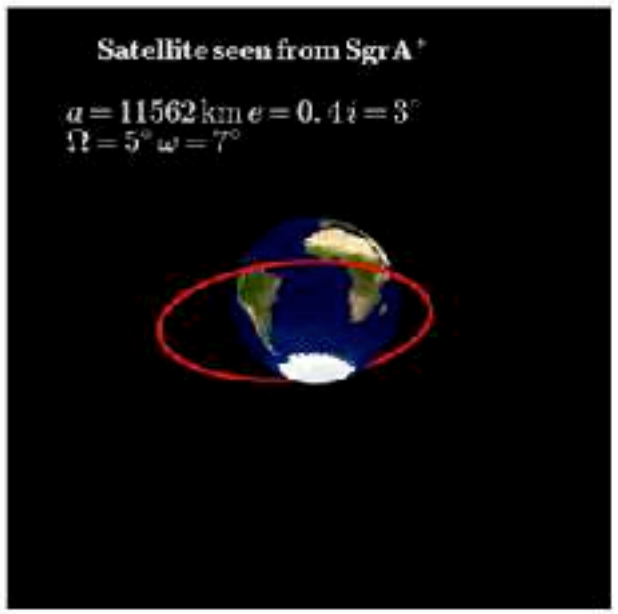

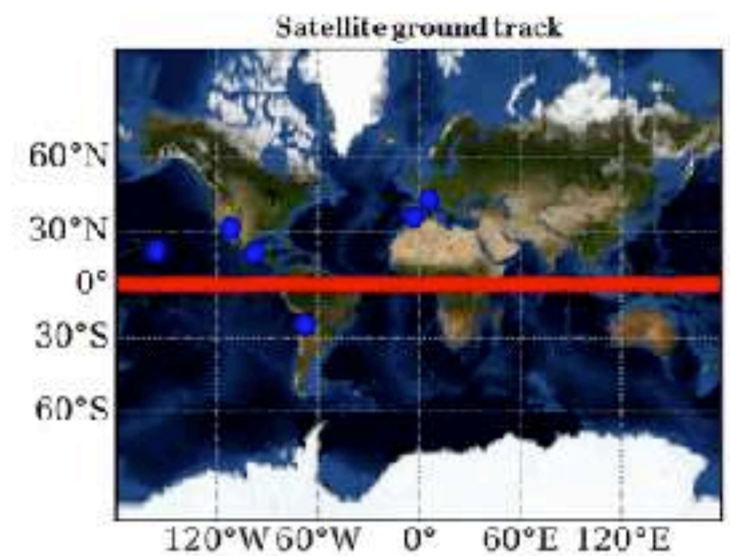

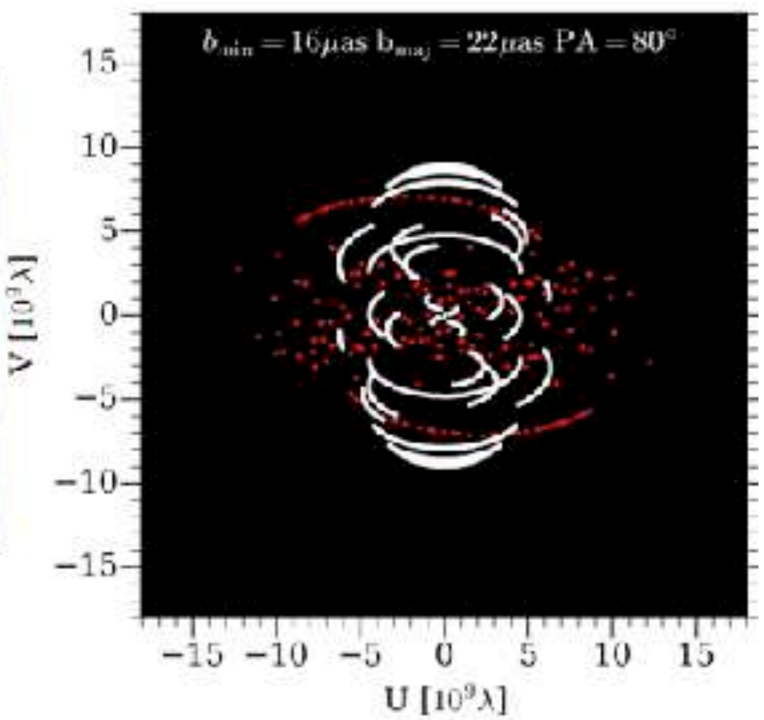

Method can be easily adopted and modified for:

- different sources (M87 or M87+Sgr A*)
- different observations schedules (6h,12h,18h,…)
- modification of ground array (where to add new antennas)

Primary Target for EHT

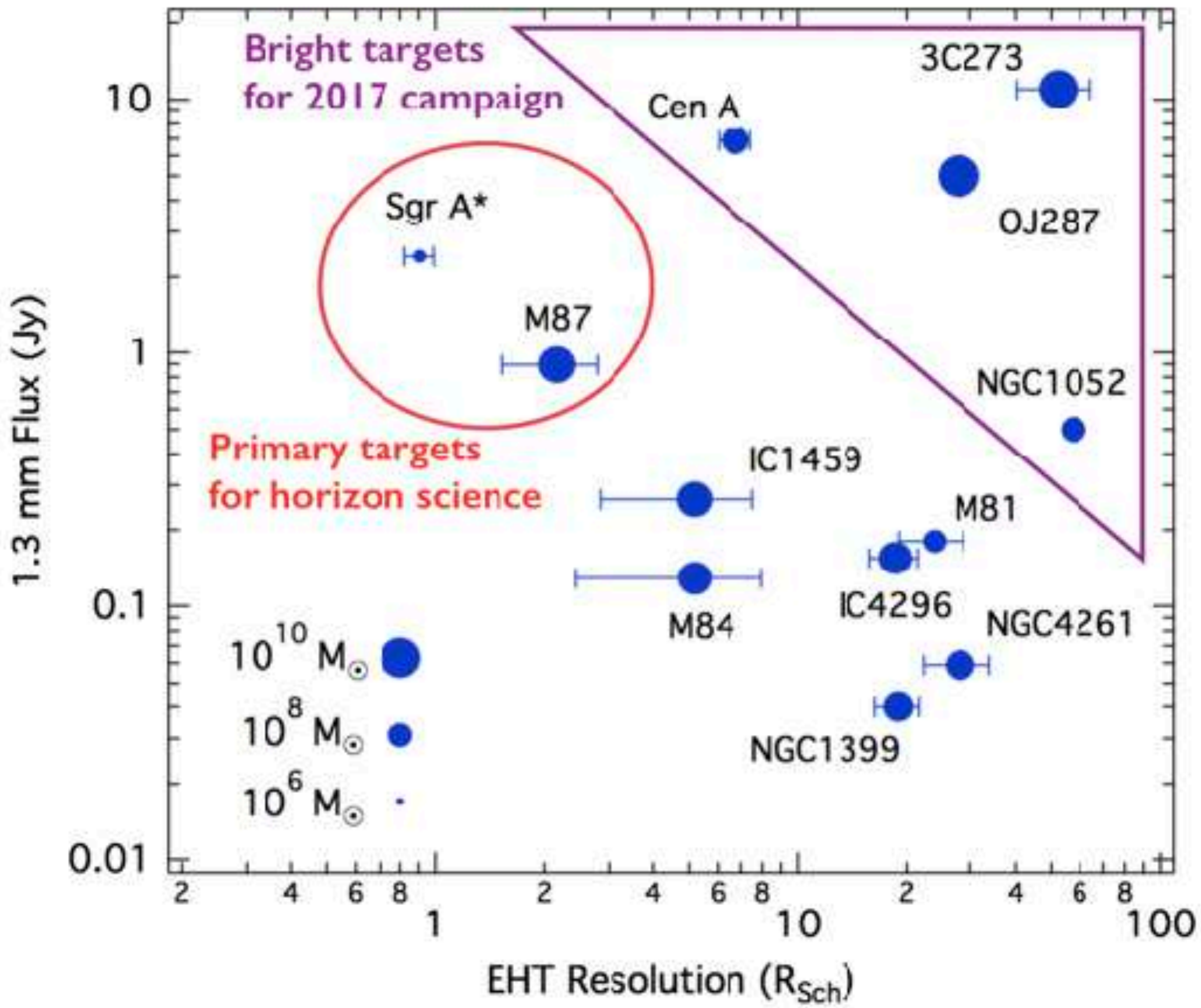

Psaltis (2018)

Event Horizon Telescope

Slowly Building Up Data

Lo-band eht-imaging on April 11

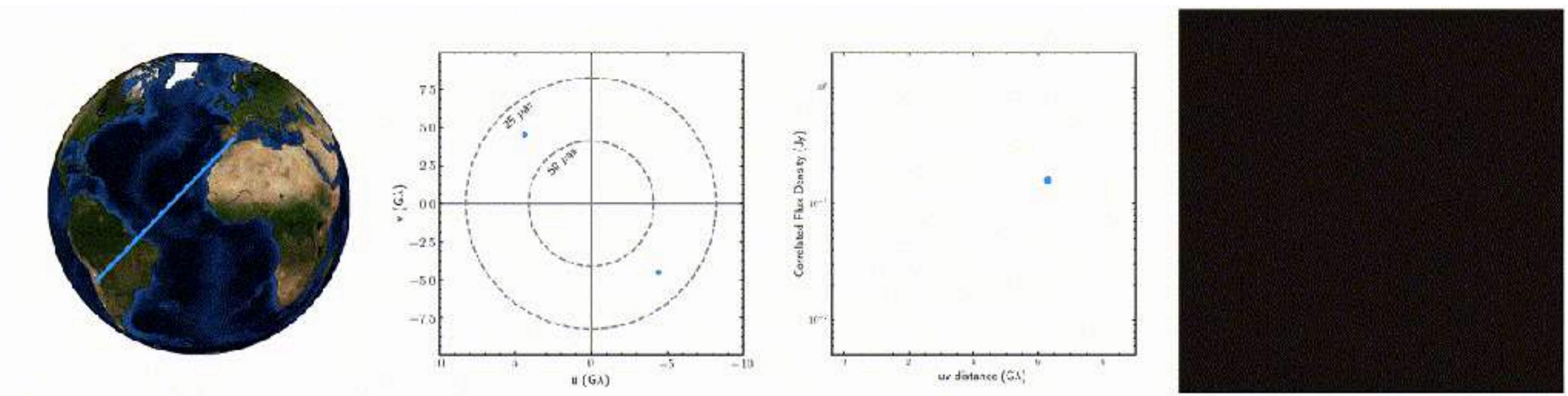

Credit: Palumbo & Wielgu

Closure Phases: Mildly asymmetric & time-variable structure

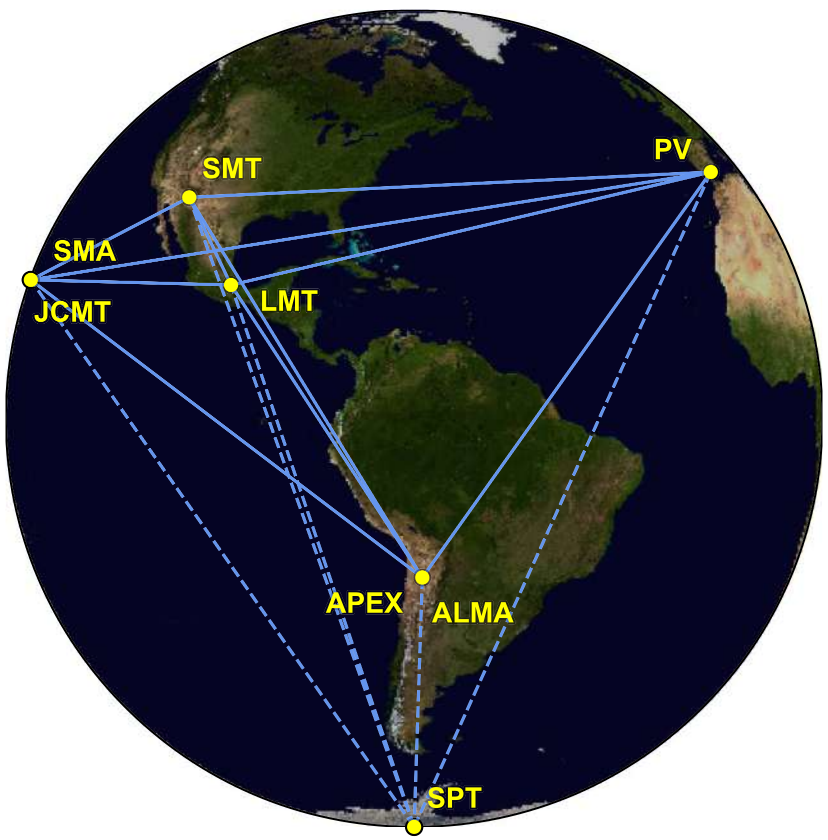

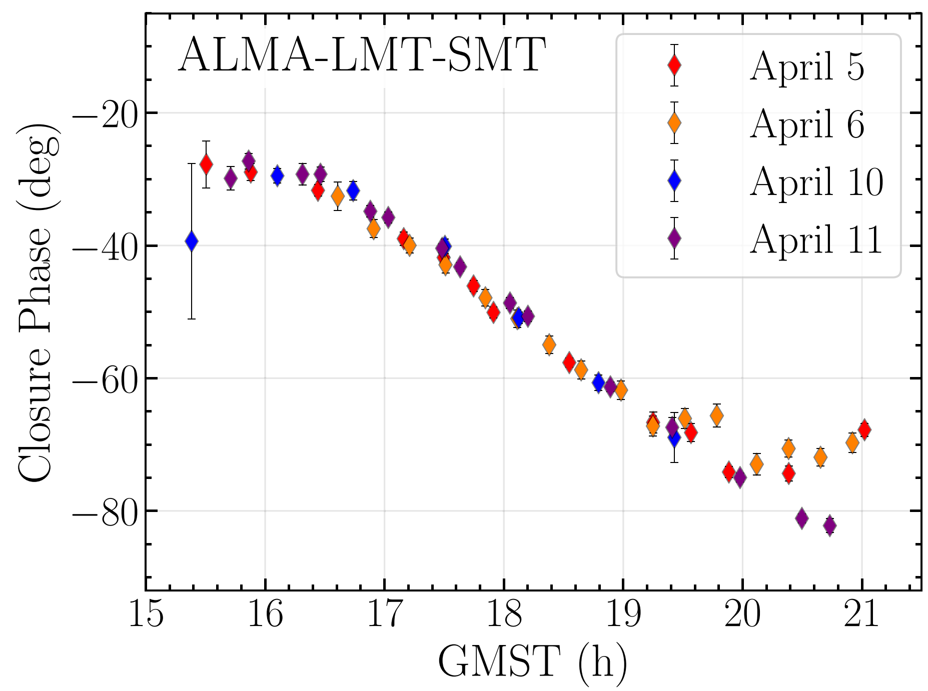

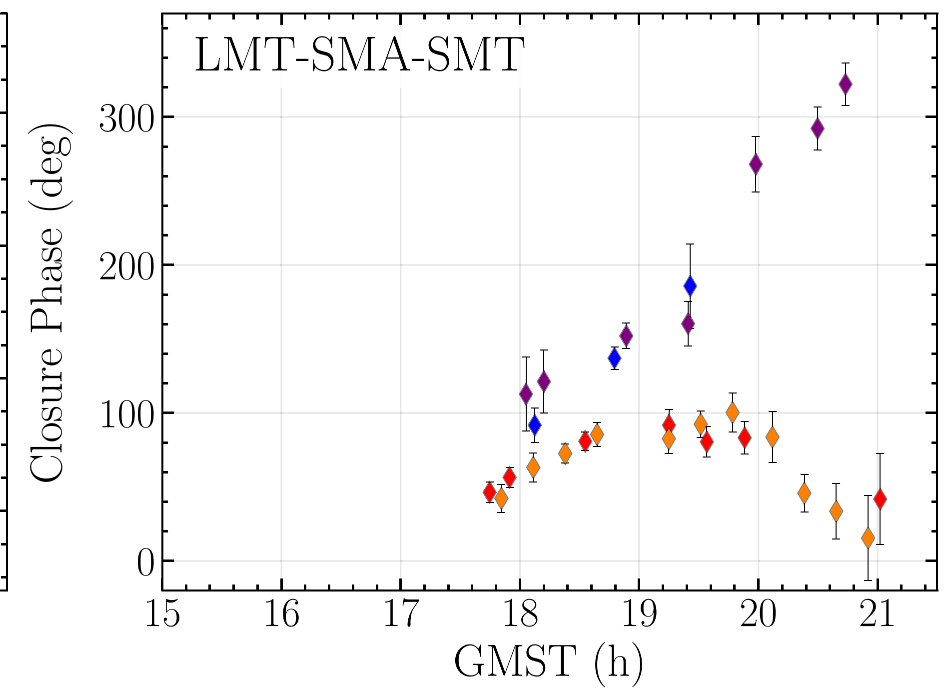

(Paper IV)

X-ray constraint

- X-ray data: simultaneous Chandra, NuSTAR observations during EHT2017 Campaign
  - 2-10 keV luminosity: $L_X = 4.4 \pm 0.1 \times 10^{40}$ erg/s

- Compare data to SEDs generated from simulations
  - X-ray flux is produced by inverse Compton scattering of synchrotron photons

- Reject models that consistently *overproduce* X-ray

- Overluminous model: mostly SANE with $R_{high} \leq 20$.

- L_X is sensitive to R_{high}, very low values of R_{high} are disfavored.

Event Horizon Telescope

Jet Power

- M87's jet power (P_{jet}) estimates range from 10^{42} to 10^{45} erg/s
- Adopt conservative lower limit on jet power, $P_{jet,min} = 10^{42}$ erg/s
- P_{jet} defined as total energy flux in polar regions where $\beta\gamma > 1$
- P_{out} defined as energy flux in all polar outflow regions (includes wide-angle, low velocity wind)
- P_{out} is *maximal* definition of jet power
- Constraint $P_{jet} > P_{jet,min} = 10^{42}$ erg/s rejects all a=0 models (P_{jet} =0). These models also have $P_{out} < 10^{42}$ erg/s
- SANE models with $|a| < 0.5$ rejected
- Most $|a| > 0$ MAD models acceptable
- P_{jet} dominated by Poynting flux; driven by extraction of black hole spin energy through Blandford-Znajek process

P_{jet}/P_{out} vs $\beta\gamma_{cut}$

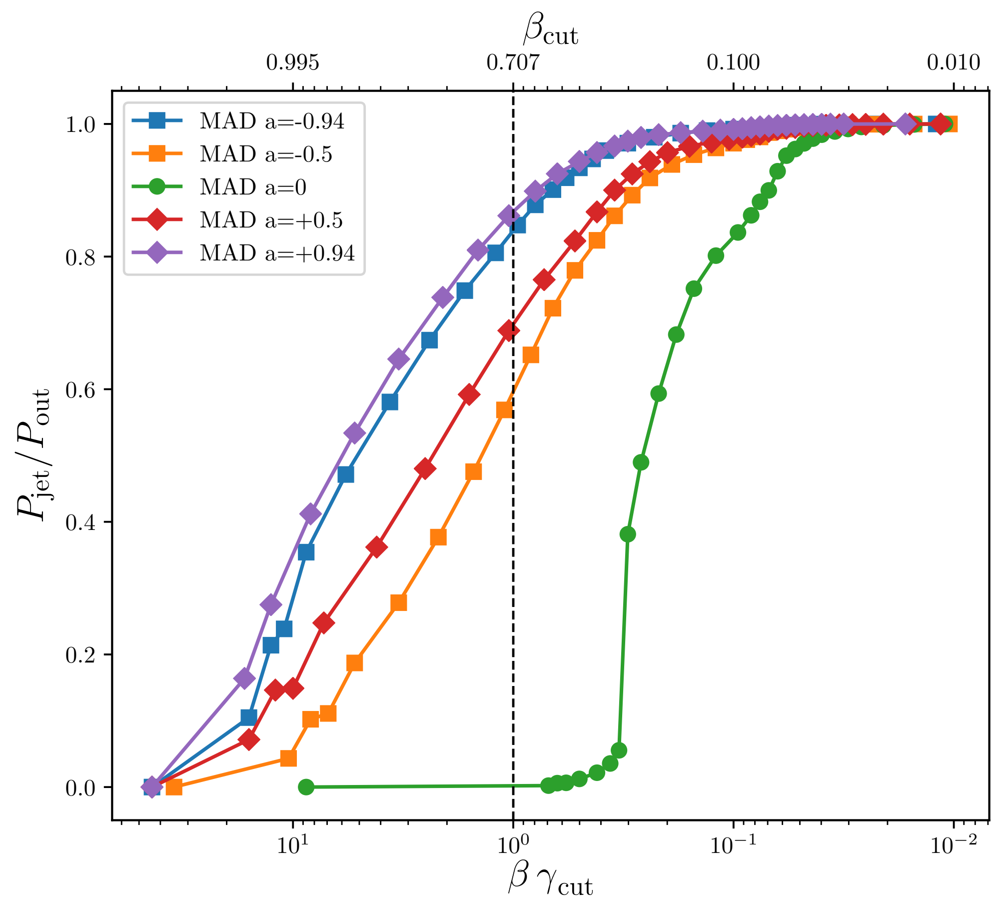

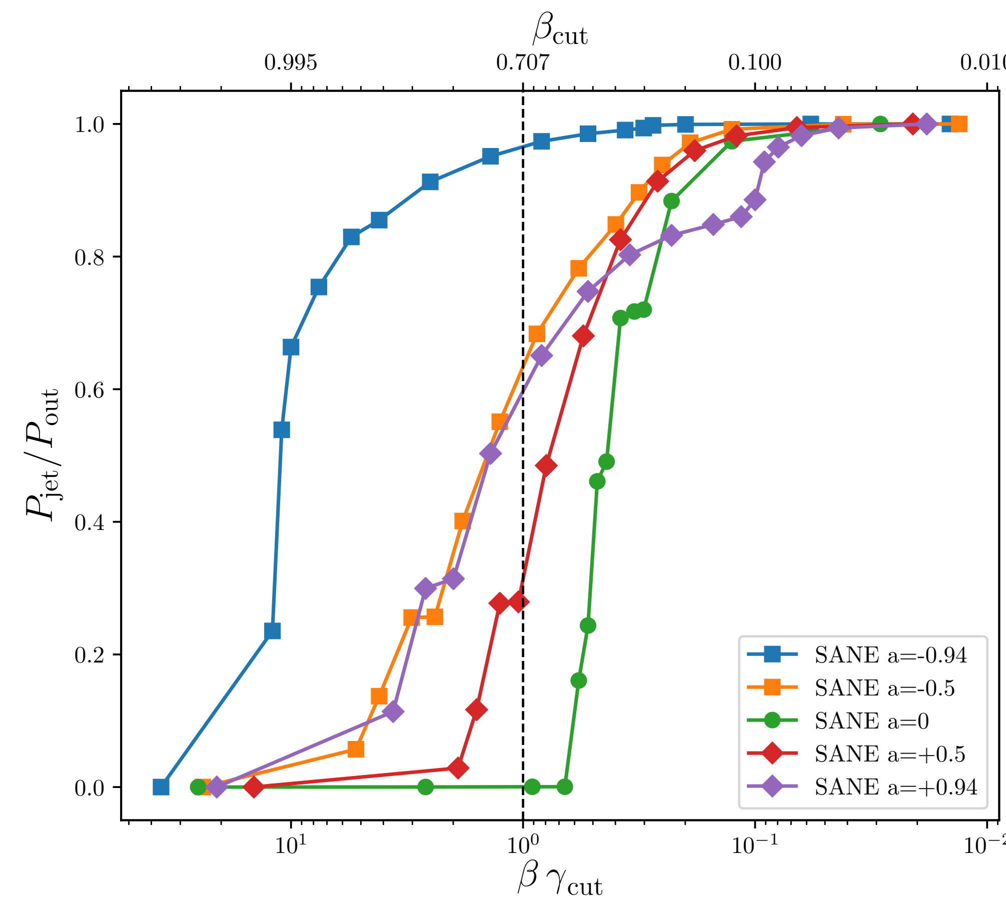

- P_{jet} depends on $\beta\gamma$ cutoff used in definition
- P_{jet} small for a = 0 because energy flux in relativistic outflo small

Event Horizon Telescope

Black Hole Photon Ring

Johnson et al. (2019

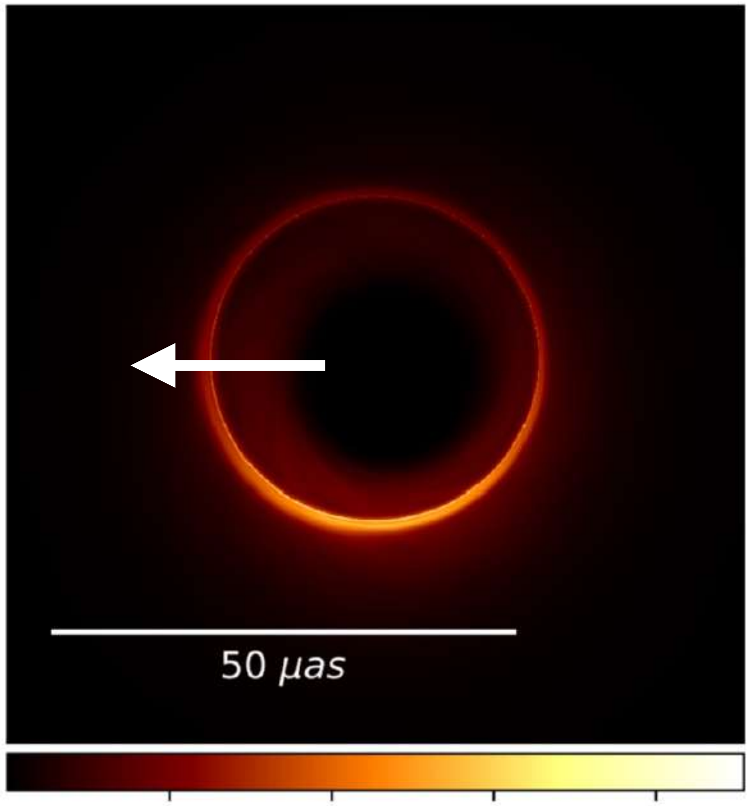

ne-average image of BH shadow,
3DMAD, a=0.94, i=17 deg

for M87

Event Horizon Telescope

Blue: perpendicular intersection to BH spin axis

Red: parallel intersection to BH spin axis

Decomposition of subrings by the number *n* of photon half-orbits from turning points in θ.

subring flux ratio

$$F^{n+1}_{\rm ring}/F^{n}_{\rm ring} \approx e^{-\gamma}$$

γ: Lyapunov exponent

a=1 case: n=1 subring contribute ~10% of total luminosity

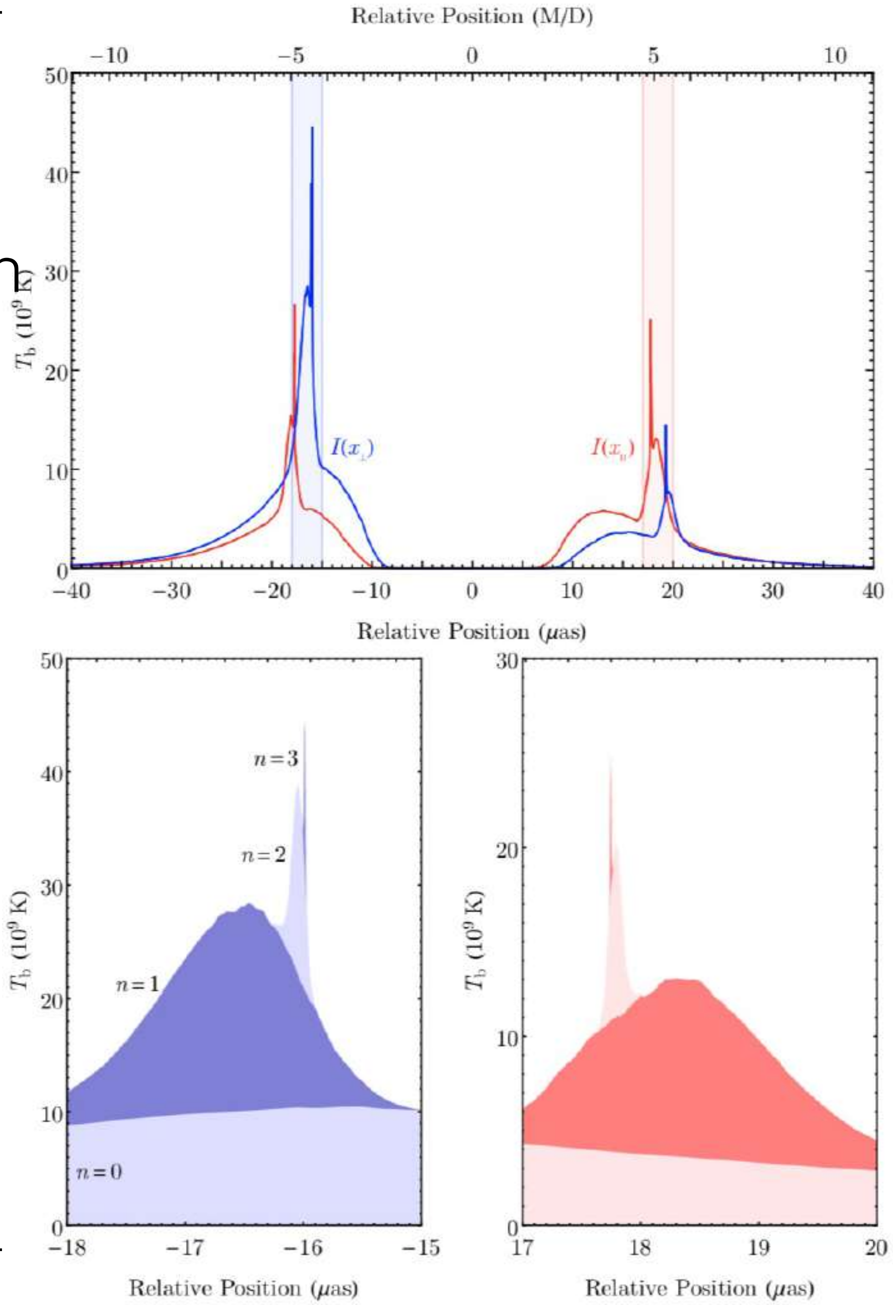

Black Hole Photon Ring

Johnson et al. (2019

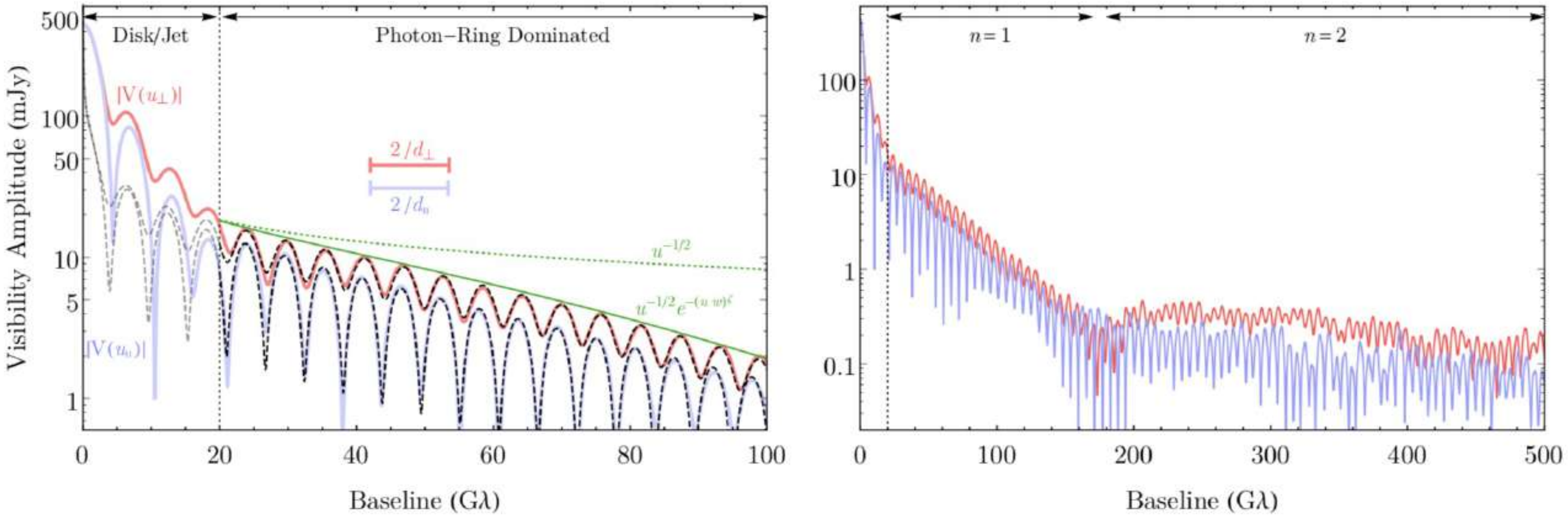

visibility amplitude of time-averaged GRMHD simulation for M87 (i=163 deg)

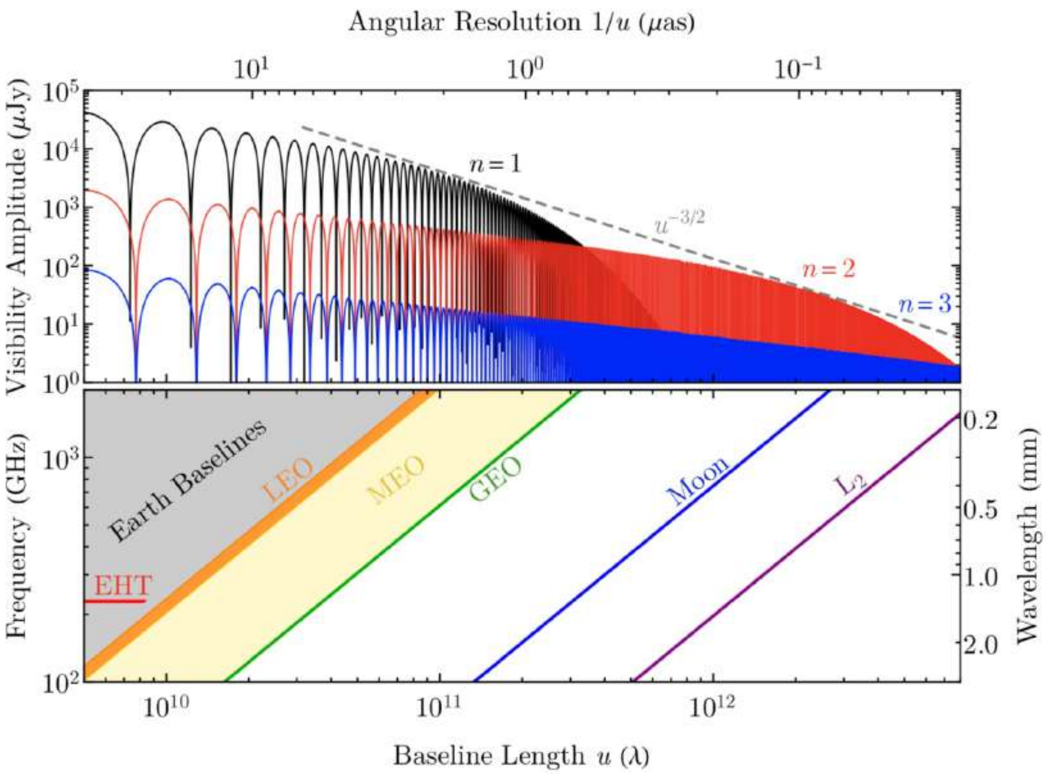

Blue: perpendicular intersection to BH spin axis

Red: parallel intersection to BH spin axis

short baseline: complex structure reflected disk/jet emission

long baseline (>20Gλ): dominated by photon ring (n=1,2,…)

LEO: low Earth Orbit: < 2000 km

MEO: Medium Earth Orbit: 2000-36,00

GEO: Geostationary orbit: 36,000 km

Effect of Changing Mass

napshot image of GRMHD simulation
MAD, spin a=0.94, Rhigh=160

Changing mass between
3 x 10^9 and 6 x 10^9 M_{sun}

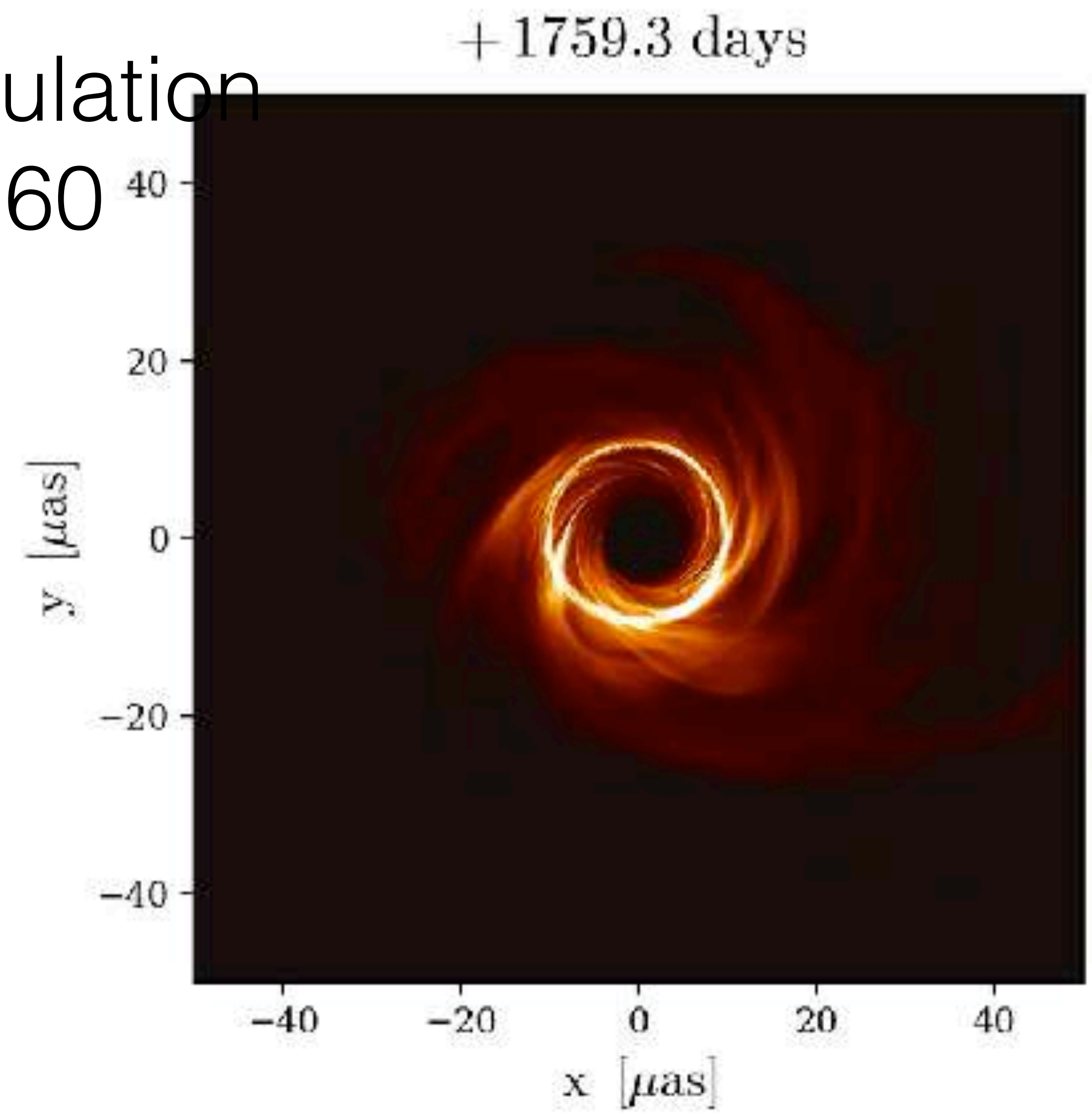

Credit: G. Wong, B. Prather, C. Gammie (Illino

Effect of Changing Inclination

napshot image of GRMHD simulation
MAD, spin a=0.94, Rhigh=160

Changing inclination
from163 to 0 degree

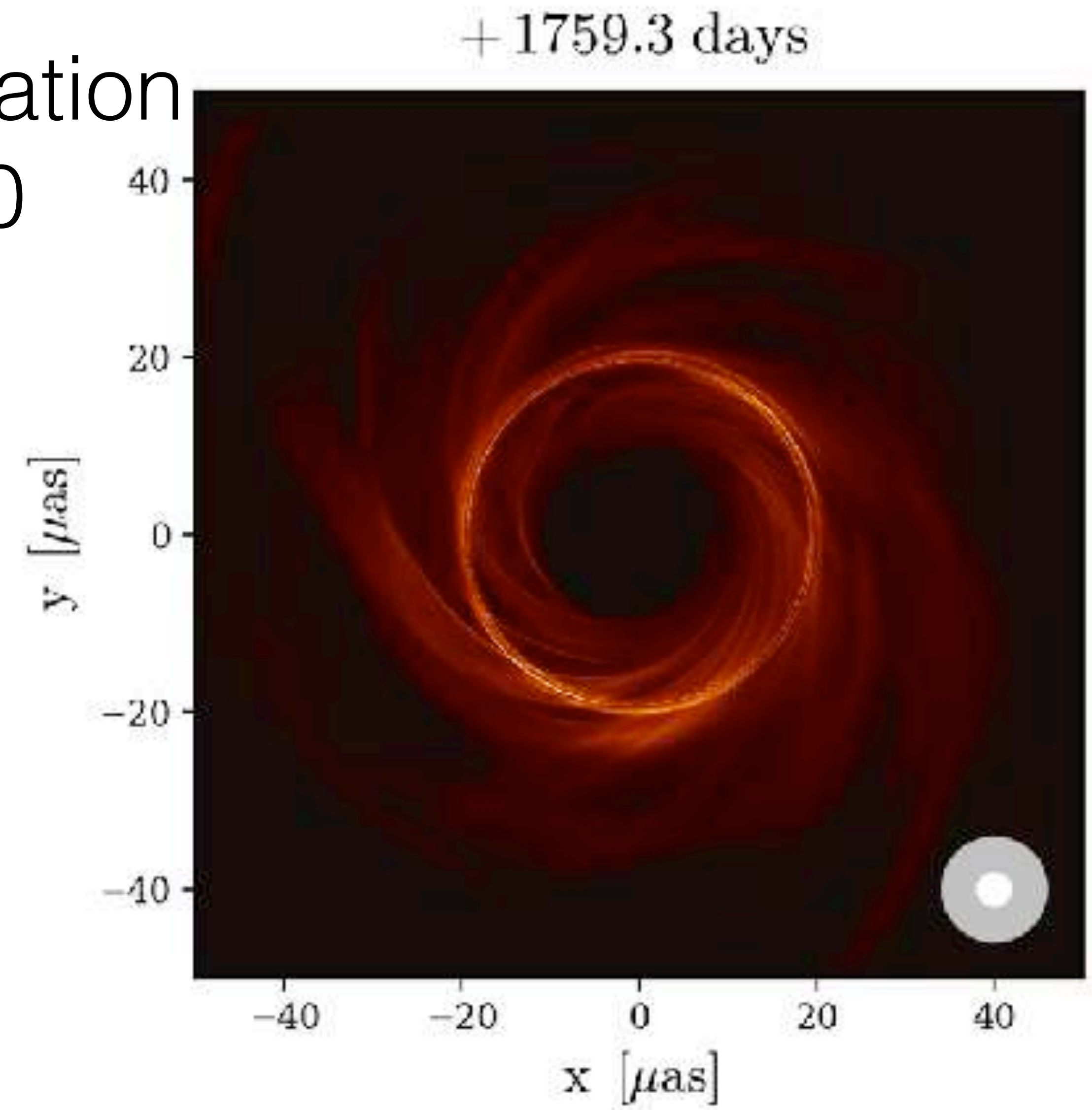

Credit: G. Wong, B. Prather, C. Gammie (Illino

M87 Theoretical Images

Movies of time evolution of GRRT image of M87

GRMHD simulation, SANE, a=0.94

Movie: Z. Younsi, L. Weih, C. Fromm, L. Rezzolla
Frankfurt BHCam team

M87 Theoretical Images

Movies of time evolution of GRRT & convolved images of M87

GRMHD simulation, SANE, a=0.94

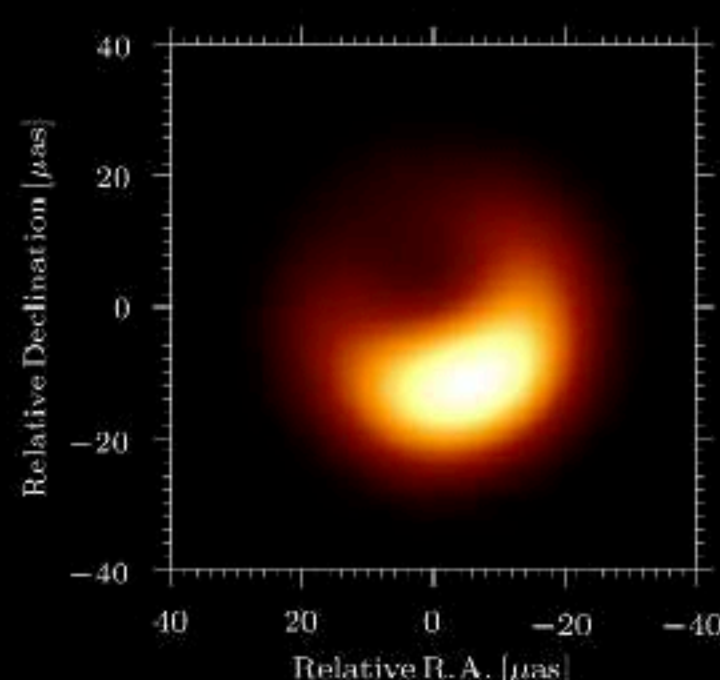

Movie: Z. Younsi, C. Fromm, L. Weih, L. Rezzolla
Frankfurt BHCam team

Effect of Changing Inclination

Snapshot image of GRMHD simulation
SANE, a=0.94

Changing inclination angle (from 163°)

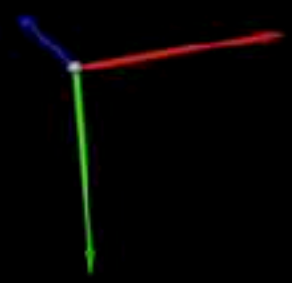

Movie: Z. Younsi, L. Weih, C. Fromm, L. Rezzolla
Frankfurt BHCam team

Spherical Projection of Density Evolution

color shows
log(ρ)
on surface
$r = 10\ GM/c^2$

pole to equator
contrast ~ 10^5

MAD, a=0

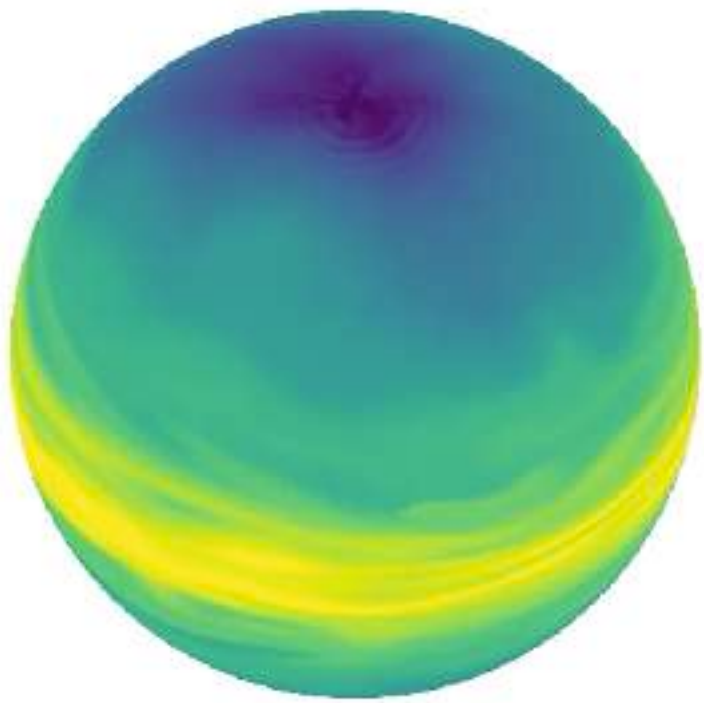

SANE, a=0

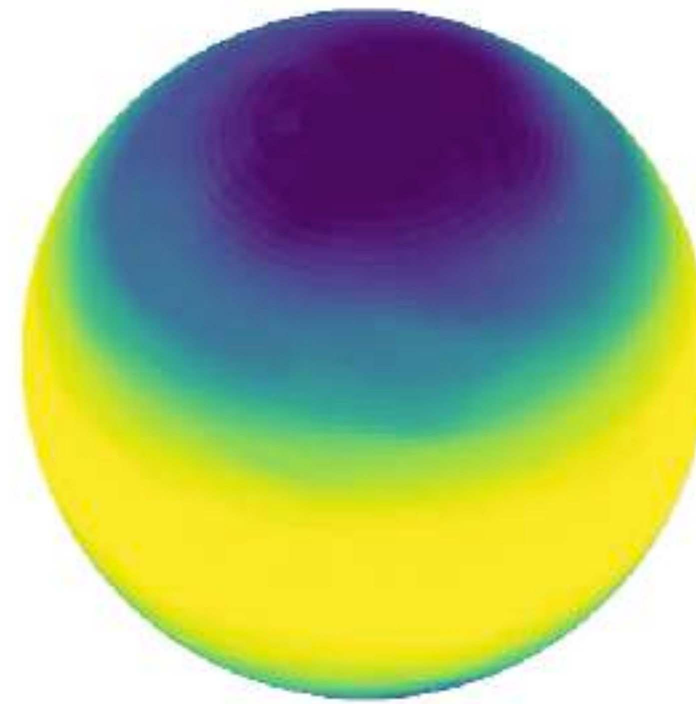

Credit: G. Wong, B. Prather, C. Gammie (Illino

Spherical Projection of Density Evolution

color shows
$\log(\rho)$
on surface
$r = 10\ GM/c^2$

pole to equator
contrast ~ 10^5

MAD, a = -0.94
retrograde

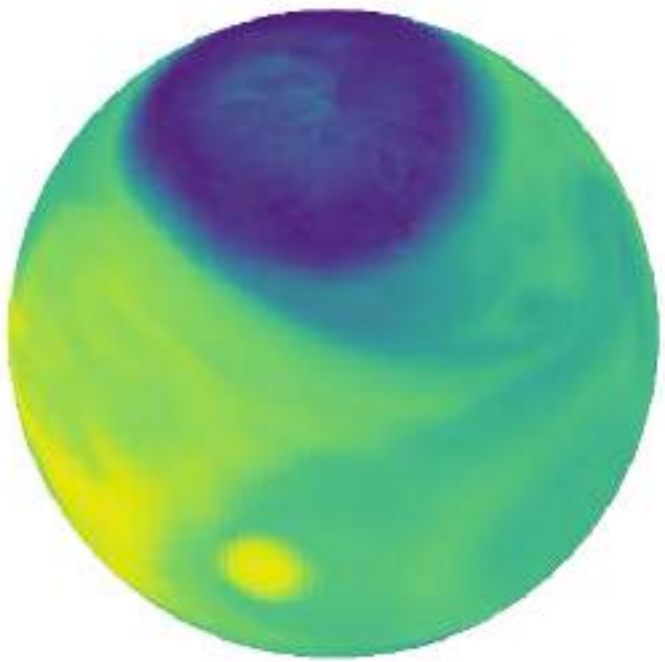

BH spin: clockwise
matter: counter-clockwise

MAD, a= +0.94
prograde

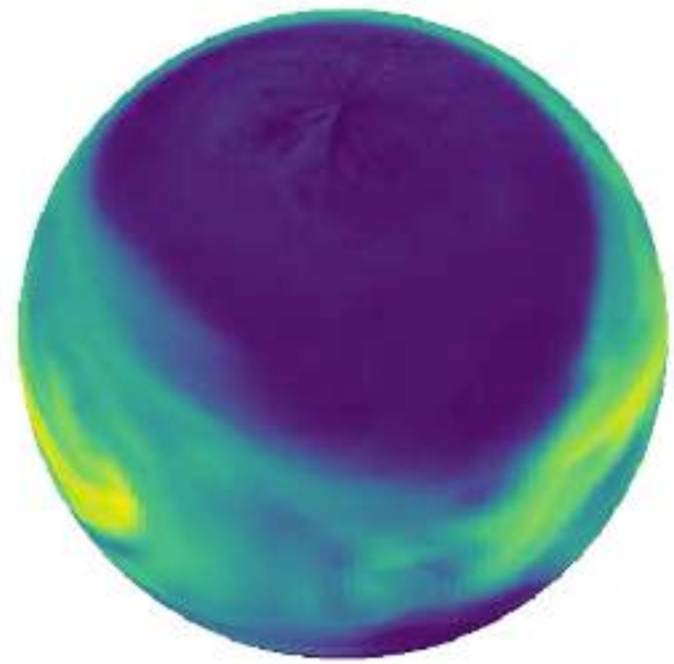

BH spin: counter-clockwise
matter: counter-clockwise

Credit: G. Wong, B. Prather, C. Gammie (Illino

Spherical Projection of Density Evolution

color shows
log(ρ)
on surface
$r = 10\ GM/c^2$

pole to equator
contrast ~ 10^5

SANE, a = -0.94

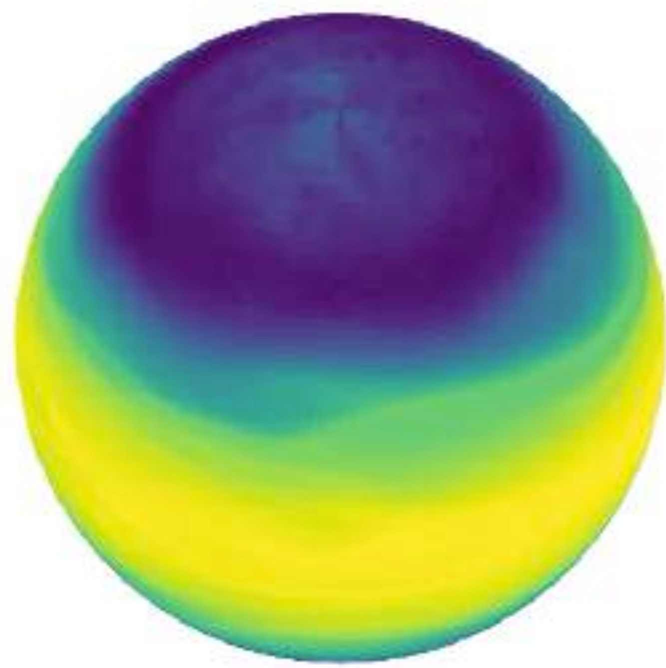

BH spin: clockwise
matter: counter-clockwise

SANE, a= +0.94

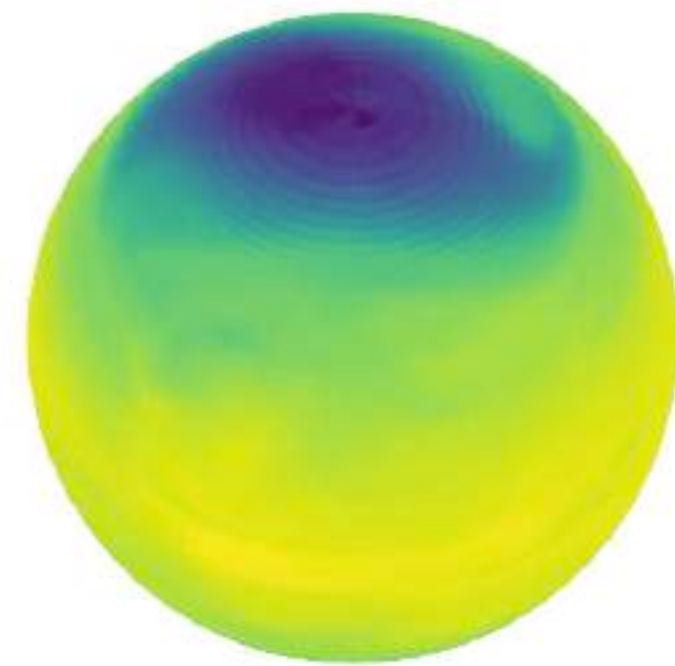

BH spin: counter-clockwise
matter: counter-clockwise

Credit: G. Wong, B. Prather, C. Gammie (Illino

Event Horizon Telescope

Credit: Dom Pesce
(Paper VI)

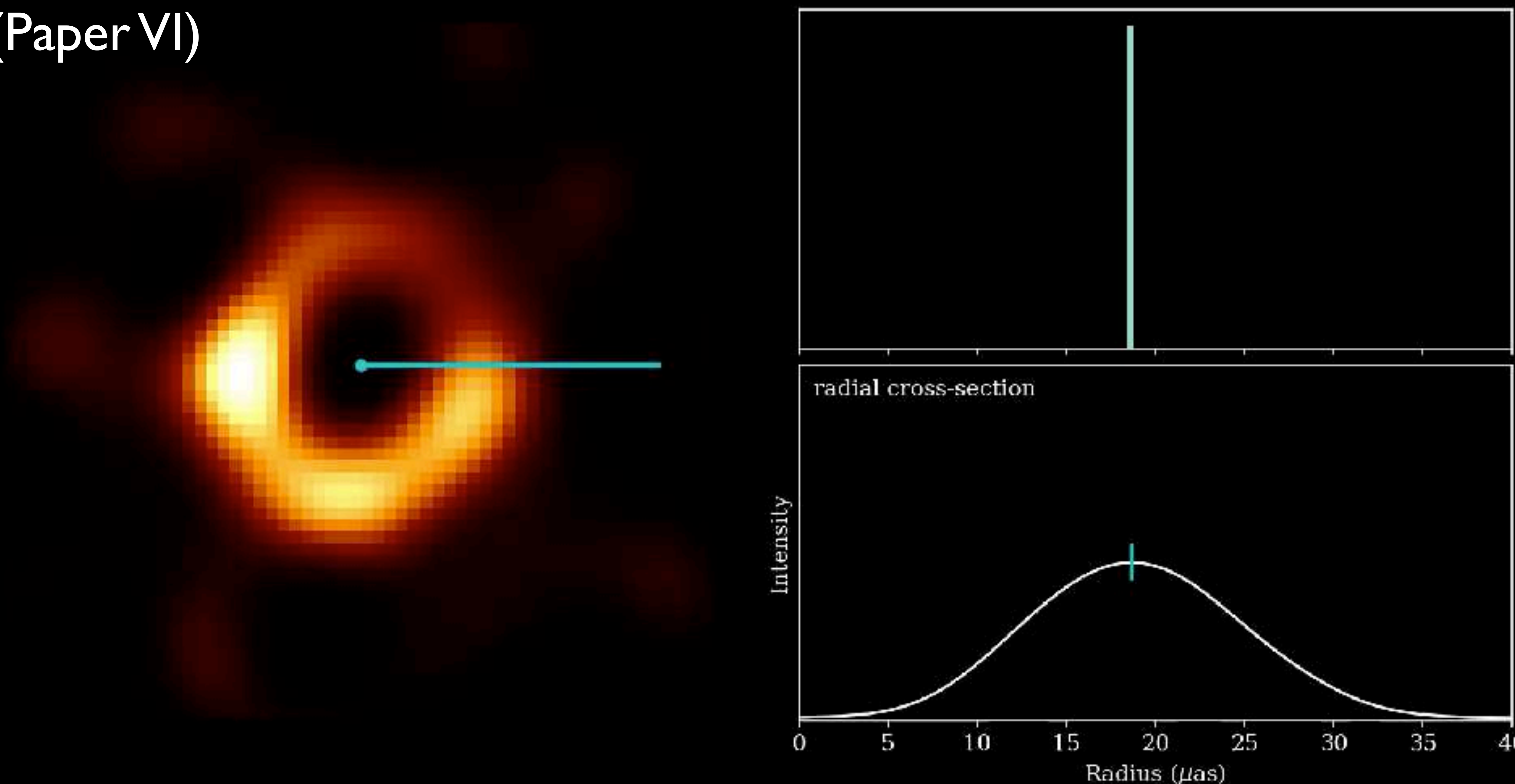

Credit: Dom Pesce
(Paper VI)

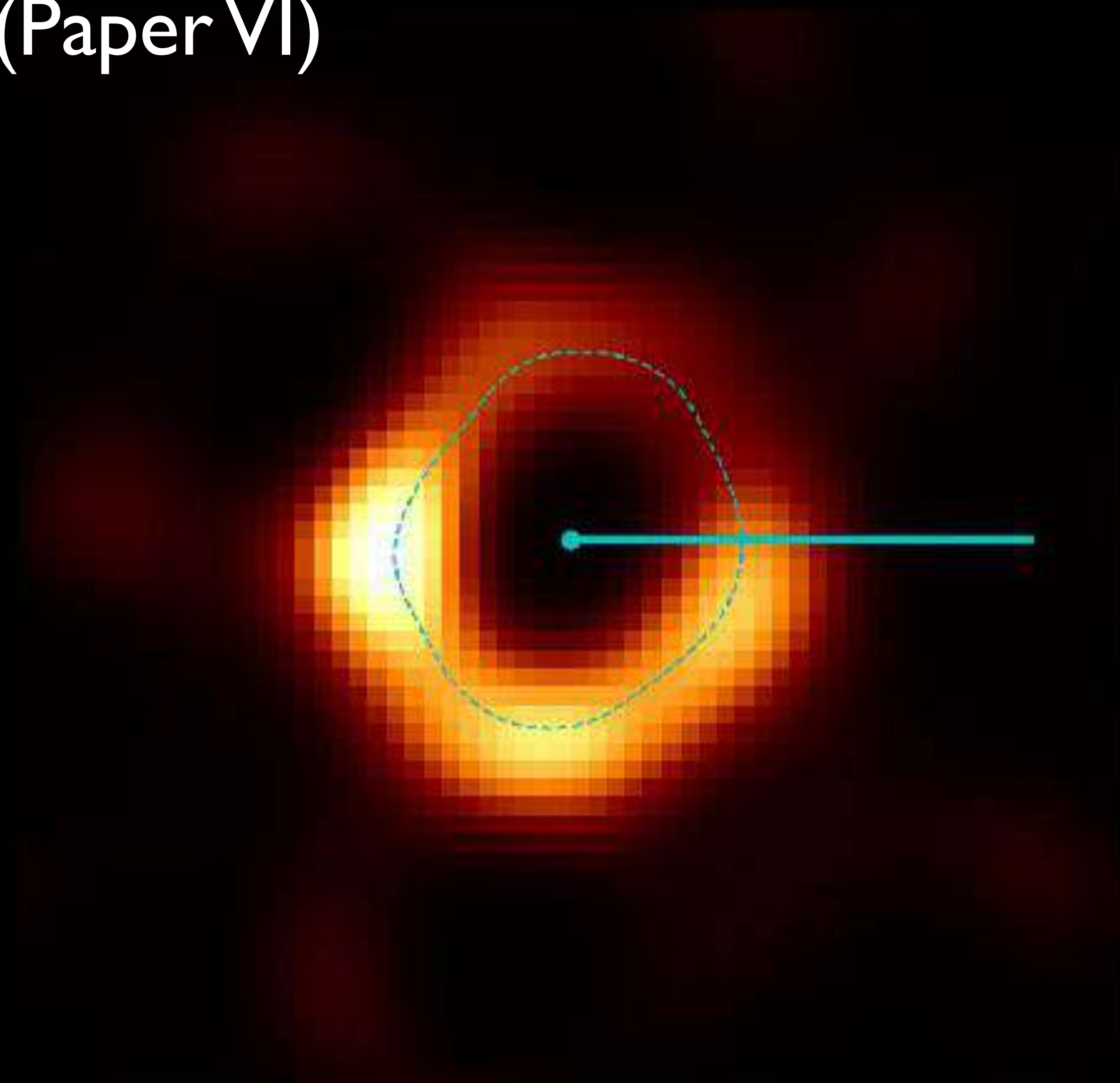

diameter and uncertainty

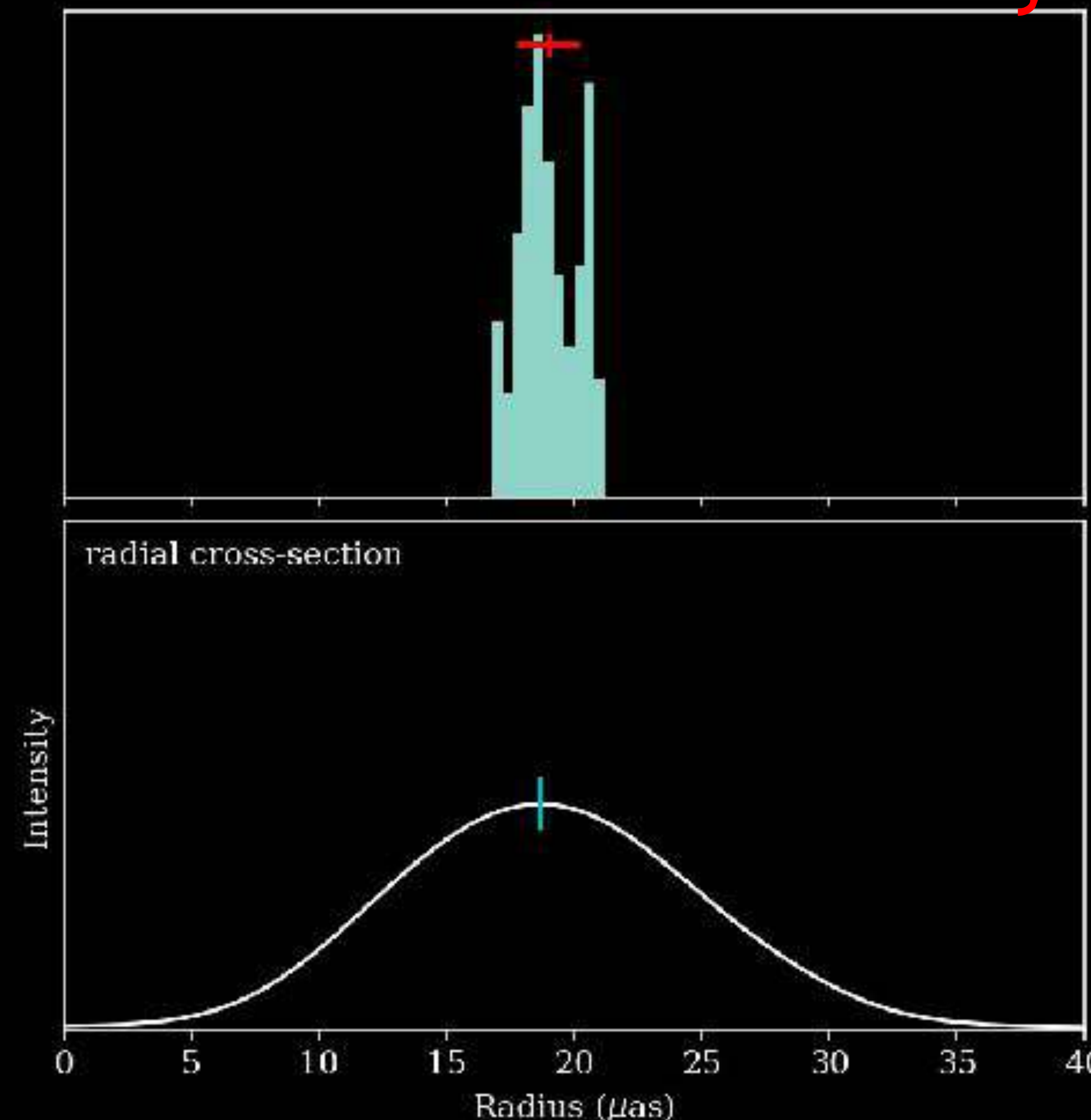

Credit: Dom Pesce
(Paper VI)

Image
domain

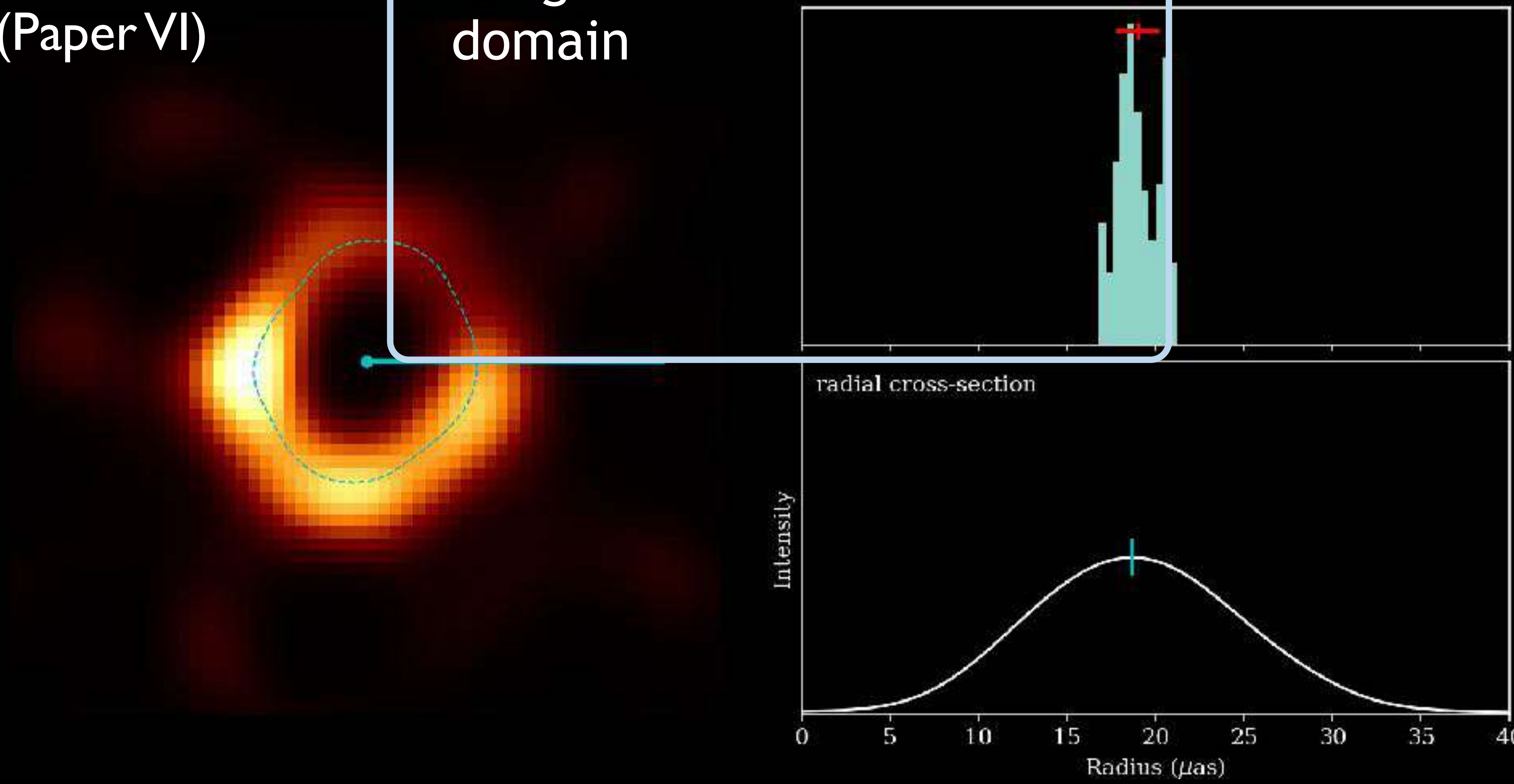

Credit: Dom Pesce (Paper VI)

Image domain

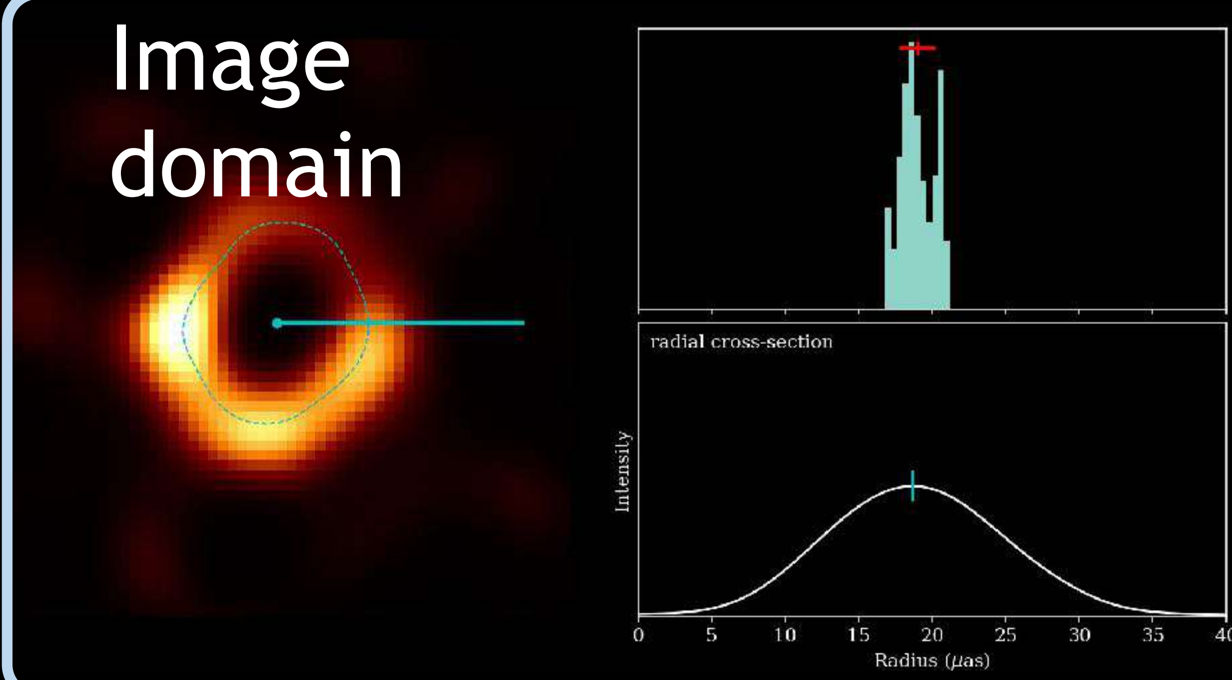

Geometric models

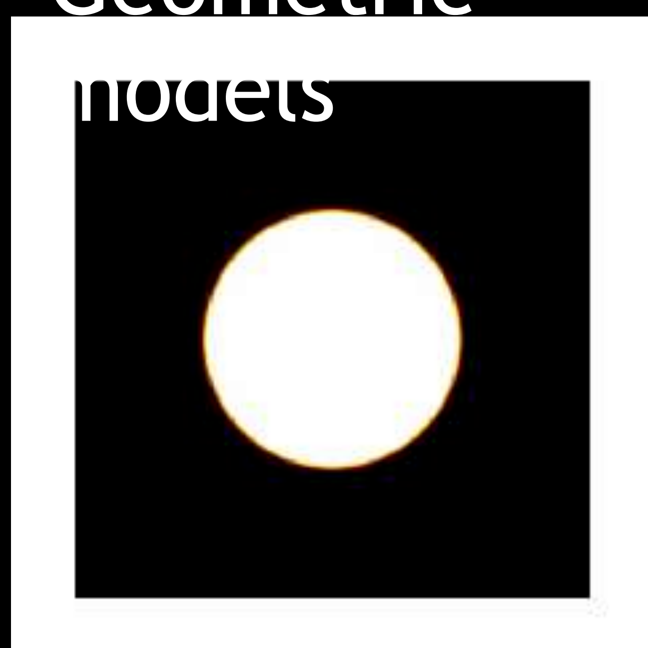

Simulations*